TECHNISCHE
UNIVERSITÄT
DARMSTADT

Physik

PNIPAM-Coated Brushy Beads and How They Collapse

At the faculty of Physics of the Technischen Universität Darmstadt

Submitted in the fulfilment of the requirements for the degree of
Doctor rerum naturalium (Dr. rer. nat.)

Doctoral thesis
by David VAN DUINEN

First assessor: Prof. Dr. Hans-Jürgen Butt
Second assessor: Prof. Dr. Regine von Klitzing

Darmstadt 2020 (year of the viva voce)

van Duinen, David: PNIPAM-Coated Brushy Beads and How They Collapse
Darmstadt, Technische Universität Darmstadt
Year thesis published in TUprints: 2021
URN: urn:nbn:de:tuda-tuprints-200413
Date of the viva voce: 16.12.2020

David **van Duinen**

Physicist, PhD candidate

Summary

I am currently finishing my PhD thesis at the Max-Planck Institute for Polymer Research in Mainz, Germany. My thesis topic is responsive polymer coatings, for which I developed an experimental optical method. Of the many aspects of PhD research – experiments, analysis, reporting, outreach, etc. – one of the things I enjoy most is discussion of results or analyses, both within my team and finally externally at conferences. Part of what I really liked when I was in Twente is the approach to technology and innovation. Making new innovations useful and applying these is great. While completing my studies, I also consistently participated in student organisations and found this work quite enjoyable. After I complete my PhD, I see myself working in a field related to physics and technology, driving new innovations and perhaps coordinating these. I believe that science and technology are incredibly important to society, and I would love to be a part of the infrastructure connecting them. On the personal side, in my spare time I enjoy sports and the outdoors, gaming, reading, and music.

Education

Max-Planck Institute for Polymer Research

Mainz, Germany

PhD in Physics — *Expected 2020*

- About stimuli-responsive polymer coatings, reacting to changes in temperature and solvent.
  I characterised the coatings' responses with a novel combination of an optical technique and analysis method that I developed.
- I am supervised by Prof. Dr. H.-J. Butt and Dr. R. Berger.
- During the PhD, I gave several presentations within the group in the regular group seminars and retreats as well as externally.
- The defence will take place within the department of physics at the Technical University of Darmstadt.
- The work was published in the scientific journal Langmuir (*link*).
- Exchange
  Shanghai and Huainan, China – As part of the German DAAD exchange, I travelled to China to gain expertise in AFM measurements with Prof. Dr. Yi Zhang and his group at SINAP. I also visited Prof. Dr. C. Xue in Huainan.

University of Twente

Enschede, the Netherlands

MSc in Applied Physics — *Diploma 2016*

- Optics and Biophysics specialisation.
- Master thesis
  Optical Sciences group – Supervised by Dr.Ir. J.M. Huijser and Prof. Dr. J.L. Herek.
  Argonne, United States – During my thesis I also joined measurements at the ANL. The results were published in J.Phys.Chem. (*link*).
- Internship
  Seville, Spain – At Abengoa Research I investigated layers of perovskite, a rather novel material for photovoltaic solar cells.

University of Twente

Enschede, the Netherlands

BSc in Advanced Technology — *Diploma 2013*

- This study provides a broad scientific and technological basis, which is combined with some courses in business administration and planning.

Workshops

- Conflict management (Mainz) with Matthias Mayer.
- Presenting (Mainz) with Millie Baker.
- Managing Cultural Dynamics (Enschede) with Jitske Kramer.
- Board training (Enschede) with Ulberthe Wielinga.

Honors & Awards

Oct. 2018 **Best Poster Award,** MPI-P Poster day — *Mainz, Germany*

Apr. 2018 **Best Poster Award,** 14th Zsigmondy Colloquium — *Mainz, Germany*

Presentation

Conference of the European Colloids and Interface Society

KU Leuven, Belgium

Oral presentation — *Sept. 2019*

- Title: PNIPAM-coated Brushy Beads and How They Collapse: How Environment Affects Brownian Motion

Conference of the International Association of Colloids and Interface Scientists

Rotterdam, the Netherlands

Poster presentation — *May. 2018*

- Title: The Influence of a Temperature-Responsive Polymer Brush on the Brownian Motion of a Microbead

Zsigmondy colloquium

Max-Planck Institute for Polymer Research, Mainz, Germany

Poster presentation — *Apr. 2018*

- Title: The Influence of a Temperature-Responsive Polymer Brush on the Brownian Motion of a Microbead
- Awarded the Best Poster Award

Meeting of the German Physical Society (DPG Tagungen)

Technical University of Berlin, Germany

Oral presentation — *Mar. 2018*

- Title: How a responsive polymer brush layer influences the Brownian motion of a microbead

Invited talk

Anhui University of Science and Technology, Anhui, China

Oral presentation — *Oct. 2017*

- Title: Surface forces at high hydrostatic pressure

Zsigmondy colloquium

Leibniz-INM, Saarbrücken, Germany

Poster presentation — *Apr. 2017*

- Title: Force Measurements of Microspheres Trapped with a Laser at High Hydrostatic Pressure

UTwente MESA+ Day

Enschede, the Netherlands

Poster presentation — *Sept. 2015*

- Title: Shedding light on molecule-nanoparticle interactions
- Here I presented on my master's thesis.

Activism and Extracurricular Activities

S.A. Astatine

University of Twente

Board member (full- and part-time) — *Sept. 2011 - Sept. 2013*

- For one year, I was a full-time board member of Astatine, which had about 400 members. For the second year I focussed on finishing my BSc, and was part-time member of the board.
- I had several functions, including secretary and external relations.
- This time was rewarded with the Certificate Recognition of Extracurricular Activities of the UTwente and the Student Union.

D.K.V. Euros

University of Twente

Chair of the board (part-time) — *Oct. 2013 - Oct. 2014*

- As the chair of the club I regularly planned and conducted meetings with my own board, the whole club, and other external organisations.

Other activities

UT and Mainz

Teaching assistant, first aid (BHV 2012-2017), several committees, trainer, organising an open-air rock festival

Skills and languages

Software Matlab, MS Office, LaTeX, Thunderbird, EndNote, Python, Windows, Mac OS
Science Experimental, Optics, Spectroscopy, Laboratory Skills, Data Analysis, Presenting

Dutch Mother tongue
English Native level, International Baccalaureate A1 (comparable CEFR to C2)
German Fluent (living and working)

Eigenständigkeitserklärung - Declaration of Authorship

Erklärung gemäß §9 Promotionsordnung

Hiermit versichere ich, dass ich die vorliegende Dissertation selbstständig angefertigt und keine anderen als die angegebenen Quellen und Hilfsmittel verwendet habe. Alle wörtlichen und paraphrasierten Zitate wurden angemessen kenntlich gemacht. Die Arbeit hat bisher noch nicht zu Prüfungszwecken gedient.

I declare that this thesis and the work presented in it are my own work, for which I have used no other sources or help than those stated in this thesis. Any literal or paraphrased citations are always properly attributed. This work has not been used for an examination before.

David VAN DUINEN

Datum und Unterschrift - Date and signature

"Everything must be made as simple as possible. But not simpler."

Albert Einstein

Contents

List of Figures

List of Tables

List of Abbreviations

APD	**A**valance **P**hoto**D**iode
AFM	**A**tomic **F**orce **M**icroscopy
ATRP	**A**tom **T**ransfer **R**adical **P**olymerisation
CCD	**C**harged **C**oupled **D**evice
FIB	**F**ocussed **I**on **B**eam
fwhm	**F**ull **W**idth **H**alf **M**aximum
GPC	**G**el **P**ermeation **C**hromatography
LCST	**L**ower **C**ritical **S**olution **T**emperature
PNIPAM	**P**oly(*N*-**I**so**p**ropyl**a**crila**m**ide)
PSD	**P**ower **S**pectral **D**ensity
QCM	**Q**uartz **C**rystal **M**icrobalance
RMSE	**R**oot **M**ean **S**quared **E**rror
RICM	**R**eflection **I**nterference **C**ontrast **M**icroscopy
RMS	**R**oot **M**ean **S**quared
SEM	**S**canning **E**lectron **M**icroscope
SPM	**S**canning **P**robe **M**icroscopy

List of Symbols

A	Magnitude of drift term in PSD	$\mathrm{m^2\,s^{-1}}$
A_{contact}	Contact area	$\mathrm{m^2}$
A_{corr}	Correlated area	$\mathrm{m^2}$
C	Experimental limits in PSD	$\mathrm{m^2\,Hz^{-1}}$
d	Distance between bead and wall	m
D	Diffusion coefficient	$\mathrm{m^2\,s^{-1}}$
f	Frequency	Hz
f_k	Cut-off frequency	Hz
F	Force	N
G	Gibbs energy of a system	J
G'	Viscoelastic storage modulus	Pa
G''	Viscoelastic loss modulus	Pa
H	Enthalpy	J
I	Light intensity	$\mathrm{W\,m^{-2}}$
k	Spring constant	$\mathrm{N\,m^{-1}}$
$k_{\mathrm{B}}T$	Thermal energy at temperature T	J
l	Length of polymer chain segment	m
L	Swollen brush thickness	m
L_{dry}	Dry brush thickness	m
m	Mass of the bead	kg
M_{monomer}	Molar mass of a monomer	$\mathrm{kg\,mol^{-1}}$
M_n	Molecular weight of polymer	$\mathrm{kg\,mol^{-1}}$
n	Refractive index	-
n_{chains}	Number of polymer chains	-
N	Number of chain segments in a polymer	-
adj. $\mathrm{R^2}$	Adjusted $\mathrm{R^2}$ value describing fit quality	-
P	Laser power	W
R	Radius of the bead	m
R_{g}	Radius of gyration	m
S	Entropy	$\mathrm{J\,K^{-1}}$
t	Time	s

T	Temperature	°C or K
x	Spatial variable	m
x_c	Fraction of collapsed polymer segments	-
β	Damping coefficient	$\mathrm{N\,s\,m^{-1}}$
$\zeta(t)$	Normalised white-noise process	-
η	Viscosity	Pa s
λ	Wavelength of light	m
λ_D	Debye length	m
ρ	Density	$\mathrm{kg\,m^{-3}}$
σ	Grafting density	$\mathrm{m^{-2}}$
τ_p	Time constant of inertial effects	s
ϕ	Volume fraction	-
φ	Phase shift	-
χ	Flory interaction parameter	-
ψ_0	Surface potential	V

Abstract

PNIPAM-Coated Brushy Beads and How They Collapse

by David VAN DUINEN

Stimuli-responsive polymers are a group of powerful switchable materials with a broad range of applications. Induced by a stimulus, the properties of such polymers can change dramatically. One popular polymer is poly(*N*-isopropylacryamide) (PNIPAM). PNIPAM is interesting for a number of applications, including in technologies as sensors, actuators, microfluidics, and mineral retrieval, but also in biology, and in medicine. One powerful place to use them is in colloids. By themselves, colloids are a center point of interest, owing to the fact that their properties depend on their surfaces rather than on their bulk. Adding to this fact a stimuli-responsiveness will open up new possibilities for applications. What is missing to make full use of PNIPAM is a thorough understanding of its properties and how they respond to stimuli.

Understanding PNIPAM requires understanding its response to stimuli. To this end, I investigated two of PNIPAM's main stimuli: temperature and solvent. With temperature, PNIPAM mostly displays a simple collapse while above a certain temperature, the lower critical solution temperature (LCST). In some cases, however, PNIPAM has been reported to show a rather complex, not fully understood, two-stage collapse. With solvent, PNIPAM exhibits the co-non-solvency effect. PNIPAM swells well in either water or in alcohols, yet it collapses in intermediate mixtures. The exact cause of the co-non-solvency effect is still debated, however. The study of the effects of these two stimuli on PNIPAM-based colloids is not straightforward: many techniques are technologically quite involved, average over a multitude of colloids, or are invasive and change the response of the sampled colloids to stimuli. Hence, a better understanding of these two stimuli would be greatly benefited by the ability to study them in a simple, non-invasive manner.

In this thesis, I present a new method to observe responses of PNIPAM-based colloids to stimuli. The method is optical, and is based on interference and microscopy. Specifically, I studied colloidal glass beads that were coated with an end-grafted PNIPAM brush (51 ± 3 nm thick) near a glass surface. The Brownian motion of such beads is dominated by the brush layer's viscoelastic properties, which change as a response to stimuli. As a result, monitoring the

Brownian motion through interference allows observing viscoelastic changes of the PNIPAM brush in a simple and non-invasive manner. Consequently, this method allowed me to study how various stimuli affected the PNIPAM brush coating.

Taking temperature as a stimulus, I observed a two-stage collapse of the PNIPAM brush-coated beads. Upon increasing the temperature, I first observed a change at 36 °C. This change was attributed to the LCST volume collapse of PNIPAM, which induced an increase of polymer brush density and subsequent increase of viscosity of the brush layer. Then, increasing temperature above 46 °C induced a second transition. I attributed this second transition to the complete collapse of the brush layer. Upon this complete collapse, the brush layer became stiffer throughout, which made the Brownian motion more elastic. These results indicate that PNIPAM undergoes a type II-phase transition. The better understanding will play a role towards proper application of PNIPAM brush coatings.

Furthermore, I investigated the co-non-solvency effect using the same method. For this effect, there exist a few hypotheses regarding the underlying cause. One leading hypothesis is based on the preferential binding of alcohol to PNIPAM, rather than water to PNIPAM. Through monitoring the viscoelastic changes in my experiments, I provide support for the theory of preferential binding.

These viscoelastic responses to stimuli provide us with a better insight into responsive thin coatings. Being non-invasive, simple, flexible, repeatable, yet measuring single coated colloids in-situ, the optical method that I developed and described proved to be a useful tool. This method can be integrated into the standard set of techniques to investigate changes in stimuli-responsive colloids.

For the non-scientists

Stimuli-responsive polymers are a group of powerful switchable materials with a broad range of applications. One popular responsive polymer is PNIPAM, or poly(*N*-isopropylacryamide) in full. It is interesting for a range of applications as a technology in sensors, actuators, microfluidics or for mineral retrieval but also as an in-body medicine carrier. What makes PNIPAM so interesting is that it responds to stimuli: changes of its environment. For example, changing the temperature can dramatically change the properties of PNIPAM. However, exactly why and how PNIPAM responds is not completely known. Therefore, before we can fully use its potential, we first need to understand PNIPAM better.

There are several forms and shapes of polymers and of PNIPAM. I looked at PNIPAM brushes. Such brushes are basically like the brush of a broom, but very short; only about a hundred nanometer thick – a thousand times thinner than printer paper. Such brushes can be coatings. What is nice in the case of a PNIPAM brush coating, is that the coated surface becomes stimuli-responsive. I investigated such PNIPAM brush-coatings on small glass beads. To look at the response of these PNIPAM brush-coated beads, I exposed them to different temperatures. Through a special microscope set-up that I developed, I was able to study the response of the PNIPAM brush coating.

The response of PNIPAM to temperature showed an interesting result. Most of the time, PNIPAM responds at a single temperature. In my experiments, I found that there are two distinct transitions, at two distinct temperatures. I could explain these results by looking at the thin layer of the PNIPAM brush and how it changed its thickness and stiffness. In a further study, I also looked at the influence of another stimulus: solvent, and these experiments support for one of the possible theories. All in all, we now understand thin responsive coatings a little bit better, which was made possible because of the new experimental optical method that I developed.

Zusammenfassung

Viscoelastische Änderungen in Responsive Polymerbürste

von David VAN DUINEN

'Stimuli-responsive' Polymere sind eine Gruppe leistungsstarker schaltbarer Materialien mit einem breiten Anwendungsspektrum. Induziert durch einen Stimulus können sich die Eigenschaften solcher Polymere dramatisch verändern. Ein populäres Polymer ist Poly(*N*-isopropylacryamid) (PNIPAM). PNIPAM ist für eine Reihe von Anwendungen interessant, u.a. in Technologien wie Sensoren, Aktoren, Mikrofluidik und Mineraliengewinnung, aber auch in der Biologie oder in der Medizin. Ein wirkungsvoller Ort für ihre Verwendung sind Kolloide. Die Kolloide selbst stehen im Mittelpunkt des Interesses, da ihre Eigenschaften von ihrer Oberfläche statt von ihrem Volumen abhängen. Wenn man zu dieser Tatsache noch eine 'Stimuli-responsiveness' hinzufügt, eröffnen sich neue Anwendungsmöglichkeiten. Was fehlt, um PNIPAM in vollem Umfang nutzen zu können, ist ein gründliches Verständnis von den Eigenschaften und der Art und Weise, wie PNIPAM auf Stimuli reagiert.

Um PNIPAM zu verstehen, muss man die Reaktion auf Stimuli verstehen. Zu diesem Zweck untersuchte ich zwei der wichtigsten Stimuli von PNIPAM: Temperatur und Lösungsmittel. Bei der Temperatur zeigt PNIPAM meist einen einfachen Kollaps, während oberhalb einer bestimmten Temperatur, der unteren kritischen Lösungstemperatur (Englisch: 'lower critical solution temperature', LCST), ein Kollaps stattfindet. In einigen Fällen wurde jedoch berichtet, dass PNIPAM einen ziemlich komplexen, nicht vollständig verstandenen, zweistufigen Kollaps zeigt. Mit Lösungsmittel zeigt PNIPAM den 'co-non-solvency'-effekt. PNIPAM quellt in Wasser oder in Alkoholen gut auf, kollabiert jedoch in Zwischenmischungen. Die genaue Ursache des 'co-non-solvency'-effekts wird jedoch immer noch diskutiert. Die Untersuchung der Auswirkungen dieser beiden Stimuli auf PNIPAM-basierte Kolloide ist nicht einfach: Viele Techniken sind technologisch aufwendig, über eine Vielzahl von Kolloiden gemittelt, oder sie sind invasiv und verändern die Reaktion der untersuchten Kolloide auf Stimuli. Daher wäre ein besseres Verständnis dieser beiden Stimuli durch die Möglichkeit, sie auf einfache, nicht-invasive Weise zu untersuchen, von großem Vorteil.

In dieser Arbeit stelle ich eine neue Methode zur Beobachtung der Reaktionen von PNIPAM-basierten Kolloiden auf Stimuli vor. Die Methode ist optisch und basiert auf Interferenz und Mikroskopie. Insbesondere untersuchte ich

kolloidale Glasmurmeln, die in der Nähe einer Glasoberfläche mit einer 'end-grafted' PNIPAM-Bürste (51 ± 3 nm dick) beschichtet wurden. Die Brownsche Bewegung solcher Murmeln wird durch die viskoelastischen Eigenschaften der Bürstenschicht dominiert, die sich als Reaktion auf Stimuli verändern. Infolgedessen ermöglicht die Überwachung der Brownschen Bewegung durch Interferenz die Beobachtung viskoelastischer Veränderungen der PNIPAM-Bürste auf einfache und nicht-invasive Weise. Folglich konnte ich mit dieser Methode untersuchen, wie sich verschiedene Stimuli auf die Beschichtung der PNIPAM-Bürste auswirkten.

Bei der Verwendung der Temperatur als Stimulus beobachtete ich einen zweistufigen Kollaps der PNIPAM-Murmeln mit Bürstenbeschichtung. Beim Erhöhen der Temperatur beobachtete ich zunächst eine Veränderung bei 36 °C. Diese Änderung wurde dem LCST-Volumenkollaps von PNIPAM zugeschrieben, der einen Anstieg der Polymer-Bürstendichte und eine anschließende Erhöhung der Viskosität der Bürstenschicht bewirkte. Dann induzierte ein Temperaturanstieg über 46 °C einen zweiten Übergang. Ich führte diesen zweiten Übergang auf den vollständigen Zusammenbruch der Bürstenschicht zurück. Nach diesem vollständigen Zusammenbruch wurde die Bürstenschicht durchgehend steifer, wodurch die Brownsche Bewegung elastischer wurde. Diese Ergebnisse weisen darauf hin, dass PNIPAM einen Typ-II-Phasenübergang durchläuft. Das bessere Verständnis wird eine Rolle bei der korrekten Anwendung von PNIPAM-Bürstenbeschichtungen spielen.

Außerdem untersuchte ich mit der gleichen Methode den 'co-non-solvency'-Effekt. Für diesen Effekt gibt es einige Hypothesen bezüglich der zugrunde liegenden Ursache. Eine führende Hypothese basiert auf der präferenziellen Bindung von Alkohol an PNIPAM anstelle von Wasser an PNIPAM. Indem ich die viskoelastischen Veränderungen in meinen Experimenten beobachte, unterstütze ich die Theorie der präferenziellen Bindung.

Diese viskoelastischen Reaktionen auf Stimuli geben uns einen besseren Einblick in 'Stimuli-responsive' dünne Polymerschichten. Da die von mir entwickelte und beschriebene optische Methode nicht invasiv, einfach, flexibel und wiederholbar ist und dennoch einzelne beschichtete Kolloide in-situ misst, erwies sie sich als nützliches Werkzeug. Diese Methode kann in den Standardsatz von Techniken integriert werden, um Veränderungen bei auf 'Stimuli-responsive' Kolloiden zu untersuchen.

Der englische Text wurde mit Hilfe von DeepL (Link) ins Deutsche übersetzt. Anschließend habe ich die Übersetzung überprüft.

Chapter 1

Introduction

1.1 The role of responsive polymers

Today's world keeps evolving thanks to the many scientific and technological innovations. Such innovations have allowed us to do things that we could not do before, and do them better and faster. Recently, as systems and machines become more and more complex and interlinked, sensors start playing an increasingly big role in connecting everything. Sensors can help us observe the world and act accordingly. The use of sensors has been promoted by polymeric materials: the easy production and the typical low cost of polymers allows applying sensors commonly. One novelty in sensors is based on a special type of polymeric materials. There exist materials that are responsive: a small change in surroundings can lead to a drastic change of the material's properties. Subsequently, such materials provide a way of interacting with or sensing of the environment.

One popular responsive polymer is poly(*N*-isopropylacrylamide), or PNIPAM. Stimuli such as temperature or solvent cause the properties of PNIPAM to change. This response is what makes PNIPAM interesting, and it has many uses. PNIPAM is used to an academic end to help understand the denaturation of proteins, since the collapse of PNIPAM is similar and the PNIPAM molecule is much less complex than a protein is [Stu+10]. More practically, PNIPAM coatings have also been used as an enabling technology. Types of sensors, actuators, or smart surfaces rely on the responsiveness of PNIPAM [Bra+09; Chr+16; Zha+11; Sch+10]. Thus, PNIPAM is a very useful responsive polymer.

PNIPAM as a responsive polymer also plays a role in colloidal science and technology. Colloidal dispersions are governed by their surfaces [BGK03]. Therefore, having the surfaces of colloids be responsive can bring about great changes in the whole colloidal dispersion. As a result, PNIPAM-based colloids

have been envisioned or used in responsive dispersions of many kinds. Below, I provide a few examples of applications of PNIPAM-based colloids.

In mineral processing, precious materials need to be collected from low grade ore. Often, the ore is crushed and then dispersed in water. Two viable methods to separate the minerals from the dispersion are through flotation, or sedimentation. In flotation, mineral particles attach to air bubbles, which subsequently causes the mineral to rise towards the water's surface where it can be collected. To make flotation work, a key step is to attach the minerals to the bubbles. However, minerals are often hydrophilic, while air bubbles are hydrophobic. PNIPAM can play a role in flotation. Burdukova et al. investigated the interactions of adsorbed PNIPAM surfaces [Bur+10]. The PNIPAM can physisorb to hydrophilic surfaces at low temperatures, thus coating the mineral particles. Then, as temperature is a stimulus for PNIPAM, raising the temperature above a certain value renders PNIPAM more hydrophobic. Consequently, at high temperature, the mineral particles become hydrophobic, and will stick to the air bubbles. The collection method that is based on sedimentation also relies on hydrophobicity of PNIPAM at high temperatures. Here, two hydrophobic surfaces attract, causing mineral particles to aggregate. As the minerals aggregate, they sediment, which allows them to be collected. Thus, PNIPAM can play an important role in mineral collection.

A way to introduce responsiveness to colloids was investigated by Puebla et al. The issue they worked on was sensing of dilute analytes in solution. Their method was to use PNIPAM-coated gold nanoparticles to optically sense the analytes. The optical response of just the analytes was not strong enough to detect. The gold nanoparticles enhance the optical field close to the particle. Therefore, for the enhanced field to be effective, the analytes needed to be close to the nanoparticles, which they achieved using the responsive PNIPAM layer. Consequently, the response of PNIPAM to temperature allowed the successful sensing of the analytes [Pue+09]. In a similar fashion, Shamim et al. used magnetic nanoparticles to sense a biological molecule [Sha+07], illustrating that PNIPAM layers can also be applied to magnetic nanoparticles. For both the optically and magnetically active particles, the PNIPAM layer added a responsiveness. Thus, adding a PNIPAM layer can add new responsive functionalities to colloids.

Another potential use of PNIPAM is in medicine. One challenge for medicine is targeting. In many cases, only a very specific part of the body requires the medicine. Hence, it is important to get the medicine to that part of the body

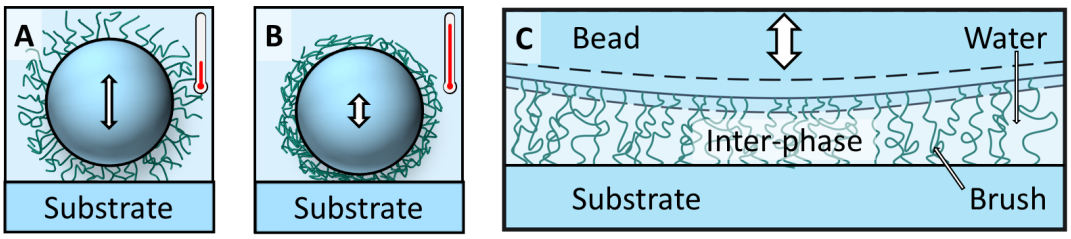

FIGURE 1.1: Cartoon of the brush coating on the bead at **A** low temperature (swollen), and **B** high temperature (collapsed). The light blue background indicates water, while the blue of the bead and the substrate indicates glass. **C** The inter-phase that exists between the bead and the substrate, which contains the polymer brush and water. The motion of the bead is influenced by the inter-phase and its state. Reproduced in part with permission from Langmuir 2019, 35, 48, 15776–15783. Copyright 2019 American Chemical Society.

where the medicine is required. Such targeting can be achieved with PNIPAM. Here, micron-sized hydrogels, called microgels, of cross-linked PNIPAM can be loaded with a medicine [Gil+00; Oh+08; Bv18]. In the collapsed state, the medicine is contained within the microgel. In contrast, in the swollen state the medicine can diffuse out of the microgel into the body. Thus, through knowledge and control of the stimulus for PNIPAM, a medicine can be administered to a specific part of the body.

In many cases, including the examples above, the function of a colloid depends on how it interacts with neighbouring colloids and its surroundings, which is dominated by viscoelastic surface properties. To this end, I investigated small colloidal beads that were coated with a PNIPAM brush at a surface (Fig. 1.1). In the case of PNIPAM, it is easy to imagine that the colloids viscoelastic properties will change when one of its stimuli is triggered, e.g. by an increase of temperature. Specifically, my experiments depended greatly on the small volume between the bead and the substrate that contained the PNIPAM brush, the inter-phase (Fig. 1.1C). Consequently, understanding the viscoelastic response of these coated beads requires understanding the inter-phase.

1.2 PNIPAM inter-phases in literature

How the inter-phase influences the function of the colloid depends on what it consists of. In my experiments, this inter-phase consists of the PNIPAM brush and water. The properties of PNIPAM have been widely studied, and

PNIPAM is most well known for its phase transition that occurs with increasing temperatures. At room temperature, PNIPAM in water is swollen: the water is a good solvent for PNIPAM. However, as the temperature increases above a certain value, PNIPAM collapses: at high temperatures water is a poor solvent. The temperature at which this transition happens is about 32 °C, the lower critical solution temperature (LCST) [HG68; Zhu+91]. This transition at the LCST drastically changes PNIPAM's properties, such as its volume, mechanical properties, optical transmittance, contact angle, or the internal solvent diffusion [HHT87; Sch+98; ZPD95; Sch92; Stu+10; Bal+03; Sui+11].

Besides temperature, another stimulus that stands in the spotlight is the solvent. For example, both pure water and pure ethanol are good solvents, causing PNIPAM to be swollen. However, mixtures of these solvents result in the collapse of PNIPAM [Sch92]. This effect was named co-non-solvency. As with the LCST collapse, solvent mixtures reduce the volume of PNIPAM [Chr+16; Koo+12; Yu+15; Yu+16; Yon+19]. Note, however, that the collapse through solvent is different from the LCST collapse. For example, the response in mechanical properties of PNIPAM differs for different stimuli [Bv18]. It is clear that PNIPAM's response to a stimulus will affect the inter-phase. Since the inter-phase determines the functionality of the colloidal beads, knowing the response to the various stimuli is important.

However, the response of PNIPAM is not fully understood, and sometimes occurs differently. For the temperature collapse, PNIPAM typically collapses as the temperature is increased, yet not always. Zhu and Napper noted that the collapse happened over a surprisingly broad temperature range, and later Shan et al. and other groups observed that PNIPAM collapsed in two stages [ZN94; Sha+04; Wu+07; TZW14]. In these studies, the two-stage collapse was attributed to heterogeneities of the PNIPAM, such as differences in PNIPAM densities. Most of the time, PNIPAM has a single LCST collapse. For applications of PNIPAM, however, the full response to temperature needs to be known, be it a one-stage or a two-stage collapse. Besides the temperature collapse, also the co-non-solvency effect of PNIPAM is not without controversy. Though there is a leading hypothesis for this effect's cause, the response of PNIPAM is not yet completely understood [Kyr+16; Bac+17a; Yon+20]. Hence, to apply responsive PNIPAM coatings to colloids effectively, an investigation of coated beads and their inter-phase and their viscoelastic response to stimuli is needed.

1.3 Techniques to investigate PNIPAM

Investigating responsive polymers can be done with various techniques. One technique that is extensively used is the quartz crystal microbalance (QCM), which can determine changes of viscoelastic properties of thin layers. In QCM, a planar sample layer is attached to a quartz crystal. Viscoelastic properties are determined through monitoring the resonances and dissipations of the crystal. This was be done under various stimuli, e.g. temperature or solvent [IB07; IB10; Hum+16; Mur+16]. Furthermore, scanning probe microscopy (SPM, often called AFM or atomic force microscopy) can be applied to characterise responsive layers, monitoring e.g. elastic properties of the layer. In this technique, a cantilever is used to probe the properties of a surface. In SPM, the force and distance between the cantilever and the surface are measured with great accuracy. From these force-distance data, the elastic modulus of the coating layer can be determined [Che+05; JBJ10; Hel+16]. Often, a sharp tip is attached at the end of the cantilever that allows a high lateral resolution. In this way, also non-isotropic coatings can be measured, for example surfaces coated with PNIPAM microgels. Through SPM, a map of the elastic modulus was thus obtained of PNIPAM microgels [Fer+10; Sch+10].

Measuring coated colloids requires a different approach. An alternative mode of SPM is to attach a colloid to the cantilever instead of a sharp tip. Often, attaching a particle is done with epoxy glue, which can potentially alter the particle. Instead, Humphreys et al. attached an uncoated particle first, and subsequently grew a brush [HWW18]. Hence, they could investigate the actual contact of a coated bead. However, regarding sample preparation, SPM is quite involved, and comparing multiple beads in quick succession in the same circumstances can prove to be a lot of work. Alternatively, spectroscopic or scattering techniques are non-invasive and can characterise both multitudes of coated colloids in dispersion or planar layers. Spectroscopy uses electromagnetic radiation that interacts with the PNIPAM. As the interaction is different for the swollen or collapsed state, the signal will vary. Examples are light or X-ray absorption spectroscopy. Besides spectroscopy, scattering techniques are also applied regularly. Here, X-rays or neutrons interact with the PNIPAM. Because of the PNIPAM layer, the direction of the incident beam is changed slightly. From this, one can distill the thickness and density of the layer. Yet, when measuring multitudes of coated beads, details are potentially obscured, which can only be seen when measuring single beads [WB05]. To measure single particles, one can apply video microscopy. The motion of

particles depends on their properties, e.g. coating thickness or adhesive properties. Tracking of the position of the particle provides information about such properties [WB05; MDT06; Bon+17]. The sampling rate of video microscopy is limited to about a kilohertz [KM15]. Therefore, video microscopy can only be applied to investigate effects or motions that occur at slower rates. This rate can be the limiting factor to measure Brownian motion. Alternatively to video microscopy are a laser-based techniques, which can sample at up to megahertz [LR13]. Laser-based measurements can thus study effects that are both slower and faster.

My experiments are aimed at characterising the inter-phase while changing a certain stimulus like temperature or solvent. Meanwhile, the experimental technique should not interfere with the measurement, and ideally measure single beads. However, experimental techniques that I discussed above leave this experimental niche open. Subsequently, I developed a method to measure and analyse the Brownian motion of single brush-coated beads. Using this method, the viscoelastic response to stimuli of coated beads and their inter-phase can be measured in situ.

1.4 Outline of this thesis

The rest of the thesis is written to answer the questions posed here. In chapter 2, I describe the synthesis of the PNIPAM brush-coated colloids that I used, and a basic characterisation of those in the dry state.

In the following chapter 3, I present the method that I developed and used to measure coated colloids. First in this chapter, I go into some depth about the sample that I measure — a PNIPAM brush-coated glass bead that adhered to a glass substrate — to confirm this situation of the sample and why this is the case. Furthermore, in this chapter I outline the set-up and its physical basis, the method of analysis of the data, and what the results of the analysis tell with regard to the inter-phase and the brush.

In chapter 4, I expose the sample to the first stimulus: temperature. As the title of this chapter hints, here I observed a two-stage collapse. I analyse these observations, and relate those to my hypothesis of what is happening within the inter-phase.

In the next chapter 5, I exposed the sample to heat in a reversed confirmation. In this case, the glass substrate was coated with the PNIPAM brush instead,

while the glass bead was kept bare.

In chapter 6, I investigated the response of the coated bead to an ethanol-water solvent mixture to examine the co-non-solvency effect.

Chapter 7 is included into this thesis because this was the would-be topic of this thesis when I started this PhD in the group of Prof. Butt. In this chapter, I discuss the Debye length of the double-layer force under extreme hydrostatic pressures up to 2.2 kbar. I acknowledge that this chapter is out of the main scope of this thesis about responsive polymer brushes. Nevertheless, I did spend a significant amount of time on this topic. In the end, I did manage to draw a few conclusions about the Debye length at such high pressures.

Finally, I place my results and findings in perspective in the conclusions chapter 8, and answer the questions that are outlined within this introduction.

Chapter 2

Thin Functional Layers: PNIPAM Brushes

Stimuli-responsive coated colloids are relevant and important (see chapter 1). In this chapter I describe how the glass colloids were coated with the PNIPAM brush. Subsequently, I show that the colloids were indeed coated. Furthermore, I describe the characterisation of the colloids and their coating in the dry state. In subsequent chapters I describe the investigation of the responses to stimuli of these coated colloids. Therefore, in this chapter I set out to confirm that the synthesis was successful.

2.1 Synthesis of PNIPAM brushes on colloids

The grafting of the brush onto the beads is described in Van Duinen et al. [vBB19], I partially re-used the text of the publication here. Grafting of PNIPAM brushes was done using atom transfer radical polymerisation (ATRP) by Gunnar Kircher, a technician in our group. The grafting started with functionalising the beads with the initiator. Here, the ATRP initiator 3-(2-bromoisobutyryl)propyl dimethylchlorosilane was used. Before use, the initiator was prepared as described by Bumbu et al. [Bum+04]. The beads that were used had a 5-µm diameter (Duke Standards™ Dry Borosilicate Glass Microspheres, 9005 series 5.4 ± 0.7 µm). First, 300 mg of dry beads was immersed in 15 mL dry toluene (anhydrous, Sigma Aldrich 99.8 %, used without purification). Next, 0.4 mL trimethylamine (Sigma Aldrich 99.8 %, distilled over CaH before use) and 0.2 mL of initiator were added. This mixture was stirred for 24 h under argon atmosphere. After mixing, the beads were allowed to sediment and the solution was decanted. Subsequently, the beads were washed nine times with methanol (Fisher chemical 99.8 %, used without

purification). Finally, the beads were dried in a vacuum oven overnight, and the beads were ready for the polymerisation.

Once the beads were dried, we used ATRP to grow PNIPAM chains on the glass beads. With CuCl, only thin PNIPAM brushes could be obtained. Therefore, CuBr was used as catalyst, instead. The polymerisation with CuBr was faster and less controlled compared to CuCl, as it resulted in a thicker layer with high polydispersity. Then, 0.97 g NIPAM (Sigma Aldrich, recrystallized from Hexane), 9.8 mg CuBr (Sigma Aldrich 98 %), and 8 mL of a DMF/water 1:1 mixture (DMF from Sigma Aldrich 99.8 %, used without purification) were mixed with the initiator-functionalised beads. In this study, all water used was MilliQ-grade (18.2 MΩ · cm). The mixture was degassed by two freeze-thaw cycles. Then, 20 µL Me6TREN (Alfa Aesar 99+ %, used without purification) was added under argon flow. The mixture was degassed by three more freeze-thaw cycles and stirred at 60 °C for 1 h. Afterwards, the beads were allowed to sediment, and the supernatant liquid was removed. Finally, the beads were washed ten times with methanol. For every wash, methanol was added and stirred for a few seconds. After stirring, the beads were left to sediment, and the supernatant methanol was removed. Before the experiments, we dispersed the beads in water.

2.2 Characterisation of the coated colloids

2.2.1 Determination of the dry brush thickness

I used the focused ion beam (FIB) and scanning electron microscope (SEM) to determine the dry thickness of the brush. First, a small droplet of bead dispersion was deposited onto a silicon substrate, which was then allowed to dry. Applying the SEM and FIB techniques raised two challenges: 1) the sample would charge, thereby hindering the techniques, and 2) the FIB can unintentionally damage polymer layers [Bas+12]. To assess challenge 1), the sample surface was made conductive by a platinum coating. To do so, the whole sample was coated with a 10 nm-thick Pt-layer by sputtering. For challenge 2), a thicker Pt-layer was locally deposited (Fig. 2.1A). Depositing of the thicker layer was done by ion-assisted Pt-deposition at a beam voltage of 30 kV and a 1 nA beam current. Thus, locally, a micrometer-thick Pt coating protected the PNIPAM-coated beads from unintended damage.

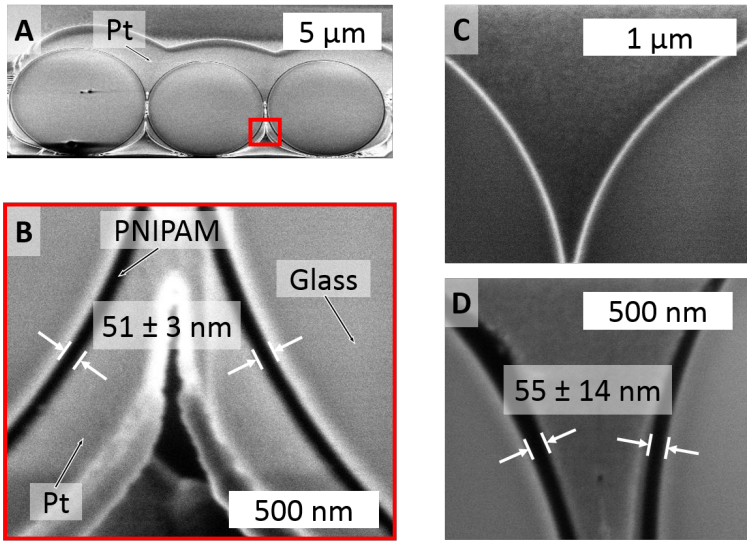

FIGURE 2.1: SEM images of cross-sections of beads. The cross-sections were produced with FIB. **A** Cross-section of three PNIPAM-coated beads and the protective Pt-layer. **B** A zoom-in of the red-rectangle that is showed in A. I attribute the dark layer to PNIPAM. **C** A cross-section of uncoated beads without a dark layer. **D** Leaving the beads dispersed in water did not significantly change the PNIPAM layer thickness. Reproduced in part with permission from Langmuir 2019, 35, 48, 15776–15783. Copyright 2019 American Chemical Society.

The FIB was used to mill-away half of the beads shown in Fig. 2.1A, making the cross-section. For rough milling, a current of 3 nA was used. Passing the beam over a rectangular section removed half of the bead. After many passes, the bead was ultimately completely cut through. Subsequently, the cross-sectional surface was polished with the FIB. Polishing happened carefully at low currents in two steps: first at 0.5 nA and finally at 0.3 nA.

SEM was done to image the smooth cross-sections of the brush-coated beads. Imaging by SEM happened at 2 kV and at a 35° angle (Fig. 2.1). The imaging happened at an angle non-normal to the cross-section surface. This angle was corrected for by scaling the image. To confirm the existence of the PNIPAM brush, I compared the ATRP-treated beads to pristine beads (Fig. 2.1B to Fig. 2.1C, resp.). The beads look different: the treated beads display a dark region around the bead that is not present around the pristine bead. Thus, I attribute the dark region to the PNIPAM brush. The measurements were performed in a vacuum atmosphere, so these images show the brush layer in the dry state. Using the software ImageJ (Version 1.52i), I determined the layer thickness over the bead's perimeter 20 times, providing a mean thickness and a standard deviation. Through this procedure, I measured $L_{\mathrm{dry}} = 51 \pm 3\,\mathrm{nm}$, the mean dry brush thickness.

The influence of water immersion on the brush

I also investigated the effect of prolonged exposure to water on the coated beads. In some cases, dispersing the coated beads in water can degrade the layer. Initially, I used a sonic bath to disperse the dried coated beads in milliQ water. However, I found that the sonic bath degraded the brush layer. While performing the interference experiments (see chapter 3), I found that there was PNIPAM dissolved in the water phase. Consequently, I concluded that the brush layer had degraded and stopped using the sonic bath. Instead, I only used beads that were separated from each other without actively separating. In this study, the beads were left dispersed in water over the course of a day. Therefore, I checked whether water over such a period had an influence on the brush. To do so, I compared two dispersions of the same batch of beads. One of these dispersions was prepared one day prior to the other, which were subsequently exposed to water for one day longer. For the beads that were dispersed in water for one day, I found the mean dry thickness to be $55 \pm 14\,\mathrm{nm}$ (Fig. 2.1D), compared to $51 \pm 3\,\mathrm{nm}$ for the freshly dispersed beads. The differing errors could be caused by a difference in roughness between the

beads, or be an outlier as I measured a low amount of beads. Nonetheless, I found that dispersing the beads in water over the course of one day did not significantly change the dry brush thickness. Thus, I concluded that during the time of the measurements, the PNIPAM brush layer does not degrade.

The PNIPAM layer can be considered a brush

Whether or not the layer can be called a brush depends on the ratio between two layer characteristics: the grafting density and the radius of gyration. First, the grafting density σ, which describes the surface density of the polymer chains that are grafted on the substrate surface. Grafting on the beads did not allow characterisation of the degree of polymerisation. Different from the case of coating of beads, coating on a planar surface did allow this. Hence, to estimate σ for the coated bead, I considered a brush on a planar surface that was synthesised separately (see section 5.1 for more details on the planar brush). The surface functionalisation of the initiator was the same for bead or planar. Therefore, I assume that the σ for the brush on the plane and on the bead were comparable. For the planar coating, unbound PNIPAM chains could be collected, and σ could be determined. In this manner, I estimate that $\sigma = 0.2\,\mathrm{nm}^{-2}$.

Secondly, the radius of gyration determines how much space one chain occupies (Fig. 2.2A). The radius of gyration is [BGK03]:

$$R_\mathrm{g} = \frac{l\sqrt{N}}{\sqrt{6}} \tag{2.1}$$

Here, l is the chain segment length, and N the number of chains per molecule. The planar brush had properties: $L_\mathrm{dry}^\mathrm{planar} = 138\,\mathrm{nm}$ and $N^\mathrm{planar} = 4000$. Consequently, using $L_\mathrm{dry}^\mathrm{bead} = 51\,\mathrm{nm}$, I find that $N^\mathrm{bead} = 1500$. Here, I neglected any curvature effects, since the bead radius is much larger than the brush thickness. Furthermore, I assume l to be about 0.3 nm [KFA90; Plu+06; Yon+20]. With these numbers, I find that $R_\mathrm{g} = 5\,\mathrm{nm}$.

One considers the layer to be a brush when $\sigma \gg \frac{1}{R_\mathrm{g}^2}$ (Fig. 2.2B) [BGK03]. In this case, I find for the beads $0.2\,\mathrm{nm}^{-2} \gg 0.04\,\mathrm{nm}^{-2}$. Hence, I conclude that the PNIPAM coating on the glass beads can indeed be classified as a brush layer.

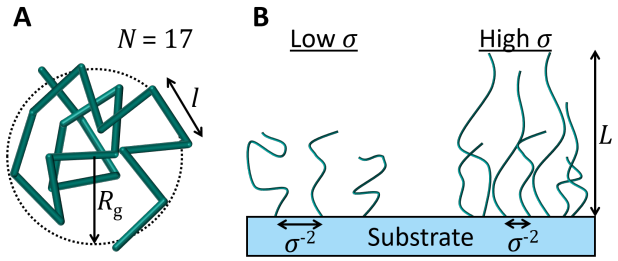

FIGURE 2.2: **A** Sketch showing the properties of a polymer chain in a good solvent. In this example, the polymer is a linear chain consisting of $N = 17$ segments of length l. The chain occupies a sphere with radius R_g. **B** Sketch of end-grafted chains. Reducing the distance between two chains, the polymer layer will be in a brush configuration.

Density of the beads

The cross-section of the one-day bead dispersion showed a peculiarity (Fig. 2.3). One bead displays what seems to be a cavity. Calibration of the bead radius in optical force measurements has been difficult in previous experiments. At the time, this difficulty was attributed to unknown bead density.[1] Such cavities in beads are an explanation for these difficulties.

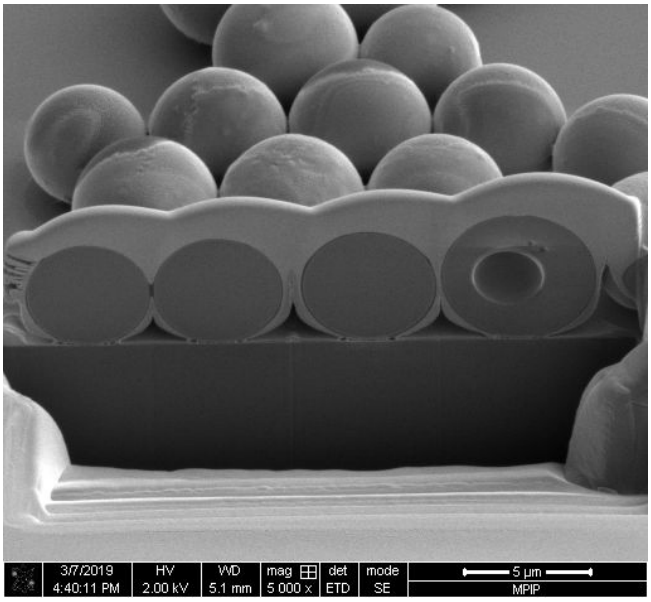

FIGURE 2.3: SEM images of cross-sections of beads that have been dispersed in water over the course of one day.

[1] During the PhD period of Dr. Dominik Pilat [Pil+16], my predecessor. Source: Verbal communication with Dr. Rüdiger Berger.

Chapter 3

Viscoelastic Characterisation by Optical Interference

In many applications, the viscoelastic properties of PNIPAM brushes on colloids play a key role. However, there is no perfect technique to measure such properties in situ. In this chapter, I will outline the method that I developed to monitor these properties of coated beads. As a model sample, I investigated a single bead that was coated with a PNIPAM brush and that stuck to a hydrophilic planar surface. First, we shall confirm that the beads were indeed sticking to the surface and what forces and processes played a role (section 3.1). In this sticky situation, the coated bead exhibited Brownian motion. We shall consider the theory behind such Brownian motion (section 3.2). To measure the Brownian motion, I developed a non-invasive method that can measure the motion of a single bead (section 3.3). Through such measurements, the spectrum of the Brownian motion was determined. The spectral properties were determined by the brush properties (section 3.4).

3.1 Adsorption of beads to a hydrophilic surface

3.1.1 PNIPAM-coated beads are not mobile

The characterisation method that I used was based on the interference of a laser. The focus of this laser was stationary. Furthermore, the measurements involved beads dispersed in water close to a horizontal planar glass surface, which is described further on in section 3.3. Therefore, to properly measure the beads, they had to be stationary. Hence, we must first confirm that the beads are not mobile and stick to the glass surface. Using a microscope, I found that the coated beads that were described in chapter 2 did not move (Fig. 3.1A). In contrast and as an example, beads that were not coated were

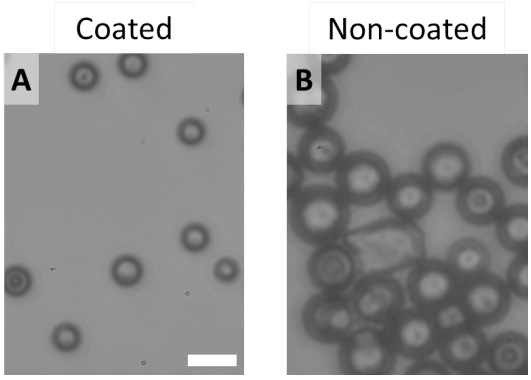

FIGURE 3.1: Microscope image of beads. **A** PNIPAM coated glass beads, 5-µm diameter. The beads stuck to the glass capillary wall and did not move. **B** In contrast, glass beads with an 8-µm diameter. The beads were aggregated, since they were able to move as these did not stick. The white scale bar corresponds to 10 µm. **A** is reproduced in part with permission from Langmuir 2019, 35, 48, 15776–15783. Copyright 2019 American Chemical Society.

able to move freely parallel to the horizontal glass surface. This movement resulted in the beads aggregating at some position (Fig. 3.1B). Thus, I conclude that the PNIPAM-coated beads stuck to the glass surface.

3.1.2 The forces that cause the coated beads to stick

Attractive bridging forces

The bead remained stationary due to attractive forces between the bead and the wall. In this case of the PNIPAM-coated bead on a glass surface, the attraction was caused by nonspecific bridging by the PNIPAM chains. At the one end of the chain at the surface of the bead, the PNIPAM chains were covalently end-grafted. At the other end, at the glass capillary wall, the PNIPAM physisorbed to the surface. Two possible pathways for such physisorption are through hydrogen bonding or Van der Waals interactions [Isr11b]. Two molecular groups specifically play important roles in hydrogen bonding: the hydroxyl groups of the glass surface (—OH), and the amide groups of PNIPAM (—CONH—). Both the oxygen and nitrogen atoms are strongly electronegative, and thus can participate in hydrogen bonds. Subsequently, hydrogen bonds formed between the PNIPAM and glass. Another possible bridging mechanism is through Van der Waals interactions, although Van der Waals interactions are not as strong as a hydrogen bonds. Every molecule has temporary dipoles induced by thermal fluctuations. These temporary dipoles

can cause an induced dipole in another molecule. This interaction between dipoles results in the attractive Van der Waals force.

There exist literature studies on the attractive interactions between PNIPAM brush-coated surfaces and hydrophilic surfaces. The interaction forces involving a PNIPAM brush-coated surface were measured with various methods: a surface force apparatus with a mica surface [Plu+06], a silicon nitride SPM tip [GKB04], or a silica colloidal probe [Mur+16; Hum+19b]. The magnitudes of the forces that these studies found varied greatly. Yet, each of them reported attractive forces, which were attributed to bridging by the PNIPAM brushes.

Repulsive steric forces

The brush also induced forces that opposed the attractive bridging, including steric repulsive forces. The PNIPAM chains were densely grafted to the surface. Because of this high grafting density, the PNIPAM density of the brush layer was very high as well. Such a high density is entropically unfavourable, which lead to an osmotic pressure away from the grafted surface. Due to this osmotic pressure, the chains stretched away from the surface and formed the brush shape. This osmotic pressure is even higher when the brush is compressed, e.g. due to attractive bridging. Thus, there was a repulsive force acting on the bead. When one knows the parameters of the polymer layer, the steric repulsion can be described by the Alexander-de Gennes equation [Ale77; DG87; But+99; Isr11b].

Repulsive electrostatic forces

In addition to the repulsive steric forces, charging of the surfaces may also result in repulsion. In our case, the glass surfaces of the wall and the bead may have dissociated with water, thereby charging the surface. This was likely the case, since the isoelectric point (or point of zero charge) of silica is at acidic conditions. In my experiments, I did not control the pH actively but instead dispersed the beads in pure water. For this reason, it is probable that the pH was above the isoelectric point and the glass was negatively charged. Therefore, I argue that both glass surfaces in the experiments were negatively charged.

The force that results from charged surfaces can be described by the double layer force. Ions that are dissolved in the liquid gather at the charged surface, thereby forming the double layer [BK10; Isr11a]. Gathering of such

ions between two surfaces leads to a high local ion concentration, which is entropically unfavourable. This results in a repulsive osmotic pressure. The range of the repulsion is determined by the Debye length, λ_D [DH23]. The Debye length is determined solely by the liquid, and depends on the concentration of ions in the liquid. In fact, ions shield charges. Thus, a higher ion concentration reduces the Debye length. For pure water, the ions consist of dissociated water ions, hydroxyl and hydronium. The concentration of the dissociated water ions is relatively low, thus resulting in a rather long Debye length. For distilled water, $\lambda_D = 300\,\text{nm}$, which corresponds to an ion concentration of 1 µM [Ste+19]. In case of added electrolytes, the Debye length reduces to 10 nm for a monovalent salt of concentration 0.1 mM [Isr11a].

3.1.3 Remarks on predicting the forces

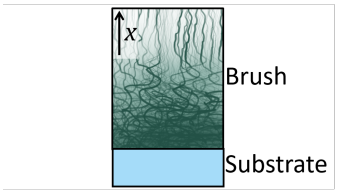

FIGURE 3.2: Sketch of the complex density profile of a PNIPAM brush. The brush density is highest close to its grafting point at the glass wall and reduces with x, away from the surface.

Polymer-mediated forces

There are a few aspects that make it difficult to predict the attractive bridging and the repulsive steric forces. PNIPAM brush layers have a complex density profile: closer to the grafted surface the density is higher than away from the surface (Fig. 3.2 and see also section 4.3) [Bal+03; Yim+05; Plu+06; Koo+12; Mur+16; HWW18; Hum+19a]. Moreover, my experiments featured coated beads that stuck to a surface. It is possible that the wall influenced the polymer density, making it difficult to predict (Fig. 3.3). Yet, both polymer-mediated forces depend on the density of the brush. Furthermore, for the bridging force, the surface of the glass wall is finite. In other words, the surface cannot accommodate endless PNIPAM, leading to additional circumstances that depend on brush compression. In addition, bridging is a dynamic and reversible process. For this reason, studies found multiple relations between force and distance, ranging from a linear to exponential dependence [Isr11b].

An upper limit for the double layer repulsion

In my experiments, I did not explicitly add electrolytes. Nonetheless, it is likely that some dissolved ions are present. These can be remnants from the brush synthesis process, in spite of repetitive rinsing with a good solvent. In these experiments, I did not determine the double layer force. Nevertheless,

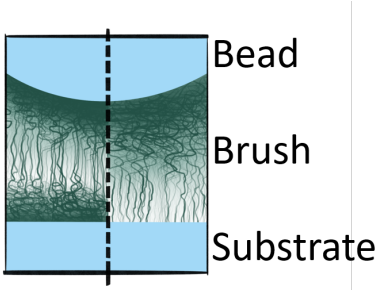

FIGURE 3.3: Two sketches of how the brush could possibly look like. The brush is covalently bound to the bead, and physisorbed on the surface of the glass substrate (the wall). The left side depicts the case where the wall induces a higher polymer density, similar to the covalently bound side at the bead. The right side shows the situation in which the wall does not influence the polymer density. Adapted with permission from Langmuir 2019, 35, 48, 15776–15783. Copyright 2019 American Chemical Society.

something can be said about its upper limit. The surfaces attracted each other, which was caused by bridging of the brush. Such attraction only occurs if the brush is in contact with the glass wall. Thus, we can conclude that the range of electrostatic repulsion is lower than the brush thickness in the swollen state. The dry brush thickness was 51 ± 3 nm, and typical swelling ratios for PNIPAM in water range from 2 to 3 [Chr+16; Yu+15]. Thus, the range of double layer repulsion is shorter than about 100 nm: shorter than the brush layer thickness.

The potential well of the bead

All in all, the uncertainties regarding the inter-phase between bead and wall prevent predicting or calculating the forces. Quantitatively, the relation to distance is exponential for both the repulsive steric and electrostatic forces, and linear for the attractive bridging force in its simplest form [Isr11a; BK10; Isr11b]. The combination of attractive bridging and repulsive forces causes a minimum in the energy landscape normal to the substrate. The bead resides within this energy minimum that is shaped by the inter-phase.

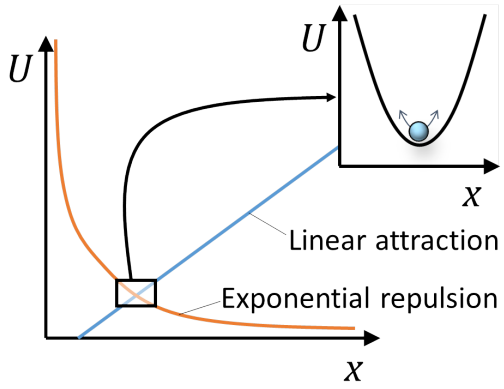

FIGURE 3.4: A sketch indicating the potential landscape of the coated bead that stuck to the capillary wall. With U the potential and x a spatial parameter normal to the surface. The inset shows a harmonic potential.

3.2 Brownian motion of a sticky PNIPAM-coated colloid

Though the beads stuck to the surface, they still wiggled. The collective bombardment by the water molecules caused Brownian motion of the bead. Meanwhile, the bead resides in the potential well. Assuming that the Brownian motion was small, the potential landscape around equilibrium of the bead could be described by a harmonic potential well (Inset Fig. 3.4). Commonly, small motions within a harmonic potential well can be described as a damped harmonic oscillator.

We shall describe the Brownian motion of a bead as a damped harmonic oscillator as Paul Langevin did in 1908 [Lan08; LG97]. The derivation is based on Newton's second law in one dimension: $F = m\frac{d^2x}{dt^2}$. Here, F is the force, m the mass of the bead, and x the dimension of motion that changes with time, t. Note that x is the displacement from equilibrium. The force acting on the bead consists of three terms: a Brownian force, damping due to viscosity, and a harmonic restoring force due to the brush. This results in the following Langevin equation [BSF04]:

$$F_{\text{Brown}}(t) - \beta\frac{dx(t)}{dt} - kx(t) = m\frac{d^2x(t)}{dt^2} \tag{3.1}$$

Here, $F_{\text{Brown}}(t)$ is the random Brownian force, β the damping coefficient, and k the harmonic oscillator spring constant. The Brownian force is described by:

$$F_{\text{Brown}}(t) = (2k_{\text{B}}T\beta)^{1/2}\,\zeta(t) \tag{3.2}$$

Here, $k_{\text{B}}T$ is the thermal energy at absolute temperature T. The variable $\zeta(t)$ is a normalised white-noise process whose average is zero and its value at time t is uncorrelated with any other time t'. In mathematical terms:

$$\langle\zeta(t)\rangle = 0 \quad \text{and} \quad \langle\zeta(t)\cdot\zeta(t')\rangle = \delta(t-t') \tag{3.3}$$

Furthermore, eq. 3.1 can be simplified. The right-hand side term in eq. 3.1 describes the inertia of the system. Inertial effects happen at a time-scale: $\tau_p = m/\beta$ [BSF04; Luk+07]. In my experiments, I measured effects at longer time scales that were significantly longer than τ_p (see e.g. section 3.4). Thus, we can drop the inertia term in eq. 3.1. Furthermore, if we divide by β, we find the following equation that describes the Brownian motion of the bead as an overdamped harmonic oscillator:

$$\frac{dx(t)}{dt} + 2\pi f_k x(t) = (2D)^{1/2}\zeta(t) \tag{3.4}$$

Here, f_k was introduced, which is the cut-off frequency defined as:

$$f_k = \frac{k}{2\pi\beta} \tag{3.5}$$

In addition, D is the diffusion coefficient and is defined by the Stokes-Einstein's equation:

$$D = \frac{k_{\text{B}}T}{\beta} \tag{3.6}$$

One way to describe motion is through the power spectral density (PSD) of the motion. Taking the Fourier transform of eq. 3.4 and using the properties of $\zeta(t)$ provides the PSD of the Brownian motion:

$$\text{PSD}(f) = \frac{D}{2\pi^2\left(f^2 + f_k^2\right)} \tag{3.7}$$

This function has a smooth Lorenztian shape with frequency f, and is the PSD of a trapped bead (Fig. 3.5). The Lorentzian spectrum is characterised by two regimes. At low frequencies, below f_k, the PSD describes a constant plateau.

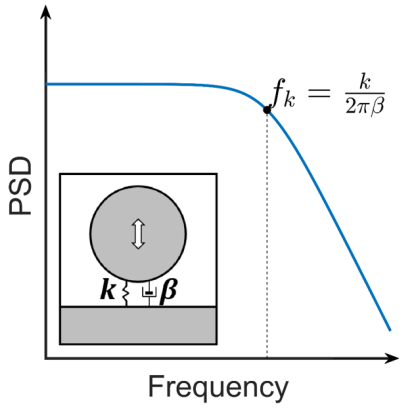

FIGURE 3.5: The theoretical plot of the PSD of an overdamped harmonic oscillator vs. frequency (eq. 3.7). The shape of the PSD is Lorentzian. The cut-off frequency f_k is indicated. Both axes are logarithmic. The inset in the bottom left shows the model that the theory is based on, which consists of a mass that moves up-and-down, a spring, and a damper.

At high frequencies, above f_k, the PSD decreases with $1/f^2$. The model and eq. 3.7 are physically very simple (inset Fig. 3.5). This physical simplicity is one beautiful aspect of this model.

The system that I investigated was overdamped. Hence, there was no resonance. This is in contrast to harmonic oscillator systems that do have a resonance, for example in SPM. The SPM cantilever in air is an underdamped system, which has a sharp resonance peak at a specific frequency. It is also possible to have resonances in cases similar to my experiments, experiments involving micron-sized beads in a fluid [Fra+11]. In these experiments, a bead was trapped in optical tweezers. The authors achieved the resonance by strong trapping, and by suspending the bead in a low-viscosity fluid away from any surfaces. In this manner, they obtained a stiff trap (high k) and reduced damping (low β). As a result, inertial forces did play a role, which resulted in a resonance.[1]

[1] I point out that the inertial effect in those experiments are more complex than described in eq. 3.1. Franosch et al. describe that the inertial effects strongly depend on the inertia of the fluid.

3.3 Method and set-up for measuring Brownian motion

3.3.1 Sample preparation

All beads that I measured were dispersed in water before use. For measuring the Brownian motion, I filled a capillary with bead dispersion (capillary: VitroCom, VitroTubes 5010, borosilicate rectangular glass capillary, nominal inner dimensions of cross-section: $0.1\,\mathrm{mm} \times 1\,\mathrm{mm}$). Filling was done by dipping the capillary in bead dispersion, subsequent capillary forces filled the capillary. Furthermore, I prevented evaporation of the water. Before capillary placement, the ends of the capillary were sealed with a highly viscous paste (Bayer, high-viscosity Baysilone paste). Then I placed the capillary on a microscope sample slide and installed it on a translation stage in the optical set-up.

3.3.2 Optical set-up

The optical set-up included a home-built inverted microscope (Fig. 3.6) [Pil+16]. Typically, a couple of beads are in view (Fig. 3.7A). Using the optical set-up, I adjusted the sample such that one of the beads was in the focus of the microscope objective. The Brownian motion of the bead in the optical focus was then investigated.

In addition to the microscope, the set-up was equipped with a laser (Coherent, Ultra Low Noise, 5 mW, $\lambda = 635\,\mathrm{nm}$, $<0.1\,\%$ RMS at below 10 MHz). The light of this laser was used to investigate the Brownian motion as it was focused onto one bead.

As the laser light propagated upwards, it reflected. There are two surfaces that played a major role in these experiments: the bead's and that of the capillary wall. Let us consider the inter-phase between the bead and wall (Fig. 3.8). Here, the laser light passes three different phases: the glass capillary wall, the PNIPAM brush inter-phase, and finally the glass bead. Each phase has its own different refractive index. Some of the light also reflected off the top surface of the bead. This does not change the measurement for two reasons. First, this reflection is weaker since it is not exactly in the focus of the microscope. Secondly, this only changes a phase shift in the reflected light off the bead, as the distance between top and bottom is constant. All in all, the reflected

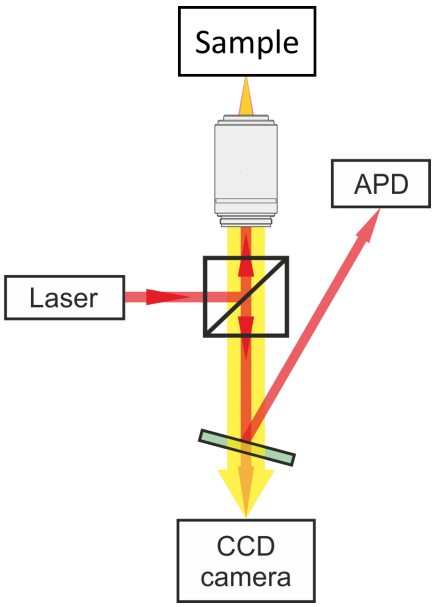

FIGURE 3.6: Schematic of the optical set-up used to detect the Brownian motion. The sample is illuminated from above by focusing white light, which is not shown in this schematic. The yellow arrows correspond to the white microscope light, while the red arrows correspond to the red interference laser. Most of the red light is filtered out before reaching the CCD camera by a tilted Notch filter (shown in green). The red light that was filtered out was detected by the APD. Reproduced in part with permission from Langmuir 2019, 35, 48, 15776–15783. Copyright 2019 American Chemical Society.

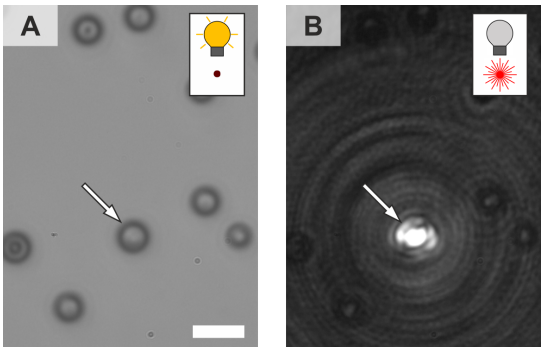

FIGURE 3.7: Microscope images of the beads that were imaged and the interference pattern from the red laser. One bead was selected. The sample was moved such that this bead was in the optical focus, indicated by the white arrow. The white scale bar corresponds to 10 µm. Reproduced in part with permission from Langmuir 2019, 35, 48, 15776–15783. Copyright 2019 American Chemical Society.

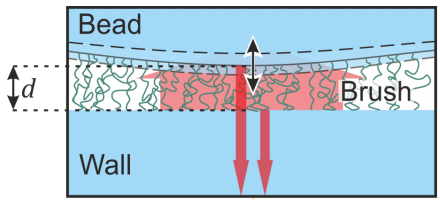

FIGURE 3.8: Schematic that indicates the reflections of the red laser. As the laser is incident from below, it first reflects off the glass capillary wall, and then off the glass bead. Reproduced in part with permission from Langmuir 2019, 35, 48, 15776–15783. Copyright 2019 American Chemical Society.

light originates mainly from two sources: the wall–brush interface, and at the brush–bead interface.

The reflected laser light interfered, as indicated by the rings that are visible in the microscope image (Fig. 3.7B). Let us consider one bead. The total reflected intensity depends on the phase difference between the two reflected light waves. Notably, the phase difference depends on the optical path length difference. In our case, the optical path length difference is twice the distance between the bead and the wall, d, times the refractive index of the brush region. As the bead moves, e.g. due to Brownian motion, d changes. This detection method is based on reflection interference contrast microscopy (RICM), and the reflected intensity, I_{refl}, can be described as follows [LS09; Pil+16]:

$$I_{\text{refl}} = I_{\text{w}} + I_{\text{b}} + 2\sqrt{I_{\text{w}} I_{\text{b}}} \cos\left(\frac{4\pi n_{\text{i}}}{\lambda} d(t) + \varphi\right) \tag{3.8}$$

Here, $I_{\text{w,b}}$ are the reflected intensity off the wall or off the bead, n_{i} the refractive index of the interface brush layer, λ the wavelength of the laser ($\lambda = 635\,\text{nm}$), and φ is a phase shift. In this case, $\varphi = \pi$, as the refractive index of the interface brush layer is lower than that of the glass bead, which causes a half-period phase shift upon reflection. Consequently, the reflected intensity depends on the Brownian motion perpendicular to the capillary wall.

We now have measured I_{refl}, which depends on d. However, we cannot determine $d(t)$ quantitatively. Typically in RICM, one can determine $I_{\text{w,b}}$ while the bead moves over a range that is bigger than wavelength of the laser. In those cases, I_{refl} crosses multiple interference minima and maxima (see chapter 7). In contrast, in this case the brush-coated bead only moved slightly due to Brownian motion: $\Delta d \ll \frac{\lambda}{2n_{\text{i}}}$. Because of this relatively small motion, my experiments did not provide values for $I_{\text{w,b}}$. Thus, rather than analysing the Brownian motion directly, we shall look at I_{refl}, instead.

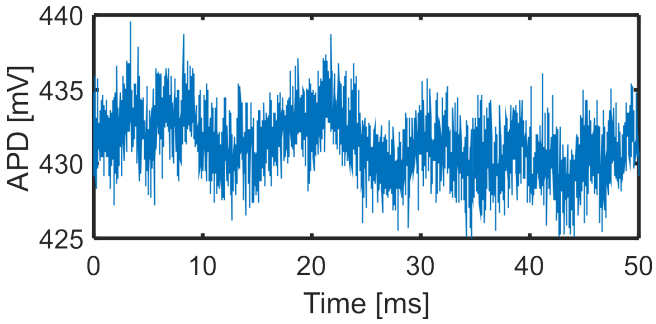

FIGURE 3.9: APD signal, I_{refl}, of a PNIPAM-coated stuck Brownian particle. Reproduced in part with permission from Langmuir 2019, 35, 48, 15776–15783. Copyright 2019 American Chemical Society.

The objective (Nikon CFI TU Plan EPI ELWD 50×) collected the reflected light. Please note that other interfaces, e.g. the top surface of the bead, were out of focus of the microscope objective. Thus, other reflections did not significantly contribute to the reflected light. After passing the objective, most of the laser light was filtered out of the beam by a tilted notch filter (Thorlabs, λ = 633 nm, fwhm = 25 nm). Finally, I_{refl} was recorded by the avalanche photodiode (APD) (Thorlabs, APD130A/M) at a sampling rate of 50 kHz.

3.4 The spectrum of the Brownian motion

To characterise the Brownian motion of a stuck bead, I measured for one minute. The motion is visible at short time-scales (Fig. 3.9). At these timescales, one can see that signal variations occurred over about 10 ms.

A suitable way to analyse the dynamics of the Brownian motion is to look at the signal in frequency space. The timescale of these variations indicates that the dynamics happen at a frequency of about $1/10\,\text{ms} = 100\,\text{Hz}$. To move from time space to frequency space, I took the square of the fast Fourier transform. This was then normalised by the sampling rate (50 kHz) and the number of data points ($60\,\text{s} \cdot 50\,\text{kHz}$). All data analysis was done with Matlab 9.2.0.538062 (version R2017a). In this manner, I computed the PSD of the Brownian motion.

Averaging is required before fitting by a least squares method. One assumption for this method is that each data point is statistically distributed around its average. Therefore, I applied an averaging method before fitting the data. Blocking, an averaging method, is useful to display data with a logarithmic axis [BSF04]. The blocked data has its data points distributed logarithmically.

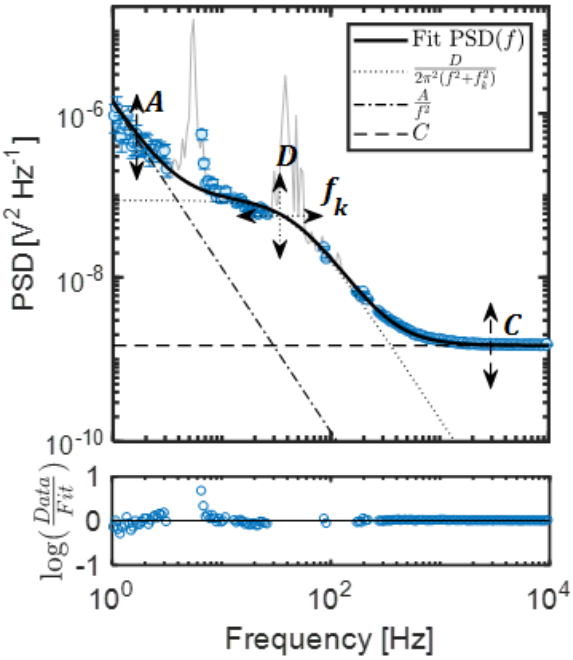

FIGURE 3.10: The PSD of a PNIPAM brush-coated glass bead that sticks to a hydrophilic glass surface (blue circles). Some regions were noise dominated and were disregarded in the fit (solid grey line). I fitted the PSD with eq. 3.9 (solid black line). The individual terms of eq. 3.9 are indicated: dotted, dash-dotted, and dotted lines. The fit parameters (A, D, f_k, and C) and their influence on the shape of the fitted equation are indicated as well. The plot below shows the residuals of the data and the fit as $\log(\frac{Data}{Fit})$. Reproduced in part with permission from Langmuir 2019, 35, 48, 15776–15783. Copyright 2019 American Chemical Society.

In contrast, the original data was distributed linearly. In my experiments, I blocked to 50 data points per frequency decade. To block the data, a number of the original data points were averaged to one blocked data point. Thereby, I used the standard deviation of the averaged data points as the error of the blocked data point. These blocked spectra will be considered in the analysis (Fig. 3.10).

We expect a Lorentzian shape for the PSD of the bead (section 3.2 and Fig. 3.5). This Lorentzian shape is apparent in the measured spectrum (Fig. 3.10 dotted line), with f_k at about 45 Hz. However, eq. 3.7 does not fully describe the measured spectrum. The measured PSD deviates at frequencies one order of magnitude below f_k, and at one order of magnitude above f_k. I attributed low frequency deviation to drifts of the set-up. Such drift caused the laser beam focus to move with respect to the bead. The beam waist was similar

to the bead radius ($2.4 \pm 0.4\,\mu m$ to $2.7 \pm 0.4\,\mu m$, respectively). Since a bead is curved, drift causes a change in I_{refl} as the light hits the bead off-centre, which is visible in the PSD. Furthermore, at high frequencies, the PSD was constant and does not depend on frequency. This frequency regime was defined by white noise in the laser or detection limit of the APD.

To describe these non-Lorentzian contributions, I added two terms to eq. 3.7 (Fig. 3.10 dash-dotted and dashed lines). For the drift I added A/f^2, and for the experimental limits at high frequencies I added C. Thus, we describe the measured PSD with the following function:

$$\mathrm{PSD}(f) = \frac{D}{2\pi^2\left(f^2 + f_k^2\right)} + \frac{A}{f^2} + C \tag{3.9}$$

The measured PSD values vary over a few orders of magnitude (Fig. 3.10). Fitting is based on calculating and minimizing the difference between the measured data and the fitted model, resulting in an overall root mean squared error (RMSE). Therefore, the relative contributions to the RMSE differ for high or low PSD values. However, the high PSD values are equally important as the low PSD values. To make these contribute more similarly to the RMSE, I fitted the logarithmic PSD values, instead.

Eq. 3.9 describes the measured data well (fitted solid line in Fig. 3.10). In particular, each of the fitted parameters is independent. Thus, the model is sensitive to each physical process.

For example, let us consider a measurement in which the drift is stronger. Then, the drift term will move upwards parallel to the y-axis, and a larger value of A will be fitted (dash-dotted line in Fig. 3.10, see also 3.4.2). However, the other contributions, the Lorentzian Brownian term and the experimental limit term, do not change.

The errors of the fitted parameters that I report are based on the 95 % confidence interval of the fit. In this measurement, each of the terms are clearly visible in the spectrum. Therefore, each parameter is well represented in the data, and the errors are small: a few percent of the value.

One other indication that the fit is good, is the residuals-plot (bottom subplot in Fig. 3.10). The residuals are close to zero, although there is a little deviation at frequencies of about 5 Hz. This frequency regime is characterised by the drift term. This deviation could indicate that the model that I used for the

drift, A/f^2, is not perfect. Nonetheless, this model was useful for the purpose of characterising the coated bead.

After all, the physics concerning the brush was visible in another frequency range of about 10 Hz to 300 Hz. In this frequency range, the deviations are small. Thus, this fit describes the Brownian motion of the bead well.

A final indication of a good fit was the root mean squared error (RMSE) value of the fit of 0.0106. An RMSE value of zero means that the model describes the data perfectly, whereas a number of one means that the overall deviation between the data and the model constitutes one decade in the PSD. Thus, the overall deviation is about one hundredth of a decade. Thus, eq. 3.9, which is based on an overdamped harmonic oscillator model and includes drift and noise terms, describes the data well.

3.4.1 Physical interpretation of the fit and its parameters

The most influential parameter is the cut-off frequency

The variable f_k in eq. 3.5 describes the damped harmonic oscillator, and is proportional to k, which corresponds to the steepness of the harmonic oscillator potential. A stiffer spring, high k, leads to a steeper potential well. Thus, in the case of the sticky brush-coated bead, a high value of f_k indicates a stiff brush.

However, f_k also inversely depends on the damping factor β. In this case of a bead that is so close to a substrate, β is dominated by viscous effects. The volume between the brush and the wall contains solvent, which can flow. There are a number of effects that contribute to β. As β describes viscous effects, I start with Stokes' law that describes the drag of a small sphere as it moves through a bulk liquid (Fig. 3.11A):[2]

$$\beta_{\text{Stokes}} = 6\pi\eta_s R \tag{3.10}$$

Here, η_s is the viscosity of the solvent, in this case water, and R is the radius of the bead.

In this case, however, the bead is sticking to a surface: it is not in bulk liquid. As a sphere is close to a surface, the liquid in between cannot move in all

[2] In this case, the Reynolds number is very small. Therefore, the flow is laminar and Stokes' law is valid. The Reynolds number is $N_{\text{Re}} = RU\rho/\eta_s$, with U the velocity of the sphere, and ρ the solvent density.

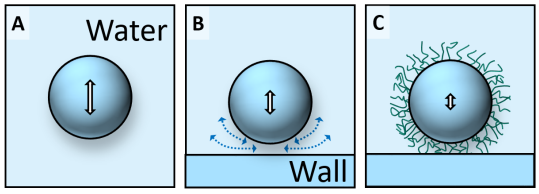

FIGURE 3.11: Sketches of contributions to the damping coefficient, β. In water, the bead experiences Brownian motion, indicated by the double-ended, open arrow. **A** The bead in bulk water with $\beta = \beta_{\text{Stokes}}$, according to Stokes' law. **B** As the bead is close to a wall it restricts water movement. Here β increases by a factor of β_d due to the drainage effect. The dotted arrows indicate the flow of water. **C** The polymer brush layer increases the effective viscosity between the bead and the wall to η_{i}, which increases β even further.

directions, as the sphere and surface will block the liquid in those directions (Fig. 3.11B). This is drainage, and increases the magnitude of β [Lor07; WC76; BK10]. To include the drainage effect, I multiplied eq. 3.10 with a factor, β_d. There is no analytical description of β_d. Nonetheless, it can be approximated fairly well by $\beta_d \approx 1 + R/d$. Thus, as the bead approaches the wall, the damping term will increase, scaling inversely with the intermediate distance, d.

Finally, there is one other relevant factor that influences the damping, namely the brush between the surfaces. The brush hinders the drainage of solvent even further (Fig. 3.11C). Mixtures of polymer and solvent have viscosities values that are manifold the values of just the solvent and scale strongly with polymer concentration [SR99; MSR03; Kam+17]. To include this effect, we replace the viscosity of the solvent, η_{s}, with the viscosity of the polymer-solvent inter-phase, η_{i}, which is not known in most cases. Thus, we end up with a new and more complete description of the damping factor:

$$\beta = 6\pi\eta_{\text{i}} R \beta_d \tag{3.11}$$

As we will look at relative changes of the PNIPAM brush-coated bead, it is practical to write the viscosity relative to the bulk: $\eta_{\text{rel}} = \eta_{\text{i}}/\eta_{\text{s}}$. Consequently, we can also write β as a function of the bulk damping by Stokes' law:

$$\beta = \beta_{\text{Stokes}} \beta_d \eta_{\text{rel}} \tag{3.12}$$

Finally, using eq. 3.12 in eq. 3.5 results in:

$$f_k = \frac{k}{2\pi\beta_{\text{Stokes}}\beta_d\eta_{\text{rel}}} \tag{3.13}$$

In conclusion, more than just the stiffness of the brush defines f_k. Changes in f_k can indicate changes of the polymer-solvent inter-phase, which is determined by the inter-phase thickness and viscosity as well as the polymer stiffness.

Discussion on the diffusion coefficient

The diffusion coefficient, D, describes the mobility of the bead, in principle. However, D cannot be measured accurately. We measure D in "arbitrary units" of $\text{V}^2\,\text{s}^{-1}$, instead of the typical $\text{m}^2\,\text{s}^{-1}$. Typically in optical tweezers applications, one calibrates D by correlating the value found in arbitrary units to the Stokes-Einstein equation, eq. 3.6 [BSF04]. However, using the Stokes-Einstein equation requires accurate knowledge about the environment of the bead. As we can see in eq. 3.12, this environment is dominated by the the polymer brush and the inter-phase, which is exactly what we are interested in and which is unknown. Thus, right now we cannot analyse D to obtain knowledge about the Brownian motion.

However, in principle it is possible to even measure D in useful units. By making a few assumptions about the optical path length in my experiments, we can gain a couple of insights and illustrate the problem. First, an assumption about the distance between the bead and wall, d, which is assumed to be twice the dry thickness: $d = 2d_{\text{dry}} = 102\,\text{nm}$ [Chr+16; Koo+12; Yu+15]. Second, I assume that the refractive index of the inter-phase, n_{i}, is between the index of water, n_{w} (=1.33), and of dry PNIPAM, n_{P} (=1.46 [Koo+12]). Specifically, let us assume that n_{i} depends on the volume fraction of PNIPAM, ϕ (notably not the optical phase shift, φ). When the layer is completely dry ($d = d_{\text{dry}}$) then $\phi = 1$, and when the layer is swollen ($d = 2d_{\text{dry}}$) then $\phi = 0.5$. In this case we assume that $n_{\text{i}} = \frac{1}{2}\left[n_{\text{P}}\phi - n_{\text{w}}(1-\phi)\right] = \frac{1}{2}\left[n_{\text{P}}\frac{51\,\text{nm}}{d} + n_{\text{w}}(1-\frac{51\,\text{nm}}{d})\right]$. With these assumptions combined with the average reflected intensity I_{refl}, we can find a linear relation between I_{w} and I_{b} (eq. 3.8).[3] Therefore, this is an underdetermined problem with one equation and two unknowns, I_{w} and I_{b}. Theoretically, adding a second interference laser with a different wavelength would introduce another equation and hence allow solving this problem. With

[3] Note that I_{w} and I_{b} are similar to I_{max} and I_{min} as found by Pilat et al. [Pil+16]; their use is interchangable [LS09].

the set-up I used, I cannot make any more sensible assumptions, and thus cannot solve this problem quantitatively.

However, using a few options that satisfy the relation between I_w and I_b will give us a possible range for $d(t)$: 2 nm to 15 nm. This leads to values of D, and subsequent η_{rel}. Although the value for η_{rel} can range over two orders of magnitude, I find that it is bigger than one. Thus, we confirm that indeed the viscosity of the polymer inter-phase is higher than that of water.

Pilat et al. used the same set-up to investigate the double layer force acting on non-coated beads of 4 µm radius [Pil+16]. For such experiments, the set-up includes an optical trapping laser that allows measuring force-distance curves (see also chapter 7). In their experiments, the bead travelled micrometers, much more than the wavelength of light, $\lambda = 635$ nm. Therefore, they could measure I_w and I_b, allowing quantitative determination of the range of d. When I apply values I_w that are on the order of this study, I find that η_i is a few ten times bigger than η_{water}, which is in line with other studies ([SR99; MSR03; Kam+17]).

3.4.2 Noises and detection limits

The measured spectra had noisy regions (solid grey lines in Fig. 3.10). These peaks were visible in every measurement, also when no bead was in the optical focus (Fig. 3.12). To find the origin of the peaks, I investigated mechanical vibrations of the optical set-up. The mechanical vibrations of the set-up were logged with an accelerometer over the coarse of one day. This measurement showed that there was significant mechanical noise of the set-up itself. Therefore, we can attribute the noisy regions to mechanical noise of the set-up. Through encasing the set-up with a foam box and disconnecting the lab from the building's ventilation system this noise was reduced. Nonetheless, noise remained. Therefore, this noise was disregarded while fitting with eq. 3.9.

The model also provides values to describe the experimental limits. I allowed the set-up to equilibrate for at least 10 min before measuring. This reduced drift, and was especially required in the experiments that involve heating (e.g. chapter 4). For example, fitting the PSD of two measurements gave $A = 0.09 \pm 0.02\,\mu V\,s^{-2}$ and $A = 1.6 \pm 0.2\,\mu V\,s^{-2}$, for a low and high drift measurement, respectively (Fig. 3.13). Thus, equilibrating can greatly improve a measurement, reducing the effect of drift by orders of magnitude.

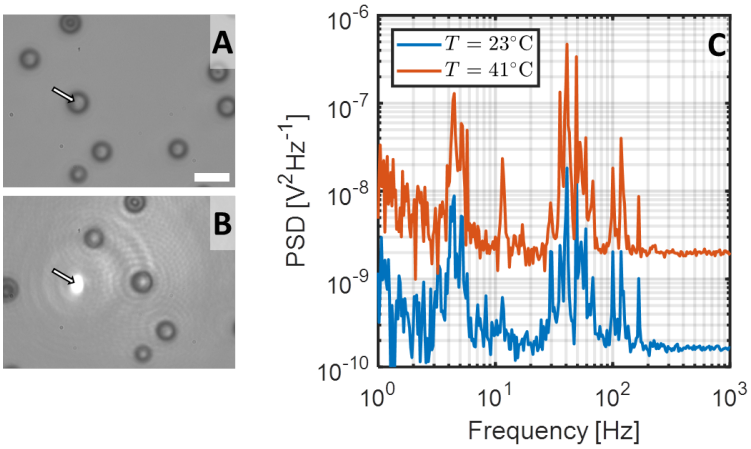

FIGURE 3.12: **A** Microscope image of a set of beads. A bead is in the optical focus, indicated by the arrow. **B** In this microscope image, the sample has been moved a few micron to the right. Here, the interference laser (the white spot at the arrow) is focused on only the planar wall. Therefore, the signal, I_{APD}, was not influenced by any beads. The white scale bar corresponds to 10 µm. **C** PSD of noise in the set-up. To measure the noise, the sample was moved such as in B. Therefore, I only measured the reflection of the wall. The noisy frequencies do not differ significantly at 23 °C and 41 °C. The PSD at 41 °C has been offset by one decade for clarity.

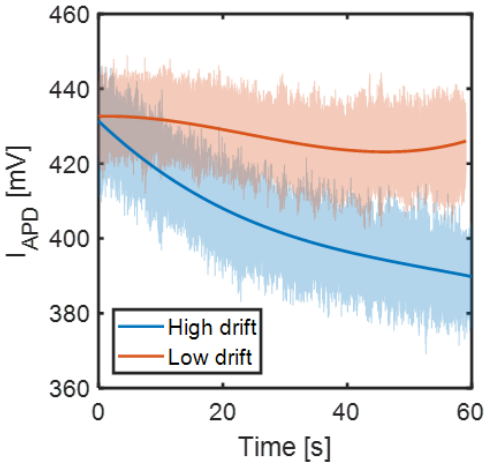

FIGURE 3.13: Two measurements of I_{APD} vs. time. The measurements are taken at 27 °C and 29 °C, both below the LCST. Both the actual data and a line to describe the trend are plotted. A measurement in which drift was low (red), and a measurement with high drift (blue). Only the drift parameter A differs significantly, the other PSD parameters are similar for both measurements.

The parameter C describes the detection limit and describes noise of the laser and the APD. Its magnitude depends on the alignment of the set-up and the incident laser intensity. Therefore, the magnitude varies between experiments.

A requirement, is that the term of the PSD that describes Brownian motion was visible. For the fit to work, this line shape has be be clearly visible (Fig. 3.10). I have also measured coated beads that did not display a clear Lorentzian spectrum. In these cases, either the parameters A or C were too high, or the Lorentzian was too weak. The latter could occur when the Brownian motion was restricted. Such restriction leads to a low diffusion coefficient, D, and thus a low plateau for the Lorentzian. In such instances, little information can be found about the coated bead. Therefore, in the experiments that I present in this thesis, the Lorentzian line shape was visible.

3.5 Summary and conclusion

The Brownian motion of a coated bead at an interface is dominated by the coating. Here, I investigated PNIPAM brush-coated beads at a glass interface. In this case, its Brownian motion was characterised through its spectral properties: the power spectral density (PSD). The main parameter of the PSD that describes the Brownian motion is the cut-off frequency (f_k). This method provides a tool to characterise individual coated colloids. Since the measurement is purely optical, colloids can be analysed without external influence: the method is non-invasive. Hence, this manner of characterisation describes the colloid in situations that are comparable to the actual application in situ. For the case of the PNIPAM-coated bead, this technique can be used to monitor the viscoelastic properties under the influence of a stimuli such as temperature or solvent.

Chapter 4

Two-Stage Thermal Collapse of a PNIPAM-Coated Bead

4.1 Temperature as a stimulus

In the previous chapter we considered the method to describe the viscoelastic properties of the bead-brush-wall system. PNIPAM collapses as the temperature is increased above to its LCST, a phenomena that has been intensively studied. However, some aspects of this response remained unexplained. The two-stage collapse has been reported sometimes, but not always. In this chapter, we explore the the response of PNIPAM to heat.

To increase the temperature, I adapted the sample holder. The microscope slide that held the sample was wrapped with a resistor wire. Then, I heated the sample by passing a current through the wire, the subsequent ohmic resistance increased the temperature. The temperature was determined with a Pt-100 sensor. The sensor measured with an accuracy of $\pm 1\,^{\circ}\mathrm{C}$, and was placed within 1 cm of the laser focus on the sample.

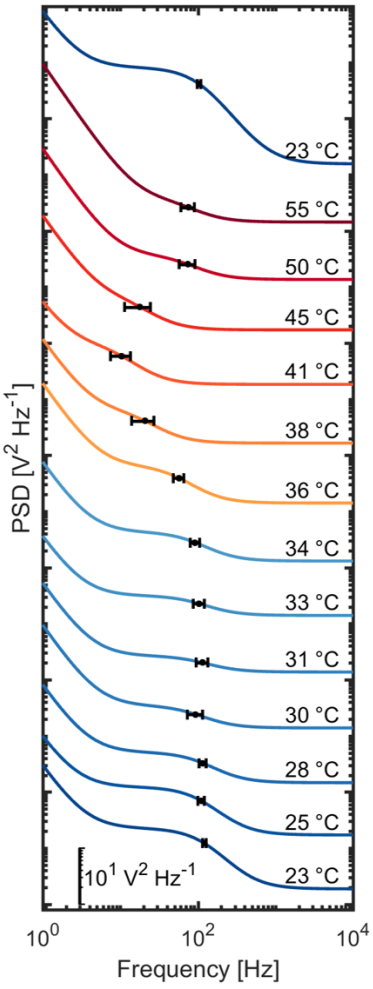

FIGURE 4.1: Fitted PSDs of a PNIPAM-coated bead at a glass wall at different temperatures. The subsequent lines are offset by one decade for clarity. Adapted with permission from Langmuir 2019, 35, 48, 15776–15783. Copyright 2019 American Chemical Society.

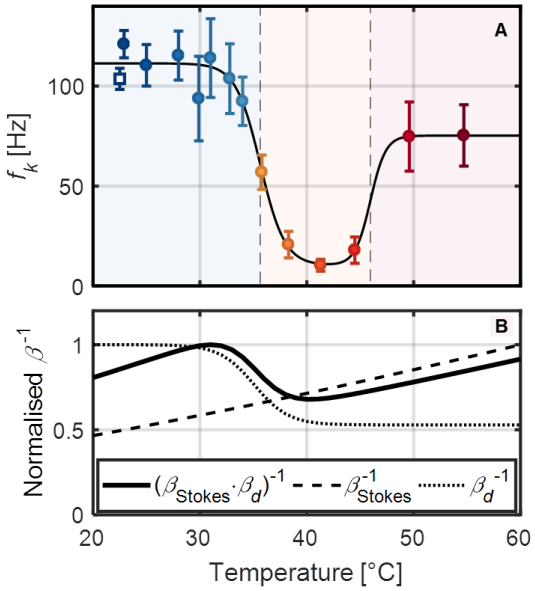

FIGURE 4.2: The influence of temperature on the spectral properties of a PNIPAM-coated bead. **A** The measured cut-off frequency, f_k, derived from the spectra in Fig. 4.1 (in that figure, f_k was indicated in black). The vertical dashed lines are drawn at 36 °C and 46 °C. **B** The normalised prediction of the damping factor (solid line). Also the individual contributions of β_{Stokes}, and β_d are also plotted (dashed and dotted lines, respectively. The x-axes in A and B have the same temperature scale. Reproduced in part with permission from Langmuir 2019, 35, 48, 15776–15783. Copyright 2019 American Chemical Society.

Through this way, I measured I_{APD} for 1 min at various temperatures, typically increasing by steps of 2 °C to 5 °C. Each signal I_{APD} was analysed accordingly (see chapter 3). Subsequently, I obtained the PSD, the power spectral density, at each temperature step (Fig. 4.1). Finally, PSD at each temperature was fitted with eq. 3.9, leading to f_k (Fig. 4.2A).

After measuring the heated sample, I allowed it to cool down overnight. PNIPAM is known for its reversible transition [Stu+10]. This is why I also determined the PSD after the sample had cooled down (top blue line Fig. 4.1). Indeed, both PSDs at 23 °C were similar, before and after heating. Thus, I confirmed that also in my experiments the collapse of the PNIPAM brush was reversible.

Before we look at the changes of f_k with temperature, let us first think about what may change. One effect of temperature is that the viscosity of the solvent, η_s, changes. As temperature increases from 23 °C to 55 °C, η_{water} will decrease

monotonically by about 40 % [LMF16]. η_{water} influences the Brownian motion of the bead through β_{Stokes}, as described by eq. 3.10. Therefore, similarly to η_{water}, also β_{Stokes} decreases monotonically by 40 %.

Furthermore, it is known that as a PNIPAM layer collapses, its volume reduces. The volume can be found to influence two relevant parameters: R, and d (in eqs. 3.10 and 3.11). The first, R, is the sum of the radius of the uncoated bead and the brush thickness. At low temperatures, the brush is swollen. The swollen brush thickness is about twice as thick as the dry thickness, $L_{\text{dry}} = 51 \pm 3\,\text{nm}$ [Chr+16; Yu+15]. The uncoated bead has a radius of $2.7 \pm 0.4\,\mu\text{m}$. Therefore, the radius changed by 2 % as the PNIPAM layer collapsed. This change is too low to be detected with the set-up that I used. Consequently, changes in R will not be considered further. In contrast, the other influence on d is significant. The distance, d, between the bead and the wall is determined by the brush thickness. The drainage factor, β_d, depends inversely on d (eq. 3.11). Therefore, as the brush collapses and d reduces, β_d increases. As the temperature is increased above the LCST, the brush thickness reduces by a factor of two, which happens over a range of 10 °C [Chr+16; Koo+12; Yu+15]. Thus, β_d increases significantly as PNIPAM collapses at the LCST, by a factor of two.

The quantity that we will finally consider is f_k, the cut-off frequency. It depends inversely on the complete damping coefficient, β and its constituents β_{Stokes}, β_d, and η_{rel} (eq. 3.13). Therefore, let us consider the inverse damping coefficients, β^{-1}. Figure 4.2B shows the normalised individual contributions $\beta_{\text{Stokes}}^{-1}$ and β_d^{-1} and their product.

As we made the prediction above that are based on established knowledge, we can now argue that f_k decreases by a predicted factor of 1.4 around the LCST transition. Importantly, we can now attribute changes that exceed the predicted factor to the two other parameters in eq. 3.13: the spring constant k, or the relative viscosity η_{rel}. These two parameters describe the inter-phase between the bead and wall surfaces. Thus, any changes beyond the predicted factor of 1.4 can be associated with k, or η_{rel}, which are the viscoelastic properties of the polymer brush in the inter-phase.

Considering f_k, the bead displayed two transitions (Fig. 4.2A). I characterised these transitions by fitting f_k with a double sigmoid function. Though this function is purely phenomenological, it describes the transition with temperature well. Previously, sigmoid functions were used to describe the collapse of

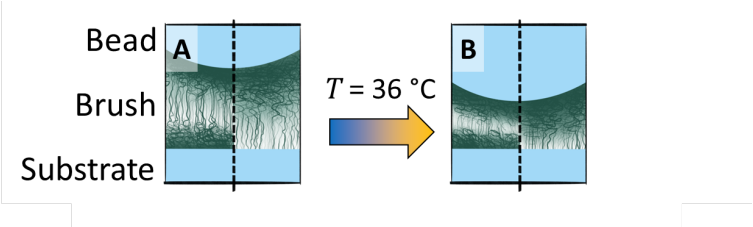

FIGURE 4.3: Sketches of the brush inter-phase for the first transition: at temperatures below (**A**) and above (**B**) 36 °C. The brush is covalently bound to the bead. The left and right parts of the sketches show different possible profiles of the brush, depending on the glass substrate–PNIPAM interaction and adsorption (see section 3.1). Adapted with permission from Langmuir 2019, 35, 48, 15776–15783. Copyright 2019 American Chemical Society.

PNIPAM. The temperature-induced change of brush layer thickness, viscoelastic dissipation, and static contact angle could be described well [Hum+16; Mic+16; Hum+19b]. In my case, the transition temperatures indicate the point of 50 % change. As the temperature increased, at 36 °C, f_k decreased by a factor of 11 over 5 °C. At even higher temperature, 46 °C, f_k increased by a factor of 7 over 5 °C.

The first transition at 36 °C exceeded the predicted factor of 1.4. Therefore, I conclude that the inter-phase viscoelastic properties had changed. I attribute this transition to the LCST collapse of PNIPAM. As PNIPAM collapsed, water was expelled from the inter-phase and the packing density of PNIPAM increased. The density of PNIPAM strongly influenced the effective viscosity. The PNIPAM chains hindered the diffusion of water [IB07], which caused the viscosity to increase. Literature reports that the viscosity increased superlinearly with polymer density [MSR03]. The observed parameter f_k is proportional to k/η_{rel} (eq. 3.13). Thus, considering the observed decrease by a factor of 11 and accounting for the predicted factor of 1.4, the first transition can be explained by an increase of η_{rel} by a factor of 8.

The observation of the decrease of f_k could also be caused by a decrease of the spring constant (eq. 3.13). Remarkably, in contrast to a decrease of the spring constant, previous studies by Ishida and Biggs and Humphreys et al. showed that PNIPAM brushes became stiffer as they collapsed [IB07; IB10; Hum+16]. Nonetheless, by examining the brush layer, this disagreement can be explained. Therefore, we have to consider the properties concerning the spring constant of the brush layer.

In the brush layer, each grafted polymer chain acts as a spring. The number

of chains that contribute depends on the grafting density, σ, and on the part of the brush that connects the bead and the wall, which is the area of contact, A_{contact}. The chains can be added like springs that are in parallel. Hence, the effective spring constant, k, can be written as:

$$k = n_{\text{chains}} k_{\text{chain}} = \sigma A_{\text{contact}} k_{\text{chain}} \tag{4.1}$$

Where k_{chain} is the spring constant of individual chains. Thus, the effective spring constant is proportional to the spring constant of the individual chains.

Because k depends on k_{chain}, we require a way to describe the spring constant of individual chains, k_{chain}. However, we know that the the brush layer was not homogeneous, it displayed a gradient (Fig. 4.3). The gradient brush density profile and the stiffness of the brush changed as temperature increased, in turn influencing the spring constant.

We can describe a single chain using two states: collapsed and swollen. Close to the substrate, the PNIPAM is dense and collapsed. Here, the chains form inter- and intrachain bonds, thereby stiffening the chain. The swollen part of the chain, away from the substrate, is not as stiff. This also implies that one single PNIPAM polymer molecule exists in two states simultaneously (Fig. 4.4). In this simplistic view, the brush has a *local* spring constant that scales with the density. Thus, due to the gradient in density, the brush also has a gradient in spring constant.

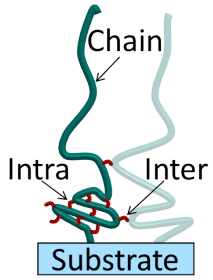

FIGURE 4.4: Examples of inter- and intrachain bonds of an end-grafted PNIPAM molecule.

The constant of one chain, k_{chain}, is a function of the local spring constant. A single spring can be considered as a combination of many spring segments, e.g. PNIPAM monomers, that are in series.

$$\frac{1}{k_{\text{chain}}} = \sum_{i=1}^{n} \frac{1}{k_i} \tag{4.2}$$

Here, n is the total number of segments, each with the local spring constant k_i. In our case, we consider the local state of PNIPAM, and thus k_i can assume two values: k_{swollen}, and $k_{\text{collapsed}}$ (Fig. 4.5AB).

$$\frac{1}{k_{\text{chain}}(x_c)} = \frac{x_c}{k_{\text{collapsed}}} + \frac{1 - x_c}{k_{\text{swollen}}} \tag{4.3}$$

Here, x_c is the fraction of the segments that are collapsed, while the fraction of swollen segments equals $1 - x_c$. Therefore, k_{chain} hardly changes for low x_c, where a large fraction of segments remains swollen (Fig. 4.5C). In contrast, the value of k_{chain} changes strongly for high x, as the collapse is almost complete. Thus, a stiffening of k can only be observed for near-complete collapse of the brush layer.

This model of springs in parallel and in series thus explain the experimental results. At 36 °C, part of the brush collapses, and hence causes the viscosity η_{rel} to increase. Yet, at this first transition, no change of stiffness can be observed. Only as the brush layer collapses completely at 46 °C can an increase of stiffness be observed (Fig. 4.6). Here, f_k increased, and k increased by a factor of 7 (Fig. 4.2). This number agrees well with literature, which reports increasing stiffnesses by about one order of magnitude [Sch+10; Che+05; Bac+17a].

The collapse of PNIPAM only sometimes occurs as a two-stage process. In 1994, Zhu and Napper observed that the collapse of PNIPAM brushes occurred over a surprisingly broad temperature range [ZN94]. Later, Shan et al. observed a two-stage collapse of PNIPAM brushes [Sha+04], which was later confirmed by other groups [Wu+07; TZW14]. These groups attributed these phenomena to heterogeneities in the brush layer (see also section 4.3). The polymer density close to the surface is higher than away from the surface. Therefore, the conditions of the polymer differ. The conditions influence the transition process. Thus, the surface changed the conditions for the PNIPAM, which lead to two distinct transitions.

The surface had another effect on PNIPAM's transition. I observed the first transition at 36 °C. Halperin, Kröger, and Winnik report that demixing temperatures can vary by up to 7 °C [HKW15]. In my experiments, the transition temperature is higher than typically reported values (31 °C to 35 °C). The LCST of PNIPAM can be raised by hydrophilic end groups. Xia, Burke, and Stöver measured the cloud point of PNIPAM chains with different end groups. They found that hydrophilic end groups could raise the LCST. Furthermore, they found that the rise of LCST was stronger for shorter PNIPAM chains. For example, chains with end group $–NH_2$ that had a M_n of 4500 Da had an LCST of 45.3 °C. Likewise, the LCST for longer chains, 16 300 Da, was 34.4 °C. In both cases, the LCST was raised considerably, by a few degrees Celsius. In my experiments, the wall and bead surfaces were glass with hydroxyl groups. Glass is hydrophilic. Therefore, the glass surface raised the LCST. Yet, in my

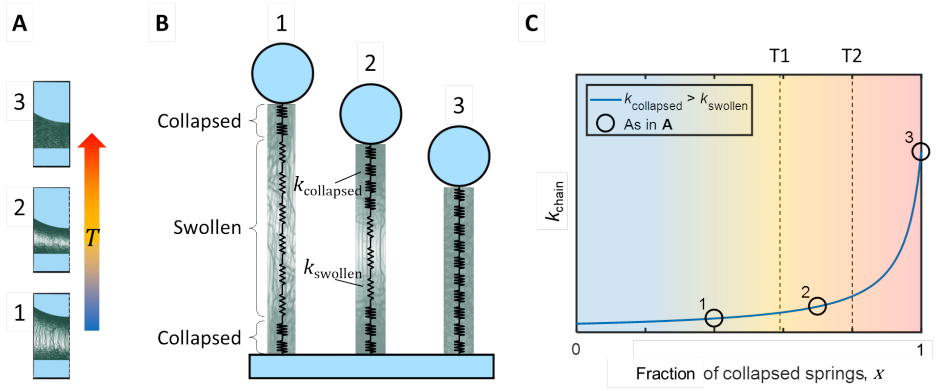

FIGURE 4.5: The spring constant of a single polymer chain can be modelled as a combination of springs in series. In this figure, I chose the case where the brush density profile is symmetric for both glass surfaces (left side of Fig. 4.3A and B). This choice has no influence on the resulting k_{chain}. **A** The sketches of the brush density profile at temperatures (T): 1: below the first transition temperature, 2: in between the two transition temperatures, 3: above the second transition temperature. **B** The spring of one chain can be considered a sum of segments in series, in this example a total of ten segments. Close to the surfaces, the brush layer is collapsed with $k_{collapsed}$. Most of the brush is swollen, with low spring constant, $k_{swollen}$. As the temperature increases above a transition, more spring segments will collapse. In these examples, the number of collapsed spring segments is for 1: four segments; 2: seven segments; 3: all ten segments. **C** A plot of the spring constant, k_{chain} vs. fraction of collapsed springs, x_c (according to eq. 4.3). The examples given (1, 2, 3) are indicated in the plot. As example, the transitions (T1 and T2) could occur at fraction x of 0.6 or 0.8.

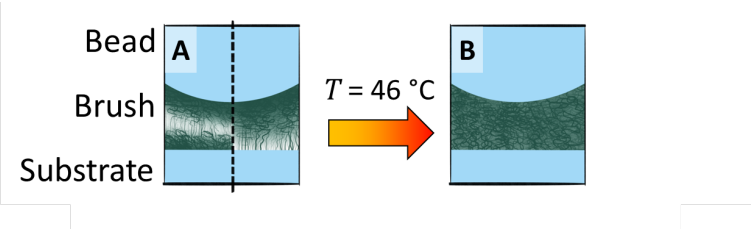

FIGURE 4.6: Sketches of the brush inter-phase for the second transition: at temperatures below (**A**) and above (**B**) 46 °C. The left and right parts of the sketch in A show different possible profiles of the brush. At temperatures above 46 °C the complete brush is collapsed. Therefore, the complete brush is drawn as a homogeneous layer with a uniform density profile. Adapted with permission from Langmuir 2019, 35, 48, 15776–15783. Copyright 2019 American Chemical Society.

experiments, I estimated that M_n was about 170 kDa, which is significantly longer than the chains of Xia, Burke, and Stöver (see section 2.2). It may be that one chain is influenced by multiple hydroxyl groups of the surface, thereby raising the LCST. Thus, I identify the first transition at 36 °C as the LCST transition.

4.2 Viscous damping dominates over other types of damping

Thus far, I have only considered damping caused by viscous effects. However, other forms of damping are possible as well, and thus should be discussed as well. One example is conformational losses from the PNIPAM chain, described by Backes and von Klitzing [Bv18] for cross-linked PNIPAM microgels. They write that conformational losses increase as PNIPAM collapses.

Such losses can be included in my model as well. In order to include these, let us add another damping term, β'_{p}, where the subscript "p" stands for polymer. I added the prime symbol to discern from β that describes viscous losses. The term, β'_{p}, can be added linearly to β in eq. 3.12, because the Brownian motion is small. Adding the polymer-related damping to the viscous damping term (eq. 3.12) results in:

$$\beta = \beta_{\mathrm{viscous}} + \beta'_{\mathrm{p}} = \beta_{\mathrm{Stokes}}\eta_{\mathrm{rel}}\beta_d + \beta'_{\mathrm{p}} \tag{4.4}$$

Previously, β was written relative to bulk value, the Stokes-Einstein drag coefficient, β_{Stokes} (eq. 3.10). The same can be done for these polymer-related losses: $\beta'_{\mathrm{rel}} = \beta'_{\mathrm{p}}/\beta_{\mathrm{Stokes}}$. Using β'_{rel}, we find the following expression for f_k, the observed parameter:

$$f_k = \frac{k}{2\pi\beta_{\mathrm{Stokes}}\left(\eta_{\mathrm{rel}}\beta_d + \beta'_{\mathrm{rel}}\right)} \tag{4.5}$$

The PNIPAM became stiffer because it formed inter-chain physical bonds. I expect these physical bonds to change the damping in a similar fashion to the stiffness. Therefore, I would expect conformational losses to increase at the same time as the stiffness would. Springs add linearly. Dashpots (dampers) add linearly as well. Hence, similar to k, I reason that β'_{rel} also changed with the transition of PNIPAM. Thus, any changes in β'_{rel} will occur at 46 °C.

At the 46 °C transition, f_k increased by a factor of 7. This increase was attributed before to a stiffening of the spring, which corresponded well to existing literature. Therefore, the denominator of the right hand side of eq. 4.5 remained constant. Since β'_{rel} can only increase, this increase could in principle have been compensated by a decrease in η_{rel}. However, we know that η_{rel} did not decrease. Consequently, we can conclude that β'_{rel} was negligible compared to η_{rel}. Hence, the damping term that I used was complete (eqs. 3.12 and 3.13): the dissipations in my measurements were dominated by the viscosity of the inter-phase polymer layer, η_{rel}.

4.3 The complex density profile of PNIPAM

Thus far, I explained some of my experimental observations to the complex density profile of the brush (as Fig. 3.2). In this section, I will discuss this density profile and why it explains the results.

The complex density profile of PNIPAM brushes has been confirmed experimentally. One of the first studies was by Balamurugan et al. in 2003 [Bal+03]. They compared the results of two techniques at different temperatures. First, surface plasmon resonance experiments provided information about the entire brush layer. Second, contact angle experiments provided information about the outermost layer of the brush, since the droplet only interacts with the surface of the brush layer. They observed that changes in the contact angle measurements occurred at a higher temperature than the surface plasmon resonance experiment. Hence, they concluded that the inner layer close to the substrate must change differently from the outer layer. Later, the complex density profile was confirmed by several different experiments: neutron reflection [Yim+05; Mur+16], small angle neutron scattering [Hum+19a], AFM [Plu+06; Mur+16; Hum+19a], ellipsometry [Koo+12], and dissipation-QCM [Mur+16; Hum+19a]. Often, this complex density profile is referred to as vertical phase separation: indicating two distinct phases in the brush.

4.3.1 Theory of vertical phase separation

Just like any other physical process, the reason for the transition of PNIPAM is to minimise its energy. The Gibbs energy of a system is defined as $G = H - TS$, with H the enthalpy, and S the entropy at temperature T. Let us distinguish between two cases: swollen and collapsed. Which case is preferred is determined by the moieties of PNIPAM. The amide moiety is hydrophilic,

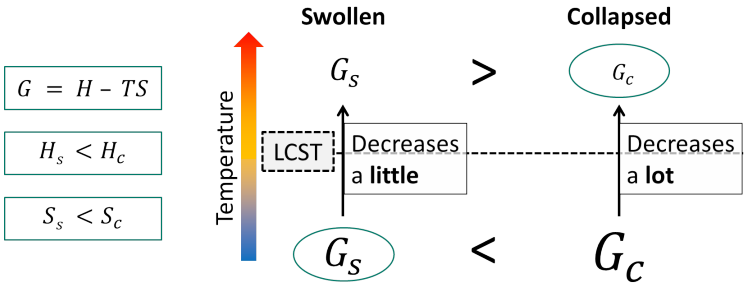

FIGURE 4.7: The Gibbs energy for hydrated and collapsed PNIPAM below and above the LCST. The font size of $G_{s,c}$ corresponds to its magnitude. The stable state is indicated by the ovals.

and participates in hydrogen bonding. These hydrogen bonds can occur with other amide moieties or with water. The enthalpy that corresponds to the swollen state, H_s, is lower than the enthalpy of the collapsed state, H_c [Ahm+09]. The other contribution to G is through entropy. The entropy is governed in a great part by the water molecules surrounding the PNIPAM. Due to the hydrophobic groups, the PNIPAM polymer backbone and the isopropyl moieties, the water molecules are restricted in their orientation. This restriction lowers the entropy. Hence, fewer water molecules are restricted in the collapsed state. Therefore, the entropy of the collapsed state, S_c, is bigger than the hydrated state, S_s. Now, we can define G for the hydrated and collapsed cases:

$$\begin{aligned} \textbf{Swollen:} \quad & G_s = H_s - TS_s \\ \textbf{Collapsed:} \quad & G_c = H_c - TS_c \end{aligned} \tag{4.6}$$

The entropy contribution, $-ST$, lowers G linearly with temperature. At low temperatures, below the LCST, $G_h < G_c$ (Fig. 4.7). Therefore, below the LCST the swollen state of PNIPAM is energetically favourable.

As the temperature increases, both G_s and G_c will decrease. Because $S_s < S_c$, the free energy of the collapsed state, G_c, will decrease more rapidly with temperature than the free energy of the swollen state, G_s. Above $T =$ LCST, the collapsed state is preferred, as $G_s > G_c$. Therefore, above the LCST the collapsed state of PNIPAM is preferred.

There is a different way, based on the same principles of minimising energy. The collapse of PNIPAM can also be explained through a phase diagram

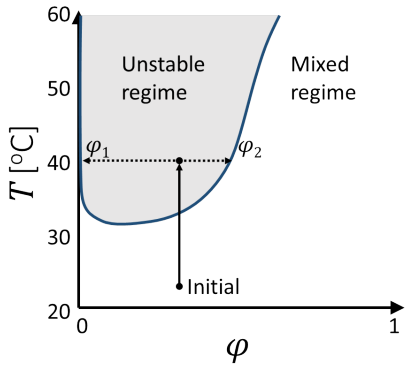

FIGURE 4.8: The phase diagram (T vs. ϕ) of PNIPAM, data taken from Heskins and Guillet [HG68]. The solid arrow indicates heating, the dashed arrows indicate phase separation.

of PNIPAM (Fig. 4.8)[1]. Let us consider the collapse of PNIPAM, where we start with the initial state at room temperature at some polymer volume fraction, ϕ that is in the mixed regime. This initial state is in the mixed regime: PNIPAM and water are mixed, thus PNIPAM is swollen. As the temperature is increased to 40 °C the system crosses past the system's spinodal into the unstable regime [HKW15]. Therefore, the system will phase separate into two phases: a water-rich (ϕ_1) and a polymer-rich (ϕ_2) phase.

At the basis of the phase diagram lies the polymer-solvent interaction parameter. This is the Flory parameter $\chi(T)$, which can describe a type I transition [HKW15]. Similarly to eq. 4.6, $\chi(T)$ depends on the temperature and describes the entropy term. However, with only the T-dependence, $\chi(T)$ cannot describe the vertical phase separation. To this end, an additional dependence on ϕ, the polymer volume fraction, is required. The new interaction parameter $\chi(\phi, T)$ describes a type II phase separation.

Often, $\chi(\phi, T)$ is described phenomenologically, where some expansion of χ describes the experimental results [HKW15]. De Gennes proposed a physical model instead [DG91]. De Gennes called it the n-cluster model, which has at times been used by groups to explain their observations [ZN96; Plu+06; HKW15; Mur+16].[2] The n-cluster model poses that clusters of monomers

[1] Note that measurements of the phase diagram of PNIPAM vary significantly [HKW15]. No systematic reason has been found for these differences. Heskins and Guillet were the first to describe the phase diagram of PNIPAM [HG68]. Therefore, I chose to show their data in Fig. 4.8.

[2] I note that in their review in 2015, Halperin, Kröger, and Winnik write: "To our knowledge the n-cluster model was never utilized to fit PNIPAM phase diagrams" [HKW15]. Yet, the authors fail to give a reason for this.

form when ϕ is high, thus leading to the ϕ dependency. The clusters consist of more than two monomers, $n > 2$, hence the name n-cluster. This model also predicts the vertical phase separation. Nonetheless, it has not been undeniably confirmed that the phase transition of PNIPAM happens in such a way, as a type II phase separation. Yet, the interaction parameter and phase diagram lay at the basis of data analysis and simulation models of different PNIPAM arrangements [Yim+05; HD09; Sch+10; HKW15; MK17].

My experiments showed the two-stage collapse of a PNIPAM brush layer, for which vertical phase separation is a requirement. Thus, my experiments added to the indications that the interaction parameter depends on ϕ as well as T, leading to type II phase separation with corresponding vertical phase separation.

4.4 Other considerations

4.4.1 Molecular interaction between PNIPAM and water

The affinity between PNIPAM and water played a role in my experiments. Many studies reported on the switch from hydrophilic to hydrophobic properties of PNIPAM-coated surfaces, often based on contact angle measurements. However, Pelton argued against that interpretation [Pel10]. Aptly titled "*Poly(N-isopropylacrylamide) (PNIPAM) is never hydrophobic*", he argued that PNIPAM is both hydrophobic and hydrophilic, independent of the temperature. Later, Tavagnacco, Zaccarelli, and Chiessi did atomistic molecular dynamics simulations on the thermal collapse of PNIPAM in water [TZC18]. Specifically, they investigated the hydration of PNIPAM. One finding was that upon collapse only about 14 % of the bonds between PNIPAM and water are lost. Hence, the interaction between water and PNIPAM only reduces slightly. In my experiments, I showed that η_{rel} increased, which I attributed to the increase of the density of PNIPAM. In contrast, in the hypothetical case that PNIPAM became hydrophobic upon collapse, the viscosity of the brush layer inter-phase (η_{rel}) should have decreased. Therefore, my experiments support the view that the affinity between PNIPAM and water does not significantly change upon collapse, and PNIPAM does not become hydrophobic.

4.4.2 Softening of PNIPAM microgels

Findings on one arrangement of PNIPAM deserves a mention in this thesis, namely microgels. Compared to the planar (2D) brushes, microgels are cross-linked 3D gels with colloidal size. Hirotsu investigated the mechanical modulus of a PNIPAM macrogel [Hir91]. Later, a number of groups report similar findings on the mechanical moduli of PNIPAM microgels [HD09; SM+11; Vou+13; Rov+19]. These studies found that the Poisson ratio has a minimum at the LCST. Moreover, this is caused by a minimum in the bulk modulus, a softening of PNIPAM.

I attributed the observed decrease of f_k at 36 °C to an increase of the viscous damping. Yet, this observation could also be the result of a softening of PNIPAM. Hence, the softening of the previously mentioned studies does appear similar to what I observed. Therefore, for completeness it is worthwhile to have a look at their analysis and discussion.

The groups used Flory-Rehner theory to describe the softening that they observed. In this theory, the moduli of a gel are described. The model is based on the balance between osmotic pressure of polymer-solvent affinity and elastic pressure from the gel network [RC+03; SM+11]. Factors such as cross-linking density, polymer-solvent interaction (χ), and polymer volume fraction (ϕ) play a role. It is the dependency of the bulk modulus on χ and ϕ that causes the softening.

However, not all groups that investigated PNIPAM gels and microgels find this softening at the LCST [Che+05; Sch+10; Fer+10; Bac+17b; Bac+17a]. Regardless of the softening, the literature studies agree that the modulus increases by about one order of magnitude as T is increased from below to above the LCST.

PNIPAM brushes and microgels are fundamentally different. First, microgels are cross-linked gels, whereas a brush is not. Second, their arrangement is very different. A microgel is a 3D spherical object. As such, it has a defined Poisson ratio and bulk modulus. Defining these parameters for a brush is doubtful. After all, a brush is an object on a surface. The brush can only expand in one dimension due to this hard surface. The Flory-Rehner theory was developed for gels that can swell in all dimensions. Using the same Flory-Rehner theory for brushes is not possible. Thus, there are significant differences between PNIPAM microgels and brushes. In addition, not all

T [C]	D [V^2/s]	err	f_k [Hz]	err2	A [V^2/s]	err3	C [V^2/Hz]	err4	RMSE [log(V^2/s)]	adj. R^2
22.9	5.94E-04	3.99E-05	1.21E+02	6.82E+00	2.80E-08	4.35E-09	1.88E-10	1.74E-12	1.16E-02	0.989
25.0	2.52E-04	3.34E-05	1.10E+02	1.04E+01	8.74E-09	2.17E-09	1.72E-10	2.14E-12	1.58E-02	0.963
28.0	9.45E-05	1.58E-05	1.15E+02	1.23E+01	7.70E-09	1.13E-09	1.47E-10	1.30E-12	1.14E-02	0.967
29.9	3.55E-05	1.35E-05	9.38E+01	2.11E+01	9.13E-09	1.57E-09	1.39E-10	1.57E-12	1.48E-02	0.936
31.0	3.28E-05	9.69E-06	1.14E+02	1.97E+01	5.05E-09	5.82E-10	1.37E-10	9.93E-13	9.36E-03	0.960
32.8	3.69E-05	1.07E-05	1.04E+02	1.74E+01	3.34E-09	5.06E-10	1.40E-10	1.16E-12	1.08E-02	0.942
34.0	4.97E-05	1.08E-05	9.24E+01	1.21E+01	7.20E-09	1.05E-09	1.31E-10	1.16E-12	1.16E-02	0.964
35.8	3.15E-05	7.80E-06	5.69E+01	8.62E+00	1.85E-08	2.45E-09	1.41E-10	1.24E-12	1.16E-02	0.977
38.3	3.71E-06	1.53E-06	2.07E+01	6.62E+00	1.11E-08	1.59E-09	1.65E-10	1.28E-12	1.05E-02	0.969
41.3	1.54E-06	4.09E-07	1.04E+01	2.99E+00	4.60E-09	1.17E-09	1.84E-10	1.48E-12	1.10E-02	0.950
44.5	2.69E-06	1.15E-06	1.80E+01	6.62E+00	1.82E-08	2.37E-09	1.72E-10	1.31E-12	1.03E-02	0.975
49.6	2.46E-05	9.19E-06	7.48E+01	1.73E+01	2.88E-08	3.61E-09	1.36E-10	1.31E-12	1.27E-02	0.972
54.7	2.27E-05	6.42E-06	7.53E+01	1.53E+01	9.44E-08	6.71E-09	1.43E-10	9.10E-13	8.32E-03	0.993
22.5	1.69E-03	7.71E-05	1.04E+02	5.29E+00	7.42E-08	1.47E-08	1.56E-10	1.77E-12	1.37E-02	0.994

TABLE 4.1: Fitted PSD parameters (eq. 3.9) while heating a PNIPAM brush-coated bead. The columns labelled "err" indicate the errors of the previous columns, and are the 95 % confidence interval values from the fit. From [vBB19].

studies report the softening. Therefore, I do not attribute my observations to softening of the brush.

4.4.3 The quality of the PSD fits and the other parameters

Before, I focused on f_k, which is the most important parameter. Here, I will discuss the other fit parameters, D, A, and C. These fit parameters were discussed in chapter 3. As I discussed before, D does hold potential. It can describe the diffusion coefficient of the stuck coated bead. However, right now it is influenced by parameters that are unknown, for example the reflected intensity that changes as the brush layer collapses. Therefore, we cannot draw any conclusions about the collapse that are based on D and discussing how it changes with T would be futile.

The fit parameter A describes the set-up drift and is not involved with the Brownian motion. Since this experiment involved heating, and materials expand, it is not unlikely that A changed. Its value did change from measurement-to-measurement. Yet, no trend can be observed with T (table 4.1). Therefore, I conclude that set-up drift due to heating was prevented by equilibrating the system.

The last fit parameter, C, describes the limit of detection of the set-up. It describes laser noise or noise in the APD detector, for example. The magnitude of C changed from experiment-to-experiment (compare e.g. Fig. 3.10 to table 4.1). I attribute this difference to alignment of the set-up. These data were taken at different days. It is likely that the optical alignment on these days differed.

Moreover, I did not observe a significant trend in C with temperature or the transitions at 36 °C and 46 °C (table 4.1). Thus, though it is likely that the refractive index of the brush changed as it collapsed, this had no significant influence on the detection limits of the set-up.

One indication for the quality of the fit can be found in two values, the RMSE and the adjusted R-squared value (adj. R^2).[3] The RMSE describes the error between fit and data points. In my case, I fitted the logarithm of the data (section 3.2). Therefore, the unit of RMSE is $\log(V^2\,s^{-1})$. A value of 1 means that the RMSE value between data and fit is one decade, whereas the hypothetical value of 0 describes a perfect match between data and fit. The other value, adj. R^2, describes the quality in a range of 0 to 1. Here, a value of 1 describes a perfect fit that describes the data completely. Note that data has variance, thus a value of 1 is not feasible. For my experiments, the RMSE value is roughly 0.01 decade, which indicates a good fit. Also adj. R^2 values are consistently close to 1. Furthermore, both values are independent of T. Naturally, having a weak Brownian signal, or high noise levels will lead to high errors in f_k. For the fit with eq. 3.9 to work, the signal magnitude of the Brownian motion should not be exceeded by A and C. In the experiments that involved heating, the errors of f_k ranged between 5 % to 30 %, depending on the clarity of the Brownian motion signal. Therefore, although the Brownian motion signal was less clear at high temperature, it lead to an error of 30 % (Fig. 4.1). This error still allowed the analysis of the collapse of the PNIPAM brush with sufficient significance.

4.5 Summary and conclusion

For the method I applied the formalism of Berg-Sørensen and Flyvbjerg, which was developed for optical tweezers calibration [BSF04]. This formalism was tailored to my experiments to study the Brownian motion of coated particles at an interface. My results show that the method is well suited to characterise single particles at different temperatures. Furthermore, the technique is unique in that it is non-invasive, easy to use and it allows comparing multiple beads in quick succession. Therefore, this method complements other techniques and fills a unique niche in that it can easily monitor the surface viscoelastic properties of single beads.

[3] The adj. R^2-value is adjusted for the degrees of freedom, the number of data points minus number of fit parameters.

Through this method, I measured the Brownian motion of a single PNIPAM brush-coated bead situated on a hydrophilic glass surface. I found that the state of the PNIPAM determined this Brownian motion. The PSD, characterised by the cut-off frequency f_k, changed with temperature. I observed a two-stage collapse in the viscoelastic properties of PNIPAM brushes. With increasing temperature, I first observed a decrease of f_k at 36 °C, and then an increase at 46 °C. The first transition was interpreted as an increase of the viscosity of the inter-phase and η_{rel}, which I identified as the LCST of PNIPAM. I also concluded that viscous losses dominated over other types of losses, for example conformational losses. The second transition was interpreted as the complete collapse of the PNIPAM layer and subsequent stiffening of the contact. The fact that there were two transitions indicates that the brush within the inter-phase consisted of two phases with distinct polymer densities. Furthermore, the two transitions indicate a type II transition, as mentioned in the review by Halperin, Kröger, and Winnik [HKW15].

Chapter 5

Temperature Collapse of a Planar PNIPAM Brush

Planar responsive polymer layers gather much interest and are suitable for many applications [Stu+10]. With the method that I developed, bare beads can be used to probe planar layers, much in the same way as described in chapter 3. In the following chapter, I describe a PNIPAM brush on a planar surface. More specifically, I investigate the temperature collapse of such brushes.

5.1 Synthesis and characterisation of the brush

5.1.1 Brush synthesis on a planar surface

The PNIPAM brush synthesis was done by Gunnar Kircher, here I describe the protocoll to make these. To clean and coat the glass slides (VWR®, VistaVision cover glass No. 1 thickness, borosilicate), they were placed in a Teflon holder. First, the slides were rinsed with dichloromethane and then allowed to dry. Then, the slides were immersed in a mixture of 4 mL hydrogen peroxide (25 %), 4 mL of 25 % ammonia solution, and 50 mL of milliQ water. In this manner, the slides were cleaned for 20 min at 80 °C. Afterwards, the slides were rinsed thoroughly, first with milliQ water, secondly with ethanol, and finally dried.

Before growing the PNIPAM brush, the slides were functionalised with the initiator for ATRP. The Teflon holder with the slides was placed in a specially designed Schlenck flask as described in [Bum+04]. The synthesis was similar to the brush on the bead as described in chapter 2). Before use, the trimethylamine was distilled over CaH. For functionalisation, the slides were immersed

in a mixture of 28 mL dry toluene (anhydrous, Sigma Aldrich 99.8 %, used without purification), 0.4 mL trimethylamine (Sigma Aldrich 99.8 %), and 0.2 mL of the initiator 3-(2-bromoisobutyryl)-propyl-dimethylchlorosilane. This mixture was stirred overnight under argon atmosphere at room temperature. Afterwards, the holder with the slides was removed from the solution and rinsed with dicholomethane, then washed for 2 h in a Soxhlet extractor that was filled with dichloromethane, and finally dried.

The brush on the slides was grown by surface-initiated ATRP, a grafting-from method as described in [Bra+09]. The slides in the Teflon holder were placed in a Schlenck flask. Subsequently, 2.72 g of NIPAM monomer (Sigma Aldrich, recrystallized from Hexane), and 19 mg of the ATRP catalyst CuCl were added. The flask was then evacuated and flushed with argon gas. Then, a 28 mL 1:1 mixture of degassed DMF and water (DMF from Sigma Aldrich 99.8 %, used without purification), 56 µL Me6TREN (tris(2-dimethylaminoethyl)amine, Alfa Aesar 99+ %, used without purification), and 22 µL of sacrificial initiator methyl-2-chloropropionate were added. The mixture was then carefully degassed by three freeze-pump-thaw cycles. Brushes were thus polymerised by stirring the mixture for 45 min at room temperature. Afterwards, the holder and slide were removed and rinsed with methanol (Fisher chemical 99.8 %, used without purification). Finally, the holder and slides were placed in a Soxhlet extractor and filled with methanol to be washed overnight. This resulted in a clean PNIPAM layer on a glass substrate.

5.1.2 Gel permeation chromatography

During synthesis of the planar brush, also some free dissolved initiator was polymerised to obtain some free linear PNIPAM. Therefore, after removing the holder and slide, there was similarly grown PNIPAM, which allowed gel permeation chromatography (GPC) characterisation. Here, the permeation of the PNIPAM through a gel phase is compared to the permeation of a known polymer, in this case polystyrene. In such a way, we found that the brush has a molecular weight, $M_n = 460\,\mathrm{kg\,mol^{-1}}$ and has a polydispersity index of 2.5. Using the molar mass of the monomer ($M_{\mathrm{PNIPAM}} = 113.16\,\mathrm{g\,mol^{-1}}$), this corresponds to about $N = 4000$.

5.1.3 Thickness of the dry layer

The thickness of the PNIPAM layer, L_{dry} was obtained using a profilometer (Stylus Profiler P-7, KLA-Tencor). First, I scratched the PNIPAM surface with a needle, thereby removing the brush layer locally and revealing the hard glass surface. Subsequently, I measured a profile perpendicular to the scratch direction. From the profile, the difference between high and low indicated the height of the dry brush. During these measurements, the relative humidity was 20.0 % and the temperature was 21.5 °C. Three different profiles at different places along the PNIPAM-coated surface were obtained. In this manner, I found the dry brush thickness $L_{\text{dry}} = 138 \pm 1\,\text{nm}$. The error is the standard deviation of the three measurements. This error is low, indicating a uniform brush layer along the glass slide.

5.1.4 Grafting density and classification of the layer as brush

To confirm that the polymer layer was indeed a brush layer, I calculated the grafting density. The grafting density, σ, is the number of chains per unit area and is given by [Chr+16]:

$$\sigma = \frac{L_{\text{dry}} \cdot N_{\text{A}} \cdot \rho}{M_n} \tag{5.1}$$

Here, L_{dry} is the dry thickness, N_{A} is the Avogadro constant, ρ is the polymer density (I used $\rho = 1118\,\text{kg}\,\text{m}^{-3}$ [Sch92]), and M_n is the molecular weight. Hence, I find that σ was on the order of $0.2\,\text{nm}^{-2}$.

To classify the layer as a brush, we need to compare σ to the radius of gyration of the polymer (R_{g}). A layer is a brush if the following condition is met (see chapter 2):

$$\sigma \gg \frac{1}{R_{\text{g}}^2} \tag{5.2}$$

Using the definition for R_{g} (eq. 2.1) and the earlier result $N = 4000$, we find that $R_{\text{g}} = 8\,\text{nm}$. Consequently, I find $0.2\,\text{nm}^{-2} \gg 0.02\,\text{nm}^{-2}$. Therefore, the condition of eq. 5.2 was fulfilled, and we can conclude that the planar PNIPAM layer was indeed a brush.

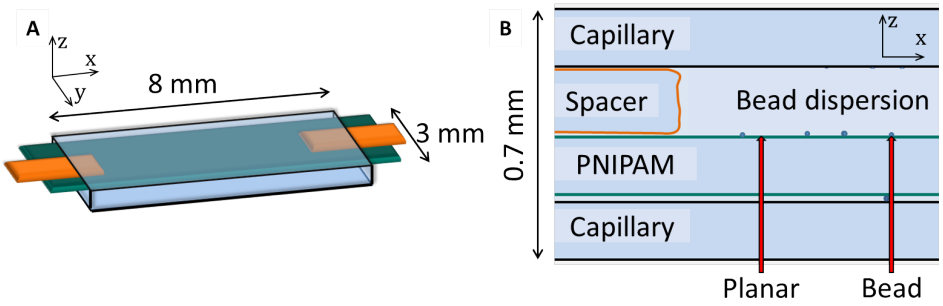

FIGURE 5.1: Sketch of the capillary containing the planar PNIPAM brush slide. **A** The side and top view of the capillary. **B** A cross-section along the long axis (x) of the capillary. The capillary has black-colored edges, the PNIPAM-coated slide has teal edges, and the spacer has orange edges. A few beads are also indicated. The dimensions that are given are approximate. The red arrows indicate the interference laser. This laser is focused on the PNIPAM-water interface. Furthermore, it can be directed on a bead or not, thus measuring just the planar PNIPAM or the planar PNIPAM-bead interaction.

5.2 Planar sample design for the optical set-up

To measure the temperature response, the sample needed to be heated while evaporation of water had to be prevented. To prevent evaporation, I placed some of the PNIPAM-coated slide inside a capillary that could be sealed. To this end, I cut a PNIPAM-coated slide into a strip with a diamond cutter. The strip was narrower than 3 mm, so it was possible to insert the strip into a capillary (Fig. 5.1). To accommodate the PNIPAM-coated strip, a bigger capillary was used than in previous experiments (VitroCom, VitroTubes 3530, borosilicate rectangular glass capillary, nominal inner dimensions of cross section: 0.3 mm $\times$ 3 mm). A glass spacer made sure that the coated slide did not adhere to the capillary ceiling. This could potentially influence the measurement, e.g. by compressing beads or by adding extra reflections. Sealing of the capillary was done with viscous paste. Subsequently, I placed the capillary on the heat-able microscope slide (as in chapter 4). During preparation of the sample, the strip could have been scratched, damaging the brush. Such damage was most likely to occur at the edges of the strip. To avoid these edges, I measured near the middle of the strip. In the end, this geometry was similar to the one used to measure the coated bead. Thus, from a technical point of view, these coated plane measurements can be compared to the coated bead results.

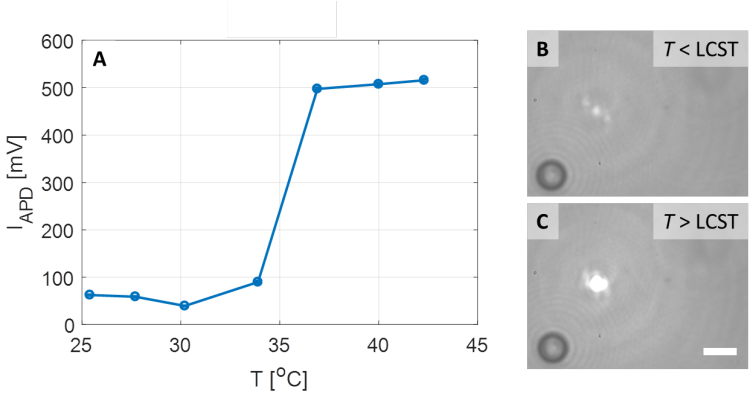

FIGURE 5.2: **A** Reflection off a PNIPAM-coated surface at various temperatures. The data points are averaged over 60 s-long signal of I_{APD}. The errors are the standard deviation and are smaller than the symbols. **B, C** Microscope images during the heating cycle. The laser spot can be seen as a bright spot. At temperatures of 29 °C (**B**), and at about 35 °C (**C**). The scale bar corresponds to 10 µm.

5.3 Results: the temperature response of a planar PNIPAM brush

5.3.1 Reflection off a planar PNIPAM brush

As PNIPAM collapses, the layer's properties change. One property is the refractive index of the layer. In turn, this leads to a different reflection off the PNIPAM-water interface, which can be measured. Hence, a simple reflection measurement can indicate the brush collapse. To this end, we first consider the planar reflection (Fig. 5.1B).

The reflected intensity, I_{APD}, was low and constant at temperatures up to 34 °C (Fig. 5.2A, B). Then, as the temperature was increased to 37 °C, I_{APD} increased strongly (Fig. 5.2A, C).

These observations are similar to those of Lord Rayleigh. Over a century ago, in 1886, he investigated the transmission of light through glass surfaces. He found that tarnished glass transmitted more light than a pristine and clean glass surface. This was caused by the intermediate tarnish layer, which had an intermediate reflective index that was between that of glass and of air. For the pristine glass, the refractive index at the glass-air interface changed abruptly from 1.5 to about 1. The tarnish caused two interfaces and thus two reflections. However, as the difference of the refractive index between tarnish-air or glass-tarnish was lower than that of glass-air, these tarnish

reflections were less intense. So much, that even the combined reflected light of both interfaces was lower than the light of the single glass-air reflection. Analytically, these observations can be described using the Fresnel equations. This theory explains my observations of I_{APD} with increasing temperature. At low temperatures, the brush layer density changed gradually away from the substrate (Fig. 5.3A). The brush density and refractive index can be considered proportional as a first order approach. Close to the glass substrate, the density of PNIPAM was high. The density gradually reduced as the brush extended into the water phase. Close to the substrate, PNIPAM had a refractive index close to that of glass [Koo+12; Chr+16]. Towards the water phase, the density of PNIPAM was low and hence the resulting refractive index was close to that of water. Thus, the PNIPAM brush layer was in effect a graded refractive index material, an anti-reflective coating.

The refractive index changed as the layer collapsed. Upon collapse, the water was expelled and the change in the density of PNIPAM was no longer gradual. This caused an abrupt change of the refractive index at the PNIPAM-water interface (Fig. 5.3B). Thus, the reflected intensity of collapsed PNIPAM was higher than for swollen PNIPAM.

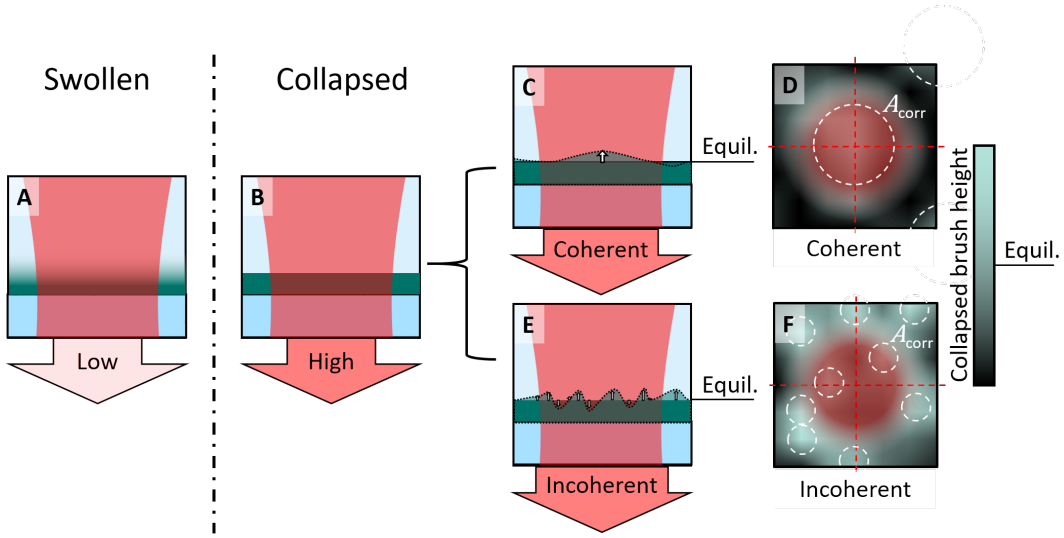

FIGURE 5.3: Cartoons of the reflective planar brush layer. The substrate (in blue) holds the brush layer (in green), and is illuminated by the interference laser that comes from below (red). The laser focus is at the PNIPAM-water interface. The reflected light is indicated by the red arrow pointing downwards. **A** The swollen brush, at low temperatures, has a gradient density profile. **B** As the brush collapses, the density profile changes abruptly towards the water phase. The reflected light off the swollen brush has a low intensity compared to the collapsed brush with a high reflected intensity. Compared to the laser spot size, the layer can have a correlated area (A_{corr}, indicated by white dashed circles) that is high: **C, D**, or low: **E, F**. Cartoons C and E are side view cross sections while D and F are top views. Hence, the reflected light for a off a surface with high A_{corr} has a high spatial coherence (C, D), while the light off a low A_{corr}-surface has a low spatial coherence (E, F).

In a similar way, I analysed the experiments of the coated bead (data of Fig. 4.1 in the previous chapter). The mean reflection signal did not show any trend with temperature (Fig. 5.4). In this experiment, the bead introduced another glass layer above the PNIPAM brush. For this reason, the contrast of refractive indices was not as strong as for the planar PNIPAM brush. Furthermore, the set-up drift had a bigger influence on curved bead measurements than it had on planar surfaces, which increased the uncertainty of this measurement (See section 3.4). Therefore, no trend in I_{APD} with T, or with PNIPAM collapse could be observed for the coated bead, and the only way to investigate the collapse with this set-up was through its Brownian motion as in the previous chapter.

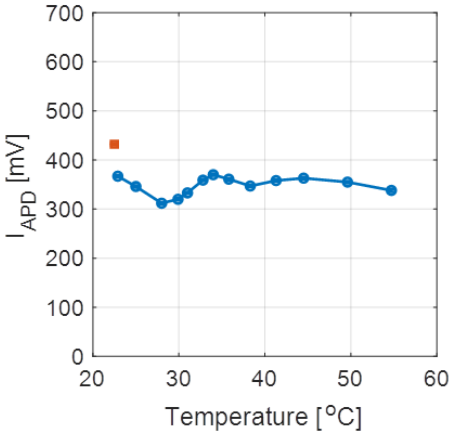

FIGURE 5.4: Reflection off the PNIPAM-coated bead of Fig. 4.1 at various temperatures. The red data point is after cooling down.

5.3.2 PSD of planar PNIPAM with increasing temperature

The refractive index difference between the planar PNIPAM layer and water is high when $T >$ LCST. In this case, there are multiple interfaces that reflect. These two reflections interfered. Similar to the interference signal of a bead, this interference signal could be influenced by thermal fluctuations in thickness and provide insight into the viscoelastic changes induced by collapse of the layer.

The interfered reflection signal can also be analysed through its PSD. At temperatures below the LCST, the PSD could be described by the last two terms of eq. 3.9: A/f^2 and C, without a discernible Lorentzian term (Fig. 5.5). However, as the temperature was increased to 37 °C, a distinct Lorentzian shape became visible, with cut-off frequency $f_k = 546 \pm 30$ Hz. At higher temperatures, this increased to $f_k = 637 \pm 39$ Hz for 42 °C. Thus, the PSD of only a PNIPAM-coated planar surface changed with temperature.

Since at $T >$ LCST, a Lorentzian shape was visible, let us consider analysing the planar layer in a similar fashion as the Brownian motion of the coated

bead. Therefore, let us assume that changes of the thickness of the planar brush describe a harmonic potential well.

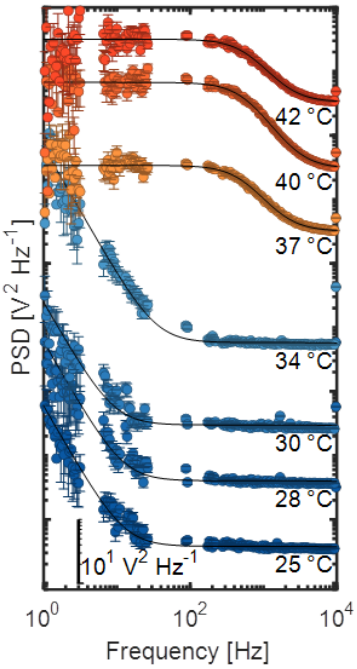

FIGURE 5.5: The fitted PSD of planar PNIPAM on a glass wall at different temperatures, corresponding to the line colours. Each subsequent line was offset by one decade for clarity. These measurements involved no beads.

In the earlier experiments, Brownian motion of a particle happened when the thermal energy was significant enough compared to the damping of the particle. The damping of the particle depended on the radius of the bead (eq. 3.2). For a planar surface, in order to observe its Brownian motion, two conditions had to be met: 1) The area of layer that is illuminated needs to move in unison (Fig. 5.3C-F). I call this area that is illuminated the correlated area, A_{corr}. 2) In general, Brownian motion only happens at small length scales. The reason is that the Brownian motion needs to be big enough to be detected. The amplitude of the motion depends on the diffusion coefficient, D. From eq. 3.6 ($D = k_{\mathrm{B}}T/\beta$), the motion amplitude is the ratio between energy and the damping coefficient. This planar surface was quite different from a sphere in a liquid for which the theory is designed, and I thus cannot define the damping coefficient in this case. However, a reasonable assumption is that in this case damping will increase with the area of the fluctuating brush layer, A_{corr}. Since the layer produced a Lorentzian shape, I assume that the motion amplitude was sufficiently large. Consequently, A_{corr} had to be limited in size so that Brownian motion could occur in my experiment. To satisfy both conditions, A_{corr} had to be as small as possible, yet similar or bigger than the laser spot size. Therefore, it follows that A_{corr} of the collapsed brush was on the order of ten square micron, similar to the laser spot size.

There are a few possible reasons why no Lorentzian shape could be observed at $T <$ LCST. First of all, the reflection off the PNIPAM-water interface at these low temperatures was too faint to be detected. In addition, a swollen brush behaves like a liquid: each chain moves individually. Hence, the correlated area was smaller than the illuminated spot (like in Fig. 5.3E, F). Therefore, the

spatial coherence of the reflected light off the PNIPAM-water interface was low, hence preventing interference. One other possibility is that the layer was very soft: the spring constant k was low. A low value for k leads to a low value for f_k. Therefore, the Lorentzian shape could have occurred at low frequencies and it was hidden by the drift term, A/f^2. For these reasons, the interference of Brownian motion was invisible in the measured I_{APD} at temperatures below the LCST. Hence, analysis of the PSD of a planar PNIPAM brush without a bead was not a viable tool to characterise the collapse of PNIPAM.

5.3.3 The PSD of a bare bead on a planar PNIPAM brush

Adding a bead introduces another interface, which should thus allow analysing the PSD for the swollen planar PNIPAM. Hence, let us have a look at the experiments in which the laser illuminated a bead instead of only the planar brush.

In this experiment, I filled the capillary with a 5 µm-diameter bead dispersion. These beads adhered to the surface, which was confirmed through the method described in section 3.1. Through analysis of the reflected light, a clear Lorentzian shape was visible in the PSD at each temperature. From these PSD, I obtained the f_k-values at each temperature (Fig. 5.6). At $T <$ LCST, I found that $f_k = 18 \pm 8$ Hz. As the temperature was increased to 37 °C, f_k had increased to 403 ± 49 Hz. Increasing the temperature further to 42 °C, f_k had increased further to 583 ± 62 Hz. Therefore, the increase of f_k over the LCST was a factor of 22. The magnitude of this change is a lot higher than what was observed for the coated bead (Fig. 4.2), and observations in literature of viscoelastic properties.

To find out why, let us have a look at f_k at temperatures below and above the LCST The value of f_k at high temperatures is similar to that of the planar PNIPAM (Fig. 5.5). Hence, I argue that the data points at T below and above the LCST have to be attributed to different origins. At $T <$ LCST, the bead reflects light, and this light subsequently describes the Brownian motion of the bead. In contrast, at $T >$ LCST, the signal of the bead remains hidden, and the signal of the planar surface becomes apparent. Therefore, during this measurement, the Brownian motion of two different things were observed. Thus, in this case, the measured changes in f_k at various temperatures cannot be used to the collapse of the planar PNIPAM brush.

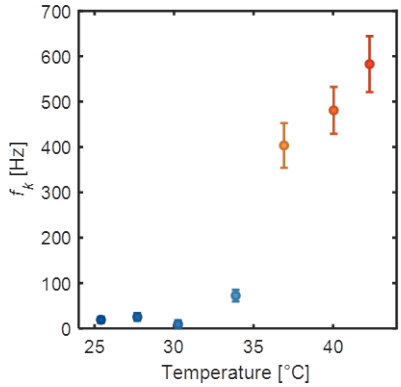

FIGURE 5.6: The influence of temperature on the spectral properties of a glass bead on a PNIPAM surface. The symbol colors correspond to T: blue indicates cold, and red indicates warm.

5.3.4 Multiple beads

One important advantage of the method that I developed is that it is easy to measure multiple beads in quick succession at identical conditions. First, the temperature was set to a certain value, and the system was let to equilibrate. Then, beads were measured one-by-one. For each bead, the sample was moved such that one particular bead was in focus of the laser.

In this way, the response of multiple beads was recorded (Fig. 5.7). One bead was disregarded, as its PSDs could not be described well with the model for the PSD (eq. 3.9). In some cases, as a result of the production of the beads, pristine beads were deformed. Such deformations influenced their reflections. I attribute this as the cause for the odd spectra of the one bead. As to the other beads, at $T <$ LCST their Brownian motion and f_k were similar.

The values of f_k of the spectra depend quadratically on R (eq. 3.13). Furthermore, the supplier's specifications of these glass beads indicated a diameter of $5.4 \pm 0.7\,\mu$m, which can even be seen through the microscope (Fig. 5.7A). Hence, differences between beads, and the influence of these differences on f_k, need to be considered.

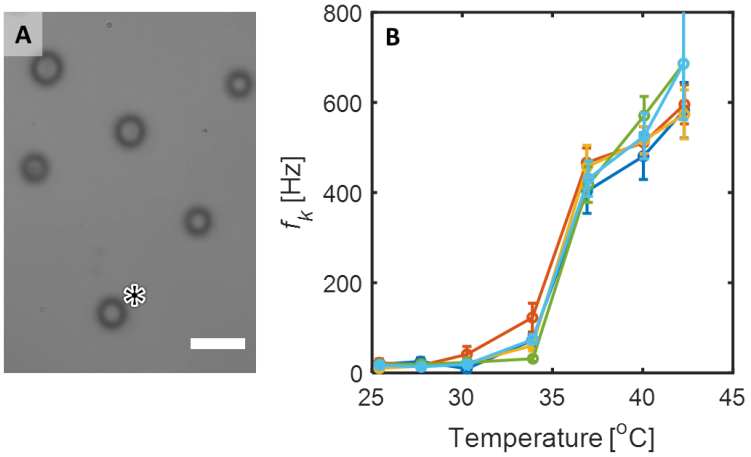

FIGURE 5.7: **A** The microscope image of multiple beads. The scale bar corresponds to 10 µm. **B** The cut-off frequency f_k that describes the PSD the measurements at temperature T. Each color corresponds to a different bead. The lines were drawn to clarify which data points belong to the same bead. The spectrum of one bead could not be described well and was thus omitted (bead indicated by asterisk in **A**).

5.4 Summary and conclusion

In addition to characterising coatings on colloids, this method also allows characterisation of planar layers. I found that at temperatures below the LCST, the brush layer acted as an anti-reflection coating. In contrast, above the LCST, the PNIPAM-water interface became more apparent, and more light reflected off it. This reflection interfered, and a Lorentzian line shape appeared in the PSD, and was subsequently analysed as a harmonic potential well. On the one hand, for such interference to occur, the illuminated area of the layer and the layer's correlated area (A_{corr}) had to be comparable. On the other hand, A_{corr} had to be limited in size for low damping, and to allow for the observed Brownian motion. Hence, I estimated that A_{corr} of the layer was similar to the laser beam spot size, a few ten square microns. Consequently, I showed that this method can be applied to characterise planar layers. For such characterisation, a bead is not required. Hence, this method can be used to analyse planar layers during operation in situ.

Tracking of the viscoelastic properties of the planar PNIPAM layer over its collapse was not possible. Using a bead as a probe for the planar layer was possible at temperatures below the LCST. However, for the collapsed PNIPAM layer above the LCST, the reflection off the PNIPAM-water interface obscured

the reflection from the bead-PNIPAM inter-phase. Adapting the set-up can remedy this unwanted PNIPAM-water reflection. By reducing the beam waist of the interference laser, most of the reflected light would originate from the bead, and less from the PNIPAM-water interface. The beam waist could be reduced by adapting the set-up with an objective with a shorter working distance.

Furthermore, I showed that multiple beads could be characterised in quick succession. Most importantly, these beads were measured in identical conditions. Compared to other techniques, measuring multiple single beads in quick succession while in the same conditions is an advantage.

Chapter 6

Co-Non-Solvency Collapse of PNIPAM

6.1 Introduction

Besides temperature, PNIPAM responds to other stimuli as well. Another stimulus of interest is the solvent. PNIPAM reacts differently to good solvents that are pure or to mixtures thereof [Sch92]. Using this response, applications are envisioned in, for example: sensors, actuators, microfluidics, gating, nanoparticle preparation, or friction control [Sui+11; Liu+12; Ito+05; Yu+17; Yu+16].

We have seen that at temperatures below the LCST, water is a good solvent for PNIPAM. Alcohols are also good solvents. Interestingly, the combination of water and alcohol is a bad solvent, which leads PNIPAM to collapse. This effect is called co-non-solvency, where water is the solvent and short-chained alcohols are the co-solvent. At a certain water-alcohol fraction, the brush thickness displays a minimum. The length of the hydrophobic chain of the alcohol shifts the fraction at which the minimum occurs, believed to be governed by the solvent-co-solvent interactions. Generally, however, the co-non-solvency effect is very similar for most short-chained alcohols [Yon+19]. Since the response is similar to methanol, I used ethanol as it is safer to work with. Ethanol has a reported minimum brush thickness at fractions ranging 15 vol % to 40 vol %. In this collapsed state the thickness of the brush decreased to 50 % of that in pure water [Yu+16; Yon+19]. I investigated the co-non-solvency response of a PNIPAM brush-coated bead at a glass surface to a water-ethanol mixture.

Compared to temperature as a stimulus, the co-non-solvency collapse leads to a similar decrease of brush thickness. Nevertheless, the collapse mechanisms

are different. For the temperature stimulus, PNIPAM binds with itself above the LCST. In pure solvent, the PNIPAM participates in hydrogen bonding with the solvent – thus swelling it, either in water or alcohol. At intermediate fractions of ethanol, PNIPAM binds very well with ethanol, the co-solvent. Simulations have showed that the co-solvent molecules preferentially bind with PNIPAM [MMK20]. The preferential binding is the leading hypothesis for the primary cause of the co-non-solvency effect [MMK14; Yon+19; Yon+20; MMK20]. For this reason, the co-solvent is the better solvent, which is apparent in the increased swelling ratio in pure ethanol (co-solvent) compared to pure water (solvent) [Yu+16; Yon+18; Yon+19]. At intermediate ethanol fractions, the co-solvent molecules can even bind with two PNIPAM monomers. Hence, bridges are formed, which subsequently cause the collapse. PNIPAM is flexible, hence such bridges can occur within one polymer chain: intrabonding, though also with other polymer chains: interbonding (see Fig. 4.4).

However, in spite of its relevance and the decades of study, the response to this type of stimulus is not yet fully understood [Kyr+16; Bac+17a; Yon+20]. As the brush collapses, some of the brush parameters change. In the experiments in this chapter, I used the method that I described in chapter 3 to study PNIPAM brush-coated beads near a glass wall in various solvents. This Brownian motion of the bead depended on the polymer that was in the inter-phase between the bead and the glass wall. The key observable was the PSD, which can be described by its cut-off frequency (f_k). Here, f_k depends on a couple of variables. For convenience, I here restate the definition of f_k, which describes the ratio between elastic (k), and viscous (β) parts of the inter-phase (eq. 3.13)[1]:

$$f_k = \frac{k}{2\pi\beta} = \frac{k}{2\pi\beta_{\text{Stokes}}\beta_d\eta_{\text{rel}}} = \frac{k}{12\pi^2\eta R\left(1+\frac{R}{d}\right)\eta_{\text{rel}}} \tag{6.1}$$

Altogether, four variables played a role in this co-non-solvency experiment, namely the bulk viscosity η, and the inter-phase's spring constant (k), thickness (d), and relative viscosity (η_{rel}), with the inter-phase like in Fig. 1.1). As the solvent changed, so did the values of these parameters. Thus, to describe the co-non-solvency effect on the PNIPAM brush in the inter-phase, I looked at these parameter.

It follows that during a collapse the thickness of a layer (d) decreases, changing

[1] I will discuss only the variables k, η, d, and η_{rel}. For a discussion on the other variables that influence the PSD, please revert to chapter 3.

f_k. Yong et al. used ellipsometry to determine the thickness of PNIPAM brushes at several water-alcohol solvent compositions [Yon+18; Yon+19]. In their studies, they found that ethanol-water mixtures reduced the brush layer thickness to half its value in pure water. This minimum occurred between 15 vol % to 30 vol % of ethanol. Furthermore, they found that ethanol is the better solvent, as the brush reached a thickness of 1.2 times the thickness in pure water, which was confirmed by Yu et al. who used SPM [Yu+16]. Therefore, I expect that the collapse and the related decrease in d pushed for a decrease of f_k.

Another brush-parameter that influences f_k is the viscosity. The bulk viscosities of solvent mixtures (η) are available in the literature. While the viscosities of water and ethanol differ only slightly, the mixture of the two is quite different. Compared to pure water, η of a mixture with 20 vol % ethanol more than doubles [Kha+12]. The value of f_k scales inversely with η. Therefore, the change in η pushed for a decrease of f_k.

In addition to the bulk viscosity, the viscosity of the inter-phase is also likely to change. As the fraction of polymer within the inter-phase increases due to the collapse, its viscosity, η_{rel}, increases as well [MSR03]. One study on linear dissolved PNIPAM reports on changes in local viscosity near the polymer [Che+11]. Chee et al. studied the co-non-solvency effect of PNIPAM with fluorescent side-groups through time-resolved anisotropy measurements. Here, they measured the fluorescence decay properties of the side group and subsequently they determined the local viscosity. They found an increase of the decay time at 30 vol % to 50 vol %, indicating an increased local viscosity in co-non-solvency conditions. One possible reason for this increase is the solvent quality of ethanol compared to water. For better solvents, I expect that the interaction between polymer and solvent molecules will be stronger. Therefore, the viscosity of the inter-phase η_{rel} was probably higher in the mixed case than in pure water. I do not know how much η_{rel} changes. Nonetheless, a higher value would lead to a further decrease of f_k.

In contrast to η and d, the spring constant k influences f_k proportionally. One study used colloidal SPM to determine the elasticity of PNIPAM brushes [Sui+11]. Here, Sui et al. investigated brushes in pure water and in mixtures of water-methanol with 50 vol % methanol. Methanol is an alcohol with a shorter chain than ethanol that also leads to the co-non-solvency collapse [Yon+19]. Sui et al. determined the apparent Young's modulus of the brush layer. The Young's modulus describes the elasticity of a material and is analogous to k in

the model that I used. Sui et al. found that the stiffness of the PNIPAM brushes increased when switched from the swollen to the collapsed state. Thus, in the co-non-solvency collapse f_k would increase as response to a stiffer brush layer.

The study by Sui et al. reports a fourfold increase of the brush stiffness as it collapsed. Thus far, I can predict changes in η, d, and k (doubling of η, halving of d, and a fourfold increase in k), while the change in η_{rel} remains unknown. Taking into account η, d, and k, these would lead to no change observed in f_k. Therefore, observed changes in f_k would be attributed to η_{rel}.

Finally, Sui et al. also discussed the dynamics of collapse and swelling. Though it was possible for them to observe collapse, they did not succeed observing the swelling. The reason was that swelling took too long, which was not compatible with their AFM technique. Using the optical interference method, I was able to investigate the dynamics of swelling.

Thus, different literature sources provide different hypotheses. In this chapter, to elucidate the co-non-solvency collapse mechanics, I investigated the viscoelastic properties of the PNIPAM-coated beads at a glass interface. I looked into how the various parameters change relatively to each other, both in steady-state and in dynamic circumstances. To do so, I applied the same optical technique and method as before, as described in chapter 3.

6.2 Method

6.2.1 Flow cell

Ideally, one measures the effect of the solvent while probing the same bead. However, such a solvent change is not possible when using the capillary sample as I did for the temperature measurements. Therefore, instead of a capillary, the bead dispersion was in an optical flow cell that had two transparent windows, top and bottom (Attofluor™ Cell Chamber, Invitrogen™ A7816). The bottom window consists of a circular microscope cover slide (VWR®, VistaVision cover glass, Round, No. 1 thickness, borosilicate, rinsed with ethanol before use). Shortly before introducing the beads in the flow cell, the beads (5 µm-diameter, PNIPAM brush-coated, see chapter 2) were dispersed in water (milliQ-grade, 18.2 MΩ cm). Following, I deposited a 10 µL-droplet of bead dispersion on the bottom window of the flow cell (Fig. 6.1). Similar to previous experiments, the coated beads sedimented and subsequently adhered to the

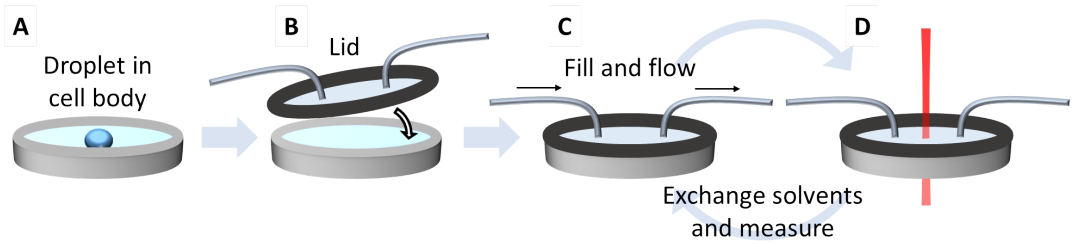

FIGURE 6.1: Measurement of the co-non-solvency experiments. **A** The flow cell has a lower windows that consists of a circular glass microscope slide on which the droplet with bead dispersion was placed. **B** A transparent lid with two tubes closes off the flow cell. **C** The tubes fill up the flow cell, and are used to replace the solvent. **D** The laser shines through the flow cell, which has two windows. The reflected laser light describes the Brownian motion of a bead.

glass surface (section 3.1). The flow cell was then installed in the optical set-up. Subsequently, the lid was put on the flow cell, and the remaining volume was filled with water. At this point, a bead was selected, and its PSD was recorded for the water as a solvent (as described in section 3.3). To change the solvent, I flowed >15 mL of the new solvent through the flow cell. The combined volume of the flow cell and the tubing involved was about 3 mL. Hence, the volume was replaced at least five times, ensuring solvent control. For this co-non-solvency measurement, I measured first in pure milliQ water, then an ethanol-water mixture with 20 vol % ethanol (Ethanol absolute $\geq$99.8 %, AnalaR NORMAPUR®ACS, Reag. Ph. Eur. analytical reagent), then pure ethanol, and then again water. All these measurements were conducted at room temperature, which was 23 °C.

6.3 Results

For each solvent, I obtained a value for f_k (Fig. 6.2). During the whole experiment and at all solvents, the bead remained in place, indicating adhesion of the PNIPAM bead to the glass substrate in all solvents. These PSDs were obtained one hour after exchanging the solvent to reach a stable state. Some of the relevant parameters for PNIPAM brushes have been discussed and reported in the literature, these well-established values are also printed in Fig. 6.2. The measured results, f_k at various solvents, are discussed in the following paragraphs.

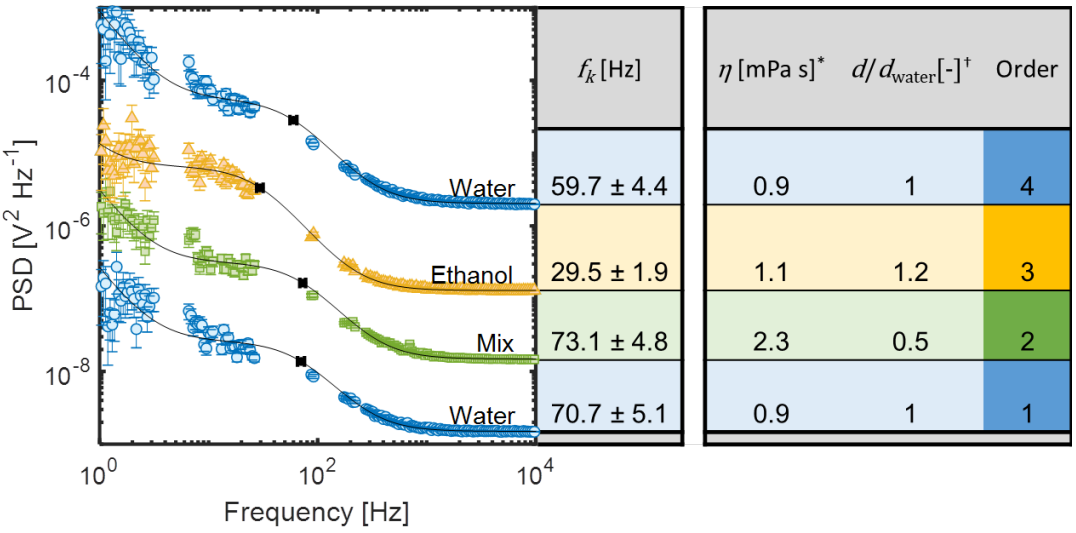

FIGURE 6.2: The effect of the co-non-solvency collapse on the PSD of a PNIPAM brush-coated bead. Each PSD has been offset in the y-axis for clarity. The order of measuring was, bottom-to-top: water (blue circles) – 20 vol % ethanol-water mix (green squares) – ethanol (yellow triangles) – water (blue circles). The table shows fitted values for f_k from the PSD, as well as the relevant and well established parameters from literature. From: *[Kha+12], †[Yu+16; Yon+18; Yon+19].

6.3.1 The water-to-mix exchange: collapse

Based on the literature studies, I expect a decrease of f_k, and the corresponding change should describe the change of η_{rel}. Remarkably, however, the PSD and the cut-off frequency f_k did not significantly change upon collapse when the solvent was exchanged from water to the 20 vol %-ethanol mixture (Fig. 6.2).

However, it is unlikely that η_{rel} did not increase. Instead, it is more likely that I should not have expected similar results of stiffness as obtained by Sui et al., for which I provide two arguments. First, the maximum collapse of PNIPAM brushes in methanol-water mixtures occurs around 30 vol % [Yon+19]. Consequently, the brush collapse that was studied by Sui et al. at 50 vol % would have provided a softer brush than one at 30 vol %. Second, Yong et al. studied brushes and the co-non-solvency effect of water mixtures with several alcohols: methanol, ethanol, 1-propanol, and 1-butanol [Yon+19]. Their results point out that the collapse was stronger for higher alcohols: the volume reduction was higher. I measured in a 20 vol %-ethanol mixture, a higher alcohol in better co-non-solvency conditions than a 50 vol %-methanol mixture. Therefore, it is not unlikely that in my experiments the layer stiffness (k) increased by more than a factor of four in co-non-solvency conditions. Thus, I interpret my results as an increase in both k and η_{rel}, in which k increased by more than a factor of 4.

6.3.2 The mix-to-ethanol exchange: re-swelling

Following, I exchanged the solvent to pure ethanol. Over this exchange, the value of f_k changed from 73.1 ± 4.8 Hz in the mix to 29.5 ± 1.9 Hz in ethanol. From literature, the bulk viscosity (η) of ethanol is about half that of the mix, reducing from 2.3 mPa s to 1.1 mPa s [Kha+12]. Furthermore, studies agree that PNIPAM brushes re-swell in ethanol compared to the mix. In pure ethanol, the co-solvent, the brush layer swells even stronger than in water, reaching 1.2 times the thickness of that in water [Yu+16; Yon+18; Yon+19]. When comparing the values to water, the influence of η and d roughly cancel out. Therefore, the low value of f_k that was observed must have originated from k and η_{rel}.

When investigating the water-ethanol mixture, the shortage of ethanol molecules lead to bridging and subsequent collapse. Now, with an abundance of ethanol molecules, neighboring binding sites need not be bridged by a single molecule. Instead one solvent molecule may accommodate a single binding

site. This lead to the re-swelling of the brush layer. Because the bridging no longer occurred, the stiffness of the brush layer (k) reduced, compared to the collapsed case.

The relative viscosity of the inter-phase (η_{rel}) describes how the local viscosity is different from the viscosity of the bulk. In this instance, the interactions between water-PNIPAM and ethanol-PNIPAM differed. As the latter interactions were stronger, it follows that η_{rel} in ethanol was higher than in water. Another reason for an increased η_{rel} compared to water is that the ethanol molecule is bigger. From the measurement, and assuming k did not significantly differ from water, I conclude that η_{rel} in ethanol was twice as high as in water. Thus, I conclude that the increased ethanol-PNIPAM interaction strength has lead to more viscous Brownian motion in ethanol than in water.

The co-non-solvency collapse was caused by preferential binding of ethanol-PNIPAM to water-PNIPAM. Hence, the characteristics of bonds between ethanol and PNIPAM were similar in the mixed solvent and the pure ethanol cases. The difference between the mixed solvent and pure ethanol case was that the layer thickness changed. Thus, the increase of η_{rel} in pure ethanol supports the interpretation that I previously made: that η_{rel} increased in the mixed solvent.

6.3.3 The ethanol-to-water exchange: return to initial conditions

Returning to water provided $f_k = 59.7 \pm 2.8\,\mathrm{Hz}$. The original value of f_k was $70.7 \pm 5.1\,\mathrm{Hz}$. These values differ only slightly. This indicates that the initial state of the coated bead and its final state were not the exact same. The confirmation of the brush changed as it collapsed and subsequently re-swelled. The brush collapsed twice. Once, during the intended co-non-solvency collapse when the solvent was changed to the mix. The brush collapsed a second time, at least partly, during the ethanol-to-water exchange. After this exchange, the ethanol within the brush layer had to diffuse out, and water diffuse into the layer. Hence, at some point after the exchange, the brush had to have experienced the co-non-solvency effect due to the effective solvent composition at that time. The twice-repeated conformational changes may have lead to the slight observed differences.

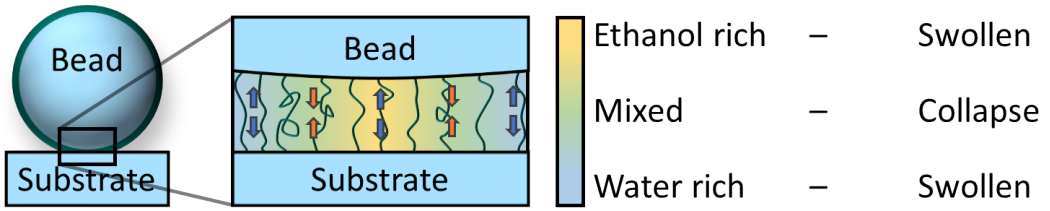

FIGURE 6.3: Sketch of the solvent composition within the brush layer inter-phase between the bead and the substrate. A zoom-in of the inter-phase between the bead and the substrate is shown as well. The coloured arrows in the zoom-in indicate the internal stresses. In the water and ethanol rich regions, the brush swells, pressing the bead away from the substrate (blue arrows). In mixed regions, the brush collapses, causing the bead to be pulled towards the surface (orange arrows).

Dynamics in the ethanol-to-water exchange

Apart from the steady-state results discussed above, I measured some dynamics during the ethanol-to-water exchange. Initially, directly after the solvent exchange, the brush was swollen with ethanol while the solvent in the bulk consisted of water. The surfaces of the bead and the wall confined the brush. Because of this confinement, there was a gradient in solvent concentration. Hence, at some point in time, the concentration gradient induced the co-non-solvency effect at some regions of the brush, while the brush remained swollen at other regions (Fig. 6.3). Hence, the effective spring constant k described the combination of swollen *and* collapsed polymer. This combination caused internal stresses within the polymer brush. In regions where the solvent conditions were good (in water and in ethanol) the ideal brush state was swollen, here the polymer chains were compressed (arrows in Fig. 6.3). At the same time, in regions where the solvent conditions were bad (in mixed solvent) the ideal brush state was collapsed, here the polymer chains were stretched. These internal stresses caused an increased stiffness of the effective spring constant k. A way to look at the stiffness is through the energy potential well that the bead was in (e.g. Fig. 3.4). Compared to the swollen case, here the bead was closer to the surface. Since the repulsive force scales exponentially, this force was significantly stronger. As a consequence, the potential well was much steeper shortly after the solvent exchange, which translates into a higher value for k.

The increased stiffness due to stresses can be seen in the time-resolved measurement (Fig. 6.4). Just after the ethanol-to-water exchange, f_k was high

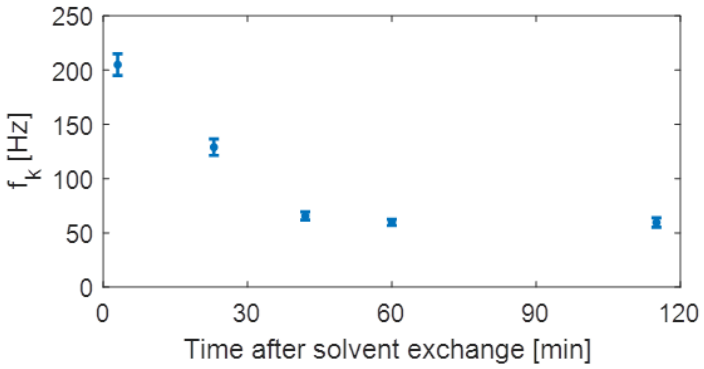

FIGURE 6.4: Values for the cut-off frequency (f_k) of the PSD, at different times after exchanging the solvent from ethanol to water.

(205 ± 10 Hz). As f_k is proportional to k, this indicates a stiff layer. With progressing time, the solvents diffused and the internal stresses relaxed over a period of one hour. This period is long compared to observations by Sui et al., who used AFM to probe the collapse of brushes in methanol-water mixtures [Sui+11]. They measured only the dynamics of the collapse, which happened in less than a minute. Furthermore, they noted that swelling "took a very long time", which prevented them from measuring the swelling, indicating that swelling took longer than the collapse. In my experiments, the transitions will take even longer. The confinement of the brush by the bead and the wall hindered diffusion. As a consequence, the full exchange of solvent within the PNIPAM brush inter-phase, a confined volume with nano- and micrometer dimensions, took one hour.

6.4 Discussion

6.4.1 Comparison to microgels described in literature

One other promising configuration of PNIPAM-based responsive colloids are microgels. As the name suggests, these are are micrometer-sized cross-linked gels. Due to their size and their ease of production, microgels have garnered a lot of interest. Some applications make use of dispersed microgel dispersions, e.g. in drug delivery [Klo15]. In other instances the microgels were deposited on a surface, thus producing a responsive coating [Sch+10; Bur+11a; Bv18]. Therefore, both microgels and brushes can be applied to produce responsive coatings and colloids. However, there are differences between such brush-based or microgel-based coatings. Those differences matter in their responses and therefore we need to understand them.

One of the more obvious differences is that microgels are cross-linked whereas brushes are not. For PNIPAM microgels, the cross-linker N,N-methylenebis-acrylamide (BIS) is often used [PC86; CV98; Bv18]. Another difference that often occurs is the temperature at which the polymerisation is done. Many brushes are synthesised at room temperature, while many microgels at 60 °C, above the transition temperature [Sch+14]. Hence, the polymer chains in a microgel are relaxed in the collapsed state, whereas they are stretched when the microgel is swollen. Furthermore, the PNIPAM polymer of brushes and microgels is in some cases different. In order to study the response of PNIPAM to stimuli, in some studies it was required to investigate a PNIPAM copolymer, for a variety of reasons. Hence, when comparing the results of studies, one must take into account all such factors.

The structural differences affect the response of PNIPAM to stimuli. For example, the cross-linker content influenced the transition by temperature. For increasing cross-linker content, the transition happened over a longer temperature range, and the reduction in volume was less [CV98; Bur+11a]. On the other hand, studies found that the role of cross-linker in gels on the co-non-solvency effect was minute [Wal+12; Sch+14]. The incorporation of a co-monomer has various influences that depend on the co-monomer used. One example of a co-monomer is acrylic acid, a weak acid that charges in water, which was used to increase the microgel size and adhesion to certain surfaces but also changed the response to temperature [Bur+11b; Bv18]. What surely played a role is the adhesion of a microgel to a surface [Bac+17a]. While investigating the mechanical properties Backes et al. found that such properties are very anisotropic and cannot be described with one average number. In a different way, brushes are also anisotropic (see e.g. Fig. 3.2). Yet, one should consider a number of factors while comparing results of microgels to brushes, as these factors influence the responses to stimuli.

A recent review article was titled *Nanomechanics and Nanorheology of Microgels at Interfaces* [Bv18]. SPM is a technology that was used to study surfaces coated with PNIPAM microgels with the co-monomer acrylic acid [Bac+17a]. The acrylic acid was negatively charged in water, which caused the microgel to swell due to electrostatic repulsion. In the measurement, the solvent ranged from water to ethanol, while SPM provided information about the mechanical properties. Specifically, they determined the viscoelastic storage (G') and loss moduli (G''), using a dynamic SPM method [Hel+16]. In addition, they calculated the loss tangent (G''/G'), which illustrates whether the properties

were dominated by elasticity or by viscous losses. Here, they found that the loss tangent increased by a factor of four in high ethanol-content mixtures. This is a remarkable result, because this most drastic increase did not occur at the minimum-volume mixture with a lower ethanol content-mixture, at 30 vol % ethanol. This was explained through the amount of solvent molecules that were present in the microgel. The co-non-solvency collapse was induced by the preferential absorption of the co-solvent molecules. However, in this collapsed state, still many solvent molecules were present. As a result, the layer did not become as stiff as in a collapse induced by temperature. Their observations match mine: the ratio between viscous losses and elasticity (the loss tangent) was high in high ethanol fractions, while at ideal co-non-solvency conditions (at 30 vol % ethanol) the loss tangent did not increase so strongly. One difference between the microgel and brush coatings is their sizes in pure ethanol. When microgels were used as a coating and were adsorbed to a surface, they were smaller in ethanol than in pure water, in contrast to results on brushes which were more swollen [Bac+17a; Yon+18]. This was possibly caused by the adsorption to a surface, since microgels in solution did have similar swelling ratios for water and ethanol as measured by dynamic light scattering [CV98]. Another cause could have been the co-monomer used by Backes et al. In water, the acrylic acid attains a charge that swells the microgel, which might not happen in high ethanol-content solvents. In terms of applications, although the brush- and microgel layers are different, their overall mechanical response to a stimulus appears similar.

6.5 Summary and conclusion

In this chapter, I described the effect of solvent on the Brownian motion of PNIPAM-coated beads at a surface, specifically in water, ethanol, and a 20 vol % ethanol and water mixture. Using the optical interference method, I described the differences of the viscoelastic properties of the brush-coated bead in these solvents. Noting that these results need to be confirmed, I have explained the observations through the volume collapse and increased brush layer stiffness in the mixture, and preferential binding of ethanol-PNIPAM to water-PNIPAM in the mixture and in ethanol. These results match observations about the viscoelastic response to solvents of microgels in the literature. Differences between brush-based and microgel-based coatings will however still occur due to the non-isotropic nature of microgels. My observations supply support to the theory of preferential binding of alcohol.

I described the temperature-induced collapse of the PNIPAM brush-coated colloids in chapter 4. Compared to the co-non-solvency collapse, differences were apparent. Hence, these results underline that the collapse mechanisms for the temperature or solvent stimuli are the result of different molecular interactions.

I showed that this method was suitable to investigate multiple stimuli, thus showing the versatility of the method. In addition, I showed that also time-resolved measurements are possible. Here I applied this method to investigate diffusion of solvents through a confined brush layer. The solvents diffused through a nano- and micrometer-sized geometry, which occurred over one hour.

6.5.1 Outlook

It would be interesting to look at intermediate ethanol-water mixtures. Yu et al. investigated PNIPAM brushes in such mixtures through SPM [Yu+16]. They determined the thickness of the brush, as well as the friction of a colloidal probe moving over the brush surface. Here, they found that the friction increased as ethanol was added to water. Surprisingly, they found that the minimum thickness of the brush, and the maximum friction happened at different ethanol fractions, at 10 vol % and 30 vol %, respectively. They attributed this to the viscoelastic interaction between the brush and the gold colloid. Similarly, Backes and von Klitzing who used SPM to determine viscoelastic properties of adsorbed microgels, reported different ethanol fractions for the point at which the volume was minimal and the point of strongest change in viscoelastic properties [Bv18]. A pointed difference is, however, that Yu et al. observed high friction at low ethanol fractions, while Backes and von Klitzing reported more viscous behaviour at high ethanol fractions. The method that I describe in this thesis is sensitive to both the thickness and the viscoelastic interaction between surface and the brush. Hence, measuring a PNIPAM-coated bead on a surface at intermediate factions of ethanol would provide more insights into how coated colloids move near surfaces.

Thus far, one main method to investigate PNIPAM microgels has been SPM. Yet, as was noted in [Bac+17a], the small size of the microgel compared to the cantilever tip prevented measuring small pure PNIPAM microgels, and instead they synthesised a co-polymer. Hence, application of the method that I introduced in this thesis (chapter 3) could be applied to microgels. One requirement would be that the focus of the interference laser be sufficiently

small. It would be important to match the beam waist to the microgel radius. This is feasible to achieve when one combines the flow-cell that was used here and a different objective. In general, optical measurements on PNIPAM microgels are possible, see e.g. [CV98; Bac+17b]. Therefore, I believe that this method could provide more insight into e.g. two-stage collapses by both temperature and solvent stimuli.

Chapter 7

Electric Double Layer at High(er) Pressure

7.1 Introduction

The blue planet earth is full with water. Here, water can be found nearly everywhere. Often, when a surface is immersed in water, this surface gains surface charges. Then, as two such immersed and charged surfaces get closer, they repulse each other. This interaction force is called the double layer force. The double layer force can be described by the properties of both the surface and the water. The surface properties mainly influence the force magnitude. The water properties dictate the range of the force, called the Debye length, named after scientist Peter Debye in 1923 [DH23]. Specifically, the Debye length depends on the number of ions in the water.

Hydrostatic pressures influences water. Both the density and dielectric constant of water increase by a few percent when the pressure increases to two kilobars [LMF16]. In addition to those properties, the structure of water changes. At ambient pressures, a water molecule has two hydration shells. It was shown that the second hydration shell is less defined as the pressure was increased up to 2 kbar [ODG94; SR00; Wir+17]. Furthermore, Wirkert et al. noted that density changes near a surface are even more pronounced [Wir+17]. All these factors can have an influence on the Debye length.

Previously, the influence of hydrostatic pressures up to one kilobar were reported by Pilat et al. [Pil+16]. They did not observe significant changes of the Debye length in this pressure range. Yet, changes of water were reported at higher pressures up to two kilobars [Wir+17]. In this chapter, I measured the double-layer force between a glass colloid and a glass wall in NaCl solution. I have extended the previous pressure range, doubling the hydrostatic pressure.

7.2 Method

For the experiments in this section, I used the same set-up as before in the previous chapters. However, this set-up was originally built by Pilat for such experiments as described here: to characterise forces at high hydrostatic pressure [Pil16]. To characterise surface forces, I determined a force-distance curve, which is analogous to an SPM force-distance curve. To obtain a force-distance curve, I determined the interaction force as function of distance. All together, these experiments can be divided into three parts. The distance was determined through interference, as previously described in chapter 3. Forces were applied using optical tweezers with a long working distance objective. High hydrostatic pressures could be achieved through a pump and an optical pressure cell. The latter two parts will be discussed in the following.

7.2.1 Optical tweezers

Laser-based optical tweezers have been used to manipulate colloids and beads. The technique was first developed by Arthur Ashkin in 1970 [Ash70]. Two years ago, optical tweezers were awarded the Nobel Prize in physics due to the technology's wide range of applications in for example physics and material science, but also biology. Generally, in optical tweezers there are two forces acting on a colloid. The first force is based on the laser focus that is in essence a strong electric field. The bead, of a dielectric material, is attracted to this strong electric field. Hence, this first force is called the gradient force, since the gradient causes the bead to be attracted towards the place where the laser is focused strongest. If strong enough, the focus will *trap* the bead, hence people often talk about optical trapping. The second force is due to the small momentum of a photon. As the bead scatters the light, the light's direction and momentum is changed. Momentum needs to be conserved, and hence a force is exerted on the bead. This force has two components, along the beams axis and transverse. The transverse component is directed towards the beam axis, and hence also traps the bead. This trapping gave control over the bead. The other component is aligned with the optical beam axis, and is essential in my force-distance experiments. In this chapter, I call this force component the radiation pressure force, F_{rp}. It is F_{rp} that was used to probe the interactions between two surfaces, where the bead itself was one of the surfaces. In the set-up that I used for glass beads, F_{rp} reached up to about a hundred pico-Newton. Furthermore, in the set-up that I used, the focusing objective had a long working distance (Nikon CFI TU Plan EPI ELWD 50×).

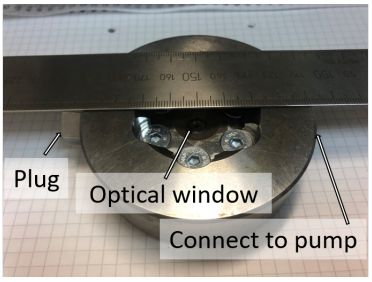

FIGURE 7.1: A photo of the optical cell. The pressure pump is not connected in this photo. The ruler is metric.

As a result, the beam waist of the beam can be considered constant over a long distance along the beam axis. Thus, the radiation pressure force on the bead was constant over a long distance. The laser that exerts F_{rp} on the bead is called the push laser (Laser Quantum, Finesse pure, $\lambda = 532\,\mathrm{nm}$). Finally, the magnitude of this force can easily be controlled through the laser power, as the force and power are proportional (see Appendix B).

7.2.2 Hydrostatic pressure

To reach high-pressure conditions, an optical cell was used [Har+03] (Fig. 7.1). Inside the cell was a sample chamber, which had two sapphire windows for optical access, and channels to connect it to the high pressure pump. Due to this direct connection to the pump, the water inside the chamber was of unknown quality. To address this, the bead dispersion was within a capillary that was sealed off with viscous paste (capillary: VitroCom, VitroTubes 5010, borosilicate rectangular glass capillary, nominal inner dimensions of cross-section: $0.1\,\mathrm{mm} \times 1\,\mathrm{mm}$, viscous paste: Bayer, high-viscosity Baysilone paste). Thus, the experiments could be conducted in a clean and controlled environment.

The optical cell was connected to an automated high pressure piston pump (SITEC Sieber - Engineering AG, motorised spindle-pump, 750.6701-sp). The system (pump, pipes, and the optical cell) was first flushed with water to remove any air pockets. Then, the system was closed off, and the pressure could be set through the interface of the pump.

7.3 Results

7.3.1 Determining the Debye length

Through the push laser, a constant force was applied on the bead for a set laser power. As the bead approached the substrate, the double-layer force became more and more significant. To characterise double-layer forces, I required a force-distance curve. Thus, knowledge about both the force and the distance were needed.

As the bead approached the substrate, I recorded the intensity of the reflected light (I_{APD}) with the avalanche photo diode (Fig. 7.2, black line). As the bead moved closer to the substrate, the reflection intensity changed periodically, as $I_{\mathrm{APD}}(d) \propto \cos\left(\frac{4\pi n}{\lambda} d\right)$ (see eq. 3.8). Hence, between the extrema, the distance d between bead and wall had changed by $\frac{\lambda}{4n} \approx 119\,\mathrm{nm}$, where $\lambda = 635\,\mathrm{nm}$ the wavelength of the interference laser, and n the refractive index of water. This means that one can back-calculate the distance the bead travelled from the last peak (Fig. 7.2, blue squares). At some point, the push laser force is cancelled out by the double-layer force, and the bead is in equilibrium. Here, it moves a little due to thermal motion, called the Brownian regime. These two regimes, the approach and the Brownian regime, were used to determine the force and distance that are needed.

First, I analyse the first regime in which the bead approached the substrate surface. The double layer force is an exponential that ranges with the Debye length, λ_{D}. For this salt concentration of 0.1 mM NaCl, the Debye length was only a few tens of nanometers. Later, I characterise the force in a different concentration, indicating that the method works for various solvent concentrations (in 7.3.2). A result of the nanometer-range Debye length, the double-layer force played a negligible role when the bead was sufficiently far away from the surface (Fig. 7.3A).

Subsequently, the total force balance can be simplified in this range. The total sum of forces is:

$$F_{\mathrm{total}} = F_{\mathrm{dl}} + F_{\mathrm{hd}} + F_{\mathrm{rp}} + F_{\mathrm{g}} \tag{7.1}$$

Here, F_{dl} is the double layer force, F_{hd} the hydrodynamic force, F_{rp} the force from the radiation pressure, and F_{g} the gravity. Since the mass of the bead was low, F_{total} was negligible. Furthermore, we know that F_{dl} was also negligible during the approach regime. As a result, F_{hd} equaled the two constant forces, F_{rp} and F_{g}. Moving through water, the bead experienced hydrodynamic drag,

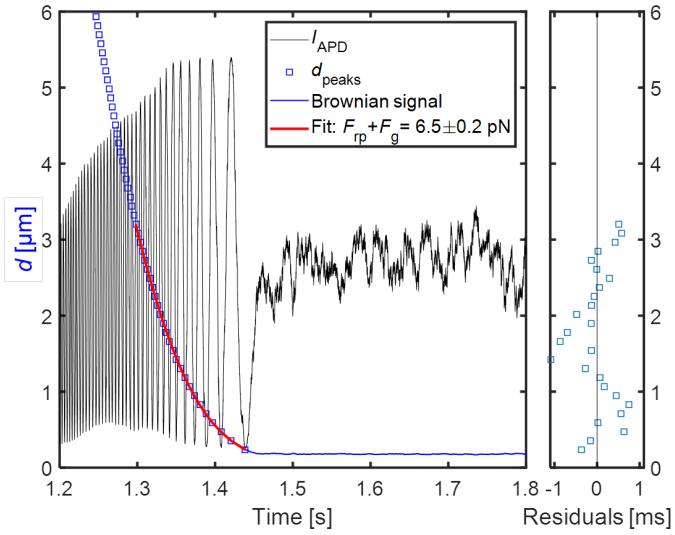

FIGURE 7.2: Fit to determine F_{rp} in double-layer measurements. I measure I_{APD} (in black, axis not shown, it ranged from 0 V to 2.66 V). The envelope is an artefact caused by lensing of the glass colloid [Pil+16]. From the maxima, I distilled d_{peaks} (blue squares), which was fitted to find F_{rp}. The fitted value was time as function of distance, hence the residuals are plotted beside the y-axis. The Brownian signal is analysed in Fig. 7.4.

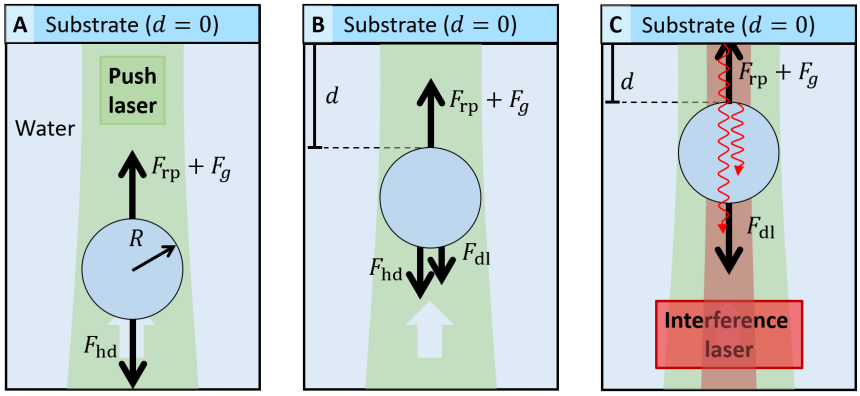

FIGURE 7.3: Schematic that describes the measurement to characterise the double layer. **A** the push laser (green) exerts a force F_{rp} through radiation pressure and pushes the glass bead upwards, while the hydrodynamic drag force (F_{hd}) opposes. **B** As the bead approaches the substrate, the double-layer force (F_{dl}) comes into play. **C** The interference laser (red) reflects off both the bead and the substrate (reflections are drawn as waves). The distance between the bead and the substrate (d) dictates the intensity of the reflected light as both reflections interfere.

described by:

$$F_{\mathrm{hd}}\left(d,\dot{d}\right) = -\beta_{\mathrm{Stokes}}\beta_d\left(d\right)\dot{d} \tag{7.2}$$

Here, d is the distance between the surfaces of colloid and plane and the dot notation describes derivative with respect to time, $\beta_{\mathrm{Stokes}} = 6\pi\eta R$ is the Stokes drag coefficient with η the viscosity of water and R the radius of the bead, $\beta_d(d)$ describes the increased drag caused by proximity to a surface. The drainage term ($\beta_d(d)$) does not have a simple exact description [Bre61]. However, here I approximate it with $\beta_d = 1 + R/d$, which is a fairly good and workable approximation [BK10; Pil+16]. Eq. 7.2 was previously solved by Pilat et al. [Pil+16]. Subsequently, this solution can be fitted to the measured data (Fig. 7.2, red line). In this instance, for this laser power ($P = 81\,\mathrm{mW}$), I found that the constant forces equal $6.5 \pm 0.2\,\mathrm{pN}$.

As the bead approaches, the double layer force starts playing a role (Fig. 7.3B). In this regime, where the forces are balanced (at $t > 1.5\,\mathrm{s}$ in Fig. 7.2), the bead does not move much and hence F_{hd} was negligible (Fig. 7.3C). An additional result of the barely moving bead is that the double layer force (F_{dl}) does not change significantly. Hence, I can equate F_{dl} to the constant forces that I found before, $6.5 \pm 0.2\,\mathrm{pN}$.

In the second regime, the bead is in equilibrium and its distance to the wall evolves around an equilibrium position, d_{eq}. The position in this regime (using eq. 3.8 and the blue line in Fig. 7.2) is Boltzmann distributed [Pil+16]. Calculating a histogram of the bead's position around d_{eq} provides $d_{\mathrm{eq}} = 179.5 \pm 0.5\,\mathrm{nm}$ (Fig. 7.4). Thus, now we know that the double layer force has a magnitude of $6.5 \pm 0.2\,\mathrm{pN}$ when the bead is a a distance of $179.5 \pm 0.5\,\mathrm{nm}$ from the substrate surface.

Now that one data point in the force-distance curve is known, I measured more. This was done by measuring another approach, at an increased laser power, which increased the radiation pressure force, F_{rp}, providing another data point. I here note that for each F_{rp}, the same bead was used. Hence, the uncertainty regarding the bead, e.g. its radius, did not propagate to the Debye length. Repeating the process for a number of laser powers provided a full set that described the double-layer force over a range of distances.

On a semi-logarithmic plot, the force-distance data appears linear (Fig. 7.5). For a sphere that approaches a planar surface, F_{dl} is given by[Isr11a]:

$$F_{\mathrm{dl}}\left(d\right) = F_0\left(\psi_0, \lambda_{\mathrm{D}}\right)\mathrm{e}^{-d/\lambda_{\mathrm{D}}} \tag{7.3}$$

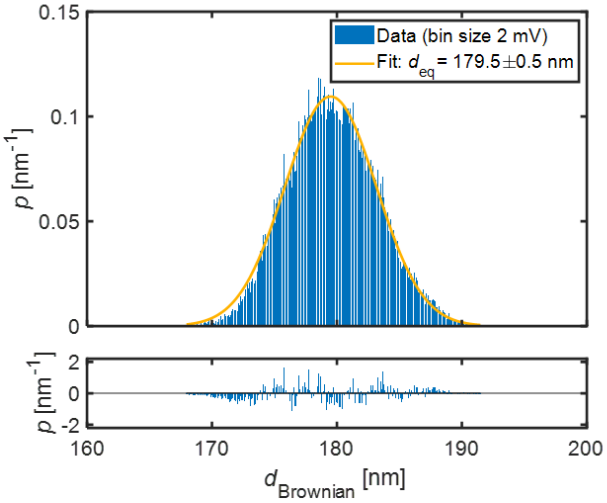

FIGURE 7.4: Histogram of the distance d in equilibrium for the double-layer force.

Here, F_0 is the magnitude of the force in which ψ_0 is the surface potential, and λ_D is the Debye length. Fitting provided $F_0 = 30.6 \pm 4.2\,\text{nN}$, and $\lambda_D = 21.3 \pm 0.4\,\text{nm}$. Pilat noted that λ_D describes the double-layer force better than F_0 [Pil16]. The reason is that F_0 is extrapolated from a relatively small range of d, thus leading to high errors in F_0. In addition, it is likely that not all beads are perfectly spherical, and it may rotate between force-distance measurements when the trap laser is turned off for a prolonged period. As a result, the surface potential of the interacting surfaces of the bead and substrate can differ between measurements. However, λ_D depends solely on the solvent, not on the surfaces. Thus, the double-layer force in this experiment is characterised by $\lambda_D = 21.3 \pm 0.4\,\text{nm}$. These results are similar to what Pilat et al. measured for a 0.1 mM-NaCl solution.

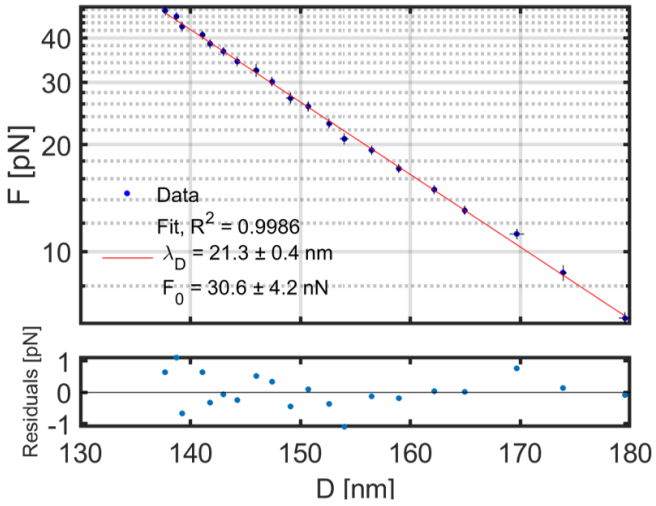

FIGURE 7.5: Force-distance curve to characterise the double-layer force in 0.1 mM NaCl (eq. 7.3).

7.3.2 The Debye length at 2 kbar hydrostatic pressure

Following, I did experimented to investigate the influence of hydrostatic pressure on λ_D, the Debye length. To do so, I determined λ_D of the same 1 mM-NaCl solvent under increasing pressures. Starting, I measured at ambient pressure using the optical cell. Then, I increased the pressure to up to 2200 bar. As the pressure was increased, the tubing that connected the pump to the optical cell expanded. This caused the cell to move slightly. As a consequence, I measured on several different beads. This should be of no consequence to λ_D, which depends solely on the solvent. However, these high pressures did lead to the cell leaking. The pressure pump had a gauge. From this, I noted that there was a decrease in hydrostatic pressure, leading to an error in the pressure of up to -50 bar.

Subsequently, I determined λ_D at various high pressures through six beads (Table 7.1). In the calculations, I corrected for changes of the viscosity caused by pressure, which changes less than 5 % over this pressure range [LMF16]. For a 1 mM solution, the theoretical value for λ_D is about ten nanometers. The values that I found are a little low, which I attribute to a higher salt concentration than 1 mM. Moreover, I did not observe a trend of λ_D with increasing pressure.

Though I observed no significant changes in λ_D over this pressure range, the properties of water have been reported to change. Comparing high pressure to ambient pressure, the dielectric constant of water increases by 8 % and its density by about 7 % [LMF16]. The square root of the dielectric constant is

Pressure [bar]	λ_D [nm]	Bead
1	7.6 ± 1.6	1
1000	8.9 ± 1.9	2
1100	7.9 ± 1.2	3
1850	7.4 ± 1.2	4
2000	7.7 ± 1.4	5
2000	9.8 ± 0.6	5
2100	9.7 ± 1.0	6
2200	7.9 ± 1.8	6

TABLE 7.1: Debye lengths of a 1 mM-NaCl solution at various pressures, measured on several beads.

proportional to λ_D, which leads to a slight increase. The density-dependence of λ_D is not as obvious. Studies showed that pressure influences the nearest neighbors of water, changing the structure [ODG94; SR00; Wir+17]. In my experiments, the closest the bead is to the surface is about 50 nm, which corresponds to many layers of water molecules. Hence, my experiments that measured the Debye length of 1 mM NaCl solution were insensitive to any changes of water structure that may have resulted from high pressure.

7.3.3 Analysis of a single approach: attractive forces

Besides the repulsive double layer force, attractive forces are just as common. Similar to the repulsive double-layer force, attractive forces often increase in strength with decreasing distances. As a result, once close to the surface, a bead will stick tightly to the surface, and releasing it may be impossible. Hence, it is impossible to obtain multiple force curves while measuring attractive forces. Consequently, it is required to obtain sufficient information of only one approach curve. In this section I outline a method that analyses a single approach.

As a bead approaches a surface, it is subject to several forces. Summed up, these forces (eq. 7.1) obey Newton's second law of motion, the force equals mass times acceleration:

$$\begin{aligned} \ddot{d} &= \frac{1}{m}\left[-6\pi\eta R\dot{d}\,(1 + R/d) - F_0 \exp^{-d/\lambda_D} + F_{rp} - F_g\right] \\ &= \frac{1}{m(R)}\left[\beta_{Stokes}(R)\dot{d}\beta_d(d) - F_{dl}(d, \lambda_D, F_0) + F_{rp} - F_g\right] \end{aligned} \tag{7.4}$$

Here I used dot notation to indicate the derivative to time. Matlab, a numerical

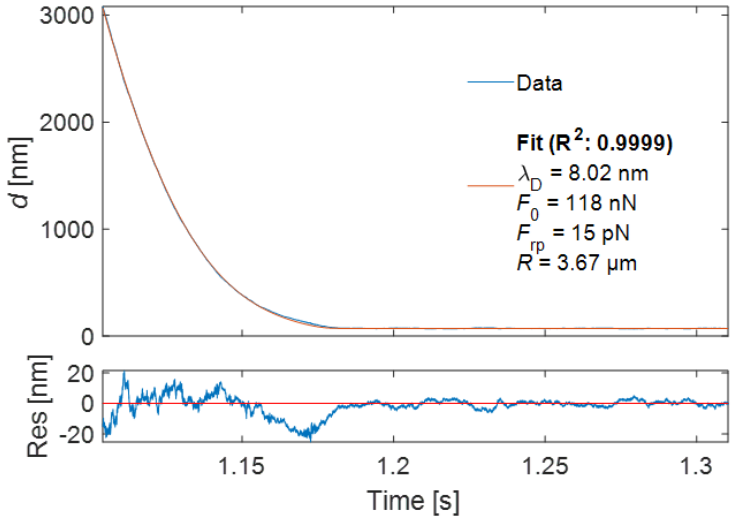

FIGURE 7.6: The approach of a bead (in blue) was fitted with the full differential equation of the forces on the bead (fit in red). No errors are displayed in the fitted parameter values as the method is preliminary. The computation was done using Matlab version 9.6.0.1072779 (R2019a).

computing program, can solve differential equations. With values for the parameters R, F_0, λ_D, and $F_{rp} - F_g$, solving eq. 7.4 provides computed values for the distance (d) over time (t). Subsequently, these computed values can be compared to the measured values. Through minimizing the difference, the optimal values of the parameters can be fitted (See also Appendix A). To illustrate this method, I used it to characterise the double layer force of the 1 mM NaCl solution of the previous section. To this end, rather than using a multitude of force-distance curves, I now used only one at a single fixed trap laser power. In this way, I was able to find values that compare well to the previously described method (Fig. 7.6).

Regardless of this seeming success, the method still needs improving. As an example, I varied the initial conditions to be random within a certain degree (e.g. vary the initial value of λ_D between 1 nm to 20 nm). Running the script ten times resulted in a variance in λ_D of less than 5 %, and about 10 % in $F_{rp} - F_g$. Another indicator for errors is the 95 % confidence interval of the fit. Here, I computed an error in λ_D of about 3 %. Therefore, it appears that variance is not very high. However, the fact that different initial values provide different solutions indicates that I found local minima, showing that this fitting procedure is not yet optimal. Notwithstanding, this analysis method does show a lot of promise and provided physical values within a reasonable range.

7.4 Summary and conclusion

In this chapter I investigated the double layer forces between two glass surfaces in salt solutions. The solvent-characterising Debye length was found for 100 µM and 1 mM-NaCl solutions. Performing such an investigation on a 1 mM-NaCl solution at high hydrostatic pressures of up to 2200 kbar showed no significant change of the Debye length. Previously, other groups have shown that the properties of water change in a certain way up to about 2 kbar, which was attributed to a changing structure of water. Therefore, I conclude that high pressure-induced changes of the structure of water had no significant influence on these double-layer experiments.

In addition, I outlined a method that allows to analyse single approaches, which is a requirement to characterise attractive forces. One interesting force to investigate would be the hydrophobic force between two surfaces in water. It is not known what exactly the physical origin is of this attraction, and several hypotheses have been proposed [MRI06]. One such hypothesis is based on the occurrence of nanobubbles, leading to capillary forces [LZ15]. With the set-up at the Max Planck Institute, hydrostatic pressure can be regulated, which increases the vapour pressure and thus should suppress the attractive forces. Thus, this optical set-up in combination with the analysis method for single approaches that I described above could play a meaningful role in understanding attractive and hydrophobic forces.

Chapter 8

Conclusions

8.1 PNIPAM response to stimuli

8.1.1 Temperature collapse

Using a new optical method, I investigated the Brownian motion of a PNIPAM brush-coated glass bead on a planar glass surface. Through its Brownian motion, I observed two transitions in the viscoelastic properties of the coated bead: at 36 °C and 46 °C. The transitions were reversible, indicating that the brush returned to its original state when the temperature was lowered. From the two transitions, I found that the brush inter-phase between the bead and the planar surface determined the Brownian motion of the bead. The first transition at 36 °C described the volume collapse of PNIPAM brush and the subsequent increase of viscosity. The second transition described the complete collapse of the brush layer, at 46 °C. I modeled this transition by describing the polymer chains as linear combinations of springs that were either swollen or collapsed. In this model, changes in elasticity of the whole brush layer could only be observed when a high fraction of the polymer layer had collapsed. Therefore, a change in stiffness could only be observed once a majority of the brush was collapsed, observed at 46 °C. Within the inter-phase, the brush layer was heterogeneous, causing the two transitions in viscosity and stiffness to occur at different temperatures.

The two-stage collapse has implications for applications. On the theoretical side, it helps understand the phase transition of PNIPAM, the two-stage collapse indicates a type II phase transition, a classification indicated by some observations [HKW15]. In addition, I showed that the losses of the Brownian motion were dominated by viscous effects. As an example on the practical side, when using PNIPAM coatings as a contact layer for colloids, the functionality

depends on the viscoelastic properties. In this instance, although the PNIPAM collapse starts at 36 °C, more changes can occur at higher temperatures. Such a two-stage response can be either a downside or an upside, depending on the application.

8.1.2 Co-non-solvency collapse

The PNIPAM-coated beads could also be collapsed through exchange of solvent. Collapsing through solvent is not yet fully understood, in spite of being technologically interesting. In these experiments I used a flow cell that allowed exchange of the solvent from water to a mixture to ethanol back to water. Preferential binding is one leading hypothesis to explain the co-non-solvency collapse. My experiments provide support for the model of preferential binding of co-solvent molecules to PNIPAM, though the experiments need to be confirmed. Furthermore, these results underline that the co-non-solvency collapse differs on a molecular level from the collapse through temperature.

Another common configuration to make a PNIPAM coating is by coating with microgels. In such cases, the substrate is covered with microgel particles. Similar to the brushes that I investigated, microgels also undergo collapse and become stiffer. However, differences between brushes and microgels exist and are based on the different geometries. Though brushes are isotropic along the surface, there is anisotropy away from the surface. In contrast, microgels themselves are highly anisotropic, and using microgels to coat surfaces therefore introduces this anisotropy. As a result, the response mechanisms of PNIPAM brushes and microgels are similar, yet different, which has to be taken into account in applications.

8.2 Optical interference method for Brownian motion

I developed a method to investigate viscoelastic properties of single coated colloids that adhered to a surface. The method and analyses the Brownian motion of the colloid through the power spectral density of the Brownian motion (see chapter 3). The experiments showed that the method works well in various situations, with controllable temperatures and solvent compositions. Hence, the method is highly versatile.

Various methods exist that are used for the characterisation of PNIPAM, as described in the introduction. The method that I developed differs from these other techniques. Single coated colloids can be measured and observed in changing environments. The basis is optics, and thus the method is non-invasive. Moreover, since the Brownian motion is measured, direct measurement of the viscoelastic properties of colloids in situ is possible, and potentially measurements in operando. Furthermore, sample preparation is fairly simple, and multiple colloids can be measured in quick succession in identical situations. Thus, this method fulfills an important niche within the range of existing techniques.

8.3 High hydrostatic pressure and the double layer force

Besides PNIPAM, I also investigated one essential interaction, the double layer force. The range of the double layer force depends on the the Debye length. Specifically, in my experiments I determined the Debye length of NaCl solutions in water at high hydrostatic pressures of up to 2.2 kbar. I found that the Debye length of a 1 mM-NaCl solution did not change significantly upon increasing the pressure. Hence, though literature shows that properties of water change with increasing pressure up to 2 kbar, this had no significant influence on the Debye length. Likely, changes in water's properties happen close to the surfaces, and did not much influence the ions between the two surfaces that form the double layer.

8.4 Outlook and further studies

8.4.1 Response of PNIPAM to stimuli

Hydrostatic pressure

PNIPAM has been reported to respond to pressure as well. The effect of pressure on PNIPAM is largely similar to temperature, and the collapsed state is preferred at pressures a little below 2 kbar at 20 °C [Ota+93; Ebe+14]. Yet, other studies indicate that though similar, pressure does hydrate the collapsed state of PNIPAM at high temperatures [Nie+17], indicating that the effect of pressure is not the same as that of temperature. Since the set-up includes a high-pressure pump and optical cell, measuring PNIPAM at high pressure

is possible. Furthermore, to my knowledge the effect of pressure on the two-stage collapse of PNIPAM has not been investigated before. Therefore, it would be interesting to investigate whether pressure shifts both transitions to lower temperatures or whether pressure affects the two transitions differently.

Temporal response of PNIPAM

The kinetics of the response to external stimuli are relevant for the development of PNIPAM's applications such as sensors or actuators, as well as for a better understanding of the collapse in general. The method that I developed measures the power spectrum of the Brownian motion. Typically in my experiments, the interesting feature was the cut-off frequency of this spectrum, which ranged from about ten to a hundred Hertz. Hence, responses to stimuli that occur at a slower rate than this can be observed. In chapter 6, I showed that this was the case after a solvent exchange from ethanol-to-water of PNIPAM, which occurred over about an hour. Thus, the method I developed can also be applied to investigate kinetics of stimuli-responsive polymer coatings.

In my experiments, exchanging the solvent took about a minute, long compared to the rate of the Brownian motion. Pressure jumps are technologically possible, with response times in the order of milliseconds, a lot faster than is possible for temperature [MCC93]. Indeed, since both temperature and pressure affect the state of PNIPAM, such jumps were used to investigate early stages of phase separation, e.g. by Niebuur et al. using a neutron scattering technique [Nie+17]. The set-up that I used does include equipment for experiments at high hydrostatic pressure up to kilobars. Hence, adapting this set-up to allow quick pressure jumps allows investigating of PNIPAM-coated colloids and the kinetics of their response to stimuli.

8.4.2 Outlook on the set-up

Dual-beam interference

My experiments were done with one interference laser. A big advantage is that the set-up is very easy to use. However, the simplicity of the set-up prevented a quantitative measure of D (see section 3.4.1) Adding another laser could prove useful. Introducing a second laser with a different wavelength would allow determining D in $\mathrm{m^2\,s^{-1}}$ [LS09]. This determining of D in more useful units would be allowed because both beam intensities can be controlled, and the beam reflectivities are similar for differing wavelengths, e.g. $\lambda = 535\,\mathrm{nm}$

and 635 nm [Pol]. Consequently, in a dual beam set-up there are the same two unknowns as in the single beam case, yet one extra equation is gained that allows to determine d quantitatively.

Smaller beam spot to extend range of possible samples

In this thesis I characterised coated beads at an uncoated planar surface. However, using the same beads but uncoated it was not possible to characterise a coated planar surface. The reason was the relative size of the laser focus to the bead radius. I argued that the beam spot size was larger than the inter-phase area, and leading to unwanted reflections that were especially pronounced in the coated-planar-surface measurements. Using a different microscope objective, it may be possible to obtain a smaller spot size. In this way, a spot size of a few hundred nanometers can be achieved. Thus, exchanging the microscope objective in the set-up can lead to characterising the planar brush, and also coated colloids with smaller radii.

Acknowledgements

I am lucky to thank many people who have contributed to the making of this thesis.

First of all, thank you, Hans-Jürgen, for having me in the group and offering this place and leading the group to do this research. Moreover, thank you for all your advice. Also thank you, Regine, for being my second supervisor from Darmstadt. Thanks especially to Rüdiger for daily supervision - I feel very lucky to have had you supervising me. I've learned so much during my time as a PhD candidate, most things from you. I also really want to thank you for all discussions and your open-door policy. We've had many discussions, and I've always felt like my opinions and my input were welcome and respected. I've really enjoyed and appreciated also the test talks of our groups, along with Stefan's group. Of course, many of the things were done within the group, whom I wish to thank! Here, I wish to name Amy and Alex specifically: you've made our office incredibly nice, interesting, and fun – pre-corona at least. Also thanks to my old office mates and our neighboring office, Alex, Amelie, Changguo, Chao, Chia-Ming, Chris, Diana, Helma, Ilka, Maren, Marjan, Ngoc, Nikhilendu, Ragini, Simon, Thomas, Uwe, Yujiao, and Xiaomei. A little extra thanks to Alex: your hospitality and friendship after meeting the group for the first time really convinced me to make the move to Mainz. I was lucky enough to find some great housemates like Claudio, who made life in Mainz enjoyable. Also many thanks to entire AK-Butt for being great colleagues. At the MPIP, we're lucky enough to have support with some of the technical aspects: many thanks for this to Gunnar, Mr. Becker, the electronics lab, and the Haustechnik.

Finally, completing a PhD without moral support is hard. However, with finishing this thesis I am now very close! Thanks to my family: Carolien, Emmelien, Ferdi, Kari-Anne, Nathaniël, Chris, and Floris - and my other family, George, Nancy and Wendy! Also thanks to my oldest friends, Anne, Casper, Guus, and Timen. Thanks for your support and interest, and practical support even, it means a lot! And thanks to oma, you were so proud of me and always so interested. Finally, a special thanks to Amy - I've been lucky enough to have run into you. Even the 'kick in the butt' that Rüdiger asked you to convey to me has helped. Your support and help definitely helped finish this thesis. I am so lucky to have run into you here in Mainz - you make me happy.

Appendix A

Matlab script to fit a single approach of a bead

The figure provides an example data set to explain the names of the data sets that were used in the Matlab script. The main input for the script is the black line, called *signal*. The data set called *timeWallEffect* is a vector containing the moments in *time* of the minima and maxima of *signal* that occur within the approach time, the star point is one such example.

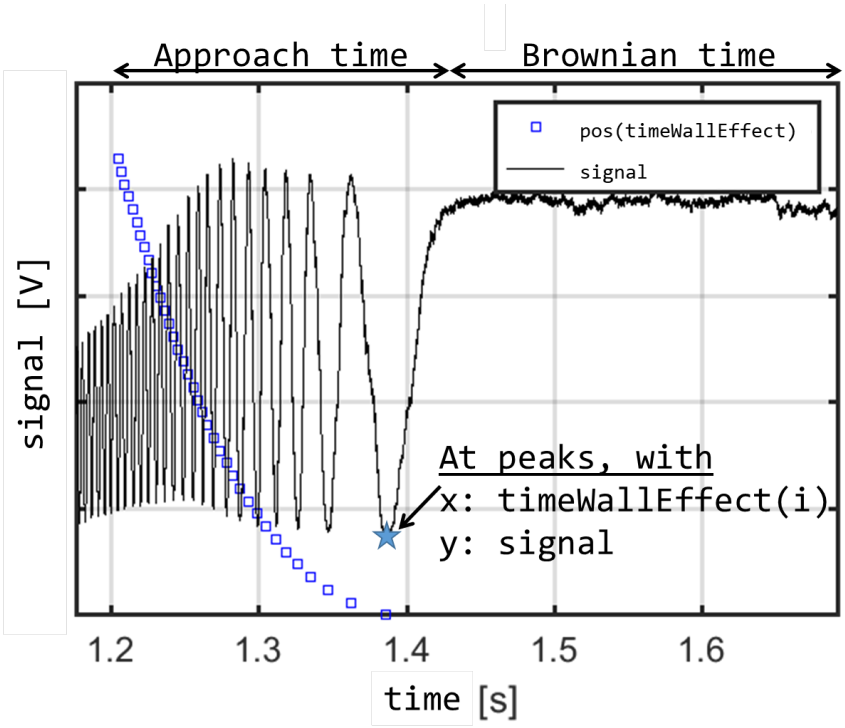

Table of Contents


```
% David van Duinen - July 2020.

% Script to fit I_APD vs time data to a differential equation that
% describes a bead that approaches a surface, in water, under the
 effect of
% the electric double layer.


% Fill time and pos with time and position in WallEffect region:
t = [];
pos = [];
errpos = [];

errI_APD = 0.02;

length_in_Brownian = 2;     % How many multiples of the approach
 (time) the brownian should last.

NoImagD_temp = 0;
for i = 1:length(timeWallEffect)-1
    if i == 1
        [~, locPeak] = min(abs(time-timeWallEffect(i)));
        [~, locPeakPlus1] = min(abs(time-timeWallEffect(i+1)));
        FirstlocPeak = locPeak;
    else
        locPeak = locPeakPlus1+1;
        [~, locPeakPlus1] = min(abs(time-timeWallEffect(i+1)));
    end


    time_temp = time(locPeak:locPeakPlus1);
    signal_temp = signal(locPeak:locPeakPlus1);


    PeakVals = [mean(signal(locPeak-4:locPeak+4))
 mean(signal(locPeakPlus1-4:locPeakPlus1+4))];
    Imax = max(PeakVals);
    Imin = min(PeakVals);

    i_plusminus_temp = mod(size(timeWallEffect),2);
    if i_plusminus_temp(2) == 1
```

```
        i_plusminus = 1;
    else
        i_plusminus = 0;
    end
    clear i_plusminus_temp

    D_temp =      acos(PlusMinus*((-1)^(i+i_plusminus)).*(2.*
 signal_temp              - (Imax+Imin))./abs(Imax-Imin)).*lambda./
(4*nMedium*pi) + (length(timeWallEffect)-i+1)*lambda/(4*nMedium);
    D_temp_min =  acos(PlusMinus*((-1)^(i
+i_plusminus)).*(2.*(signal_temp - errI_APD) - (Imax+Imin))./abs(Imax-
Imin)).*lambda./(4*nMedium*pi) + (length(timeWallEffect)-i+1)*lambda/
(4*nMedium);
    D_temp_min(imag(D_temp_min) ~= 0) = NaN;    % Remove nonreal
 elements
    D_temp_plus = acos(PlusMinus*((-1)^(i
+i_plusminus)).*(2.*(signal_temp + errI_APD) - (Imax+Imin))./abs(Imax-
Imin)).*lambda./(4*nMedium*pi) + (length(timeWallEffect)-i+1)*lambda/
(4*nMedium);
    D_temp_plus(imag(D_temp_plus) ~= 0) = NaN;    % Remove nonreal
 elements
    errD_temp = nanmax(abs(D_temp_min-D_temp), abs(D_temp_plus-
D_temp));
    clear D_temp_min D_temp_plus


    for j = 1:length(D_temp)
        if isreal(D_temp(j)) == 0
            D_temp(j) = NaN;
            NoImagD_temp = NoImagD_temp + 1;
        end
    end


    pos = [pos -D_temp.'];
    errpos = [errpos errD_temp.'];
    t = [t time_temp];
    clear time_temp D_temp signal_temp PeakVals
end

% And after the last peak:
DAfterPeak = acos(PlusMinus.*(2.*signal(locPeakPlus1+1:locPeakPlus1
 + length_in_Brownian*(locPeakPlus1-FirstlocPeak)) - (Imax+Imin))./
abs(Imax-Imin)).*lambda./(4*nMedium*pi) + lambda/(4*nMedium);
timeAfterPeak = time(locPeakPlus1+1:locPeakPlus1 +
 length_in_Brownian*(locPeakPlus1-FirstlocPeak));
DAfterPeak_min =
 acos(PlusMinus.*(2.*(signal(locPeakPlus1+1:locPeakPlus1 +
 length_in_Brownian*(locPeakPlus1-FirstlocPeak))-errI_APD) - (Imax
+Imin))./abs(Imax-Imin)).*lambda./(4*nMedium*pi) + lambda/(4*nMedium);
DAfterPeak_min(imag(DAfterPeak_min) ~= 0) = NaN;    % Remove nonreal
 elements
DAfterPeak_plus =
 acos(PlusMinus.*(2.*(signal(locPeakPlus1+1:locPeakPlus1 +
```

```
 length_in_Brownian*(locPeakPlus1-FirstlocPeak))+errI_APD) - (Imax
+Imin))./abs(Imax-Imin)).*lambda./(4*nMedium*pi) + lambda/(4*nMedium);
DAfterPeak_plus(imag(DAfterPeak_plus) ~= 0) = NaN;    % Remove nonreal
 elements
errDAfterPeak = nanmax(abs(DAfterPeak_min-DAfterPeak),
 abs(DAfterPeak_plus-DAfterPeak));
clear DAfterPeak_min DAfterPeak_plus

NoImagD_temp = 0;
for j = 1:length(DAfterPeak)
    if isreal(DAfterPeak(j)) == 0
        DAfterPeak(j) = NaN;
        NoImagD_temp = NoImagD_temp + 1;
    end
end

pos = [pos -DAfterPeak.' ];
errpos = [errpos errDAfterPeak.' ];
t = [t timeAfterPeak ];

time_oa = t;
D_oa = pos;


% Clear some variables that are used in this script, be sure to not
 use
% values of an old script.:
clear B B0 LB_B UB_B
```

Re-define the position and time vectors and prepare these for fitting:

clear errpos In case no error of the position is known, make them all equal:

```
if exist('errpos', 'var') == 0
    errpos = ones(size(D_oa));
end

[Time, Position, Weights] = prepareCurveData( time_oa, D_oa.*1e6, 1./
((errpos.*1e6).^2) );

% In case it is desired to fit until some maximum time:
maxTime = 1000;         % [s]

[~,maxTimeLoc] = min(abs(Time-maxTime));
Time = Time(1:maxTimeLoc);
Position = Position(1:maxTimeLoc);
Weights = Weights(1:maxTimeLoc);

Weights = Weights./max(Weights);            % Normalise weights, for
 the sake of the fitting.
warning('off','curvefit:prepareFittingData:removingNaNAndInf')
```

Starting positions:

```
B0(1) = 10*rand(1);                  % F_rp [pN]
B0(2) = 4 + 0.9*(rand(1)-0.5);    % R [um]  From manufacturer: 4+-0.45
 um diameter.
B0(3) = rand(1);                     % Z [nN]
B0(4) = 15+20*rand(1);               % lambdaD [nm]
B0(5) = Position(1);                 % D0
B0(6) = 0;                           % ddD0

% Bounds:
LB_B = [0     0 0 0 -10     -inf];
UB_B = [100    10 10 10000 0    inf];

% Other options for fitting:
options = optimoptions('lsqcurvefit','Display','iter');
options.MaxFunEvals = 1000;
options.TolFun = 1e-9;      % Standard is 1e-6.
options.TolX = 1e-9;        % Standard is 1e-6.
options.Algorithm = 'trust-region-reflective';  % 'trust-region-
reflective' (default) and 'levenberg-marquardt'
options.FinDiffType = 'central';
options.Diagnostics = 'off';

% Make weighin factor a global variable, so it can be used within
 another
% function as well.
global WeightsFittingODE
WeightsFittingODE = Weights;
```

Fit the data to the differential equation that is defined below:

```
f = @NonlinearBeadApproach2;
[B,Rsdnrm,Rsd,ExFlg,OptmInfo,Lmda,Jmat] = lsqcurvefit(f, B0, Time,
 WeightsFittingODE.*Position, LB_B, UB_B, options);
Rsquare = 1 - Rsdnrm / norm(WeightsFittingODE.*Position-
mean(WeightsFittingODE.*Position))^2;

% Calculate errors according to the confidence interval:
conf = nlparci(B,Rsd,'jacobian',Jmat);


% Errors of the fit:
fit_errors = (conf(:,2) - conf(:,1))./2;
```

Plot and calculate the fit along the original data:

```
FitData = NonlinearBeadApproach2(B,Time,1);
```

```
FitData = FitData./WeightsFittingODE;

figure
ax1 = subplot(30,1,1:1:22);
plot(Time,Position.*1e3)
hold on
plot(Time,FitData.*1e3)
set(gca,'Xticklabel',[])
ylabel('{\it{d}} [nm]')
xlim([min(Time) max(Time)])
legend('Data', ['\newline{\bf{Fit (R^2: ',
 mat2str(Rsquare,4),')}}\newline\lambda_D = ', mat2str(B(4),3),'
 nm\newline{\it{F}}_0 = ', mat2str(1/B(4)*B(3)*B(2)*1e3,3),' nN
\newline{\it{F}}_{rp} = ', mat2str(B(1),3),' pN\newline{\it{R}} = ',
 mat2str(B(2),3), ' ',char(181),'m'])
legend('location', 'best')
legend boxoff
set(gca, 'fontsize', 16)


% Residuals:
ax2 = subplot(30,1,25:1:29);
plot(Time,Rsd.*1e3./WeightsFittingODE)
hold on
plot(Time,zeros(size(Time)),'color','red')
ylabel('Res [nm]')
xlabel('Time [s]')
xlim([min(Time) max(Time)])
set(gca, 'fontsize', 16)

linkaxes([ax1,ax2],'x')
set(gcf, 'Position', [1190 313 700 480])
```

Define the function NonlinearBeadApproach2:

```
function FitPos = NonlinearBeadApproach2(B, t, ~)

% Starting values:
x0 = B(end-1:end);

% Matlab offers various ODE solvers.  I found that ode15s can solve
% quickest.  However, it may not be optimal.  I attempted the others
 that
% are now commented out (45, 23s, 113).  These work as well, but take
 much
% longer, by a factor of about 10.

% [t,D] = ode45(@NonlinearBeadApproach1, t, x0);
[t,D] = ode15s(@NonlinearBeadApproach1, t, x0);
%  [t,D] = ode23s(@NonlinearBeadApproach1, t, x0);
%  [t,D] = ode113(@NonlinearBeadApproach1, t, x0);
```

```
function dDdt = NonlinearBeadApproach1(t, D)


    dDdt = zeros(2,1);
    dDdt(1) = D(2);



    % [200622] Try to make it work better:

    dDdt = nan(2,1);
    dDdt(1) = D(2);


    % We're gonna fit position (in negative um) to time (in
seconds).
    % where:
    B(1);   % Frp in pN
    B(2);   % R in um
    B(3);   % Z in nN
    B(4);   % lambdaD  in nm

    % Which I then convert to um and N:
    F_rp_func = B(1)*1e-12;                          % [N]
    R_func = B(2);                                   % [um]
    Z_func = B(3)*1e-9;                              % [N]
    lambda_D_func = B(4)*1e-3;                       % [um]

    % Introducing some constants (in SI but um):
    rho_func = 2.5518e-15;                           % [kg/um3]
    eta_func = 0.91073e-15;                          % [N s/um2]

    % Calculate the mass
    m_func = 4/3*pi*R_func^3*rho_func;               % [kg]

    % Calculate values for beta drag factors:
    beta_Stokes = 6*pi*eta_func*R_func;              % [N s/um]

    % There are several ways to define the drainage factor.
    % The approximatoin by Butt and Kappl:
    if 1 == 1
        beta_d = ( 1 + R_func/abs(D(1)) );              % [-]
    end

    % An approximation by Cox and Brenner:
    if 1 == 11
        beta_d = R_func/abs(D(1)) + 1/5*log(R_func/abs(D(1))) +
0.971264;
    end

    % Alternatively, I can compute the 'analytical' value of
    % beta_d, according to Brenner.  N>200 gives problems with
    % the hyperbolic sine.  Leading to beta_d:
```

```
        if 1 == 11
            clear SUM
            SUM = 0;
            N = 200;
            alphaC = acosh(1+abs(D(1))./R_func);
            for n = 1:N
                FRAC1 = ( n.*(n+1) )./( (2*n-1).*(2*n+3) );
                NOM2 = 2.*sinh((2*n+1).*alphaC) + (2*n
+1).*sinh(2.*alphaC);
                DENOM2 = 4.*sinh((n+0.5).*alphaC).^2 - (2.*n
+1).^2.*sinh(alphaC).^2;
                SUM = SUM + FRAC1.*(NOM2./DENOM2 - 1);
                % Hyperbolic sine (sinh) is a quickly increasing
 function.  The following
                % lines can be used to find the value of n at which
 sinh returns
                % inf instead of a value.  However, it is costly to
 run.
                %         if sum(isnan(SUM)) ~= 0
                %             (['n=',num2str(n)])
                %             return
                %         end
                clear FRAC1 NOM2 DENOM2
            end
            beta_d = 4/3.*sinh(alphaC) .* SUM;          % [-]

        end


        F0_func = 1/lambda_D_func*R_func*Z_func;        % [N]

        dDdt(2) = 1e6*1/m_func*(...                          % [kg-1]
            - beta_Stokes * beta_d * D(2)...            % [N]
            - F0_func*exp( -abs(D(1))/lambda_D_func )...% [N]
            + F_rp_func...                              % [N]
            );

    end


% Add weighing factor:
global WeightsFittingODE

% Sometimes, Matlab does not solve properly and returns D that is
 shorter
% than it should be.  Do a check here, and display the length as an
% indication of what went wrong:
AA = size(WeightsFittingODE);
BB = size(D);
if AA~=BB
    disp('AA is size of weights, BB is the size of the found D.  AA
 and BB should be equal.')
    disp(['AA:',mat2str(AA),'\newlineBB = ',mat2str(BB)])
end
```

```
FitPos = WeightsFittingODE.*D(:,1);

end
```

Published with MATLAB® R2019a

Appendix B

Radiation pressure force

In the optical trap experiments, the radiation pressure force, F_{rp}, is proportional to the laser power. The laser power was controlled and increased, while the bead was monitored using interference. Through the method described in chapter 7, I obtained F_{rp} that the laser exerted on the bead. Here, it is clear that F_{rp} is proportional to the laser power (Fig. B.1). Fitting this with a linear function provided that for each watt of laser power, F_{rp} increased by 127 pN. Furthermore, the y-intercept (-3.7 pN) corresponds to the weight of the bead. This value compares well to the calculated value, using a radius of 4 µm, and a bead density of 2.55 g cm^{-3}.

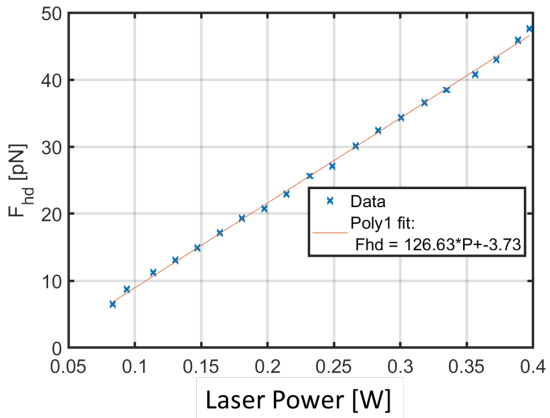

FIGURE B.1: Radiation pressure force is proportional with laser power. The data is the same as in Fig. 7.5.

Bibliography

[Ahm+09] Z. Ahmed, E. A. Gooding, K. V. Pimenov, L. Wang, and S. A. Asher. "UV resonance Raman determination of molecular mechanism of poly(*N*-isopropylacrylamide) volume phase transition". In: *J. Phys. Chem. B* 113 (2009), pp. 4248–4256.

[Ale77] S Alexander. "Adsorption of chain molecules with a polar head a scaling description". In: *Journal De Physique* 38 (1977), pp. 983–987.

[Ash70] A. Ashkin. "Acceleration and trapping of particles by radiation pressure". In: *Phys. Rev. Lett.* 24 (1970), pp. 156–159.

[BGK03] H.-J. Butt, K. Graf, and M. Kappl. *Physics and Chemistry of Interfaces*. Wiley-VCH Verlag & Co. KGaA, 2003.

[BK10] H.-J. Butt and M. Kappl. *Surface and interfacial forces*. Weinheim: Wiley-VCH, 2010.

[BSF04] K. Berg-Sørensen and H. Flyvbjerg. "Power spectrum analysis for optical tweezers". In: *Rev. Sci. Instrum.* 75 (2004), pp. 594–612.

[Bac+17a] S. Backes, P. Krause, W. Tabaka, M. U. Witt, and R. von Klitzing. "Combined Cononsolvency and Temperature Effects on Adsorbed PNIPAM Microgels". In: *Langmuir* 33 (2017), pp. 14269–14277.

[Bac+17b] S. Backes, P. Krause, W. Tabaka, M. U. Witt, D. Mukherji, K. Kremer, and R. von Klitzing. "Poly(*N*-isopropylacrylamide) Microgels under Alcoholic Intoxication: When a LCST Polymer Shows Swelling with Increasing Temperature". In: *ACS Macro Lett.* 6 (2017), pp. 1042–1046.

[Bal+03] S. Balamurugan, S. Mendez, S. S. Balamurugan, t. O'Brien M. J., and G. P. López. "Thermal Response of Poly(*N*-isopropylacrylamide) Brushes Probed by Surface Plasmon Resonance". In: *Langmuir* 19 (2003), pp. 2545–2549.

[Bas+12] N. Bassim, B. De Gregorio, A. Kilcoyne, K Scott, T Chou, S Wirick, G Cody, and R. Stroud. "Minimizing damage during

FIB sample preparation of soft materials". In: *J. Microsc.* 245 (2012), pp. 288–301.

[Bon+17] G. Boniello, J. Malinge, C. Tribet, E. Marie, and D. Zanchi. "Reversible and dynamical control of aggregation and soft adhesion of T-responsive polymer-coated colloids". In: *Colloids Surf., A* 532 (2017), pp. 510–515.

[Bra+09] C. Bradley, N. Jalili, S. K. Nett, L. Q. Chu, R. Förch, J. S. Gutmann, and R. Berger. "Response Characteristics of Thermoresponsive Polymers Using Nanomechanical Cantilever Sensors". In: *Macromol. Chem. Phys.* 210 (2009), pp. 1339–1345.

[Bre61] H. Brenner. "The slow motion of a sphere through a viscous fluid towards a plane surface". In: *Chem. Eng. Sci.* 16 (1961), pp. 242–251.

[Bum+04] G. G. Bumbu, G. Kircher, M. Wolkenhauer, R. Berger, and J. S. Gutmann. "Synthesis and Characterization of Polymer Brushes on Micromechanical Cantilevers". In: *Macromol. Chem. Phys.* 205 (2004), pp. 1713–1720.

[Bur+10] E. Burdukova, H. Li, N. Ishida, J. P. O'Shea, and G. V. Franks. "Temperature controlled surface hydrophobicity and interaction forces induced by poly (*N*-isopropylacrylamide)". In: *J. Colloid Interface Sci.* 342 (2010), pp. 586–592.

[Bur+11a] A. Burmistrova, M. Richter, C. Uzum, and R. von Klitzing. "Effect of cross-linker density of P(NIPAM-co-AAc) microgels at solid surfaces on the swelling/shrinking behaviour and the Young's modulus". In: *Colloid Polym. Sci.* 289 (2011), pp. 613–624.

[Bur+11b] A. Burmistrova, M. Richter, M. Eisele, C. Üzüm, and R. von Klitzing. "The effect of co-monomer content on the swelling/shrinking and mechanical behaviour of individually adsorbed PNIPAM microgel particles". In: *Polymers* 3 (2011), pp. 1575–1590.

[But+99] H.-J. Butt, M. Kappl, H. Mueller, R. Raiteri, W. Meyer, and J. Rühe. "Steric Forces Measured with the Atomic Force Microscope at Various Temperatures". In: *Langmuir* 15 (1999), pp. 2559–2565.

[Bv18] S. Backes and R. von Klitzing. "Nanomechanics and Nanorheology of Microgels at Interfaces". In: *Polymers* 10 (2018), p. 978.

[CV98] H. Crowther and B Vincent. "Swelling behavior of poly-*N*-isopropylacrylamide microgel particles in alcoholic solutions". In: *Colloid Polym. Sci.* 276 (1998), pp. 46–51.

[Che+05] X. Cheng, H. E. Canavan, M. J. Stein, J. R. Hull, S. J. Kweskin, M. S. Wagner, G. A. Somorjai, D. G. Castner, and B. D. Ratner. "Surface Chemical and Mechanical Properties of Plasma-Polymerized *N*-isopropylacrylamide". In: *Langmuir* 21 (2005), pp. 7833–7841.

[Che+11] C. K. Chee, B. J. Hunt, S. Rimmer, I. Soutar, and L. Swanson. "Time-resolved fluorescence anisotropy studies of the cononsolvency of poly(*N*-isopropyl acrylamide) in mixtures of methanol and water". In: *Soft Matter* 7 (2011), pp. 1176–1184.

[Chr+16] S. Christau, T. Möller, F. Brose, J. Genzer, O. Soltwedel, and R. von Klitzing. "Effect of gold nanoparticle hydrophobicity on thermally induced color change of PNIPAM brush/gold nanoparticle hybrids". In: *Polymer* 98 (2016), pp. 454–463.

[DG87] P. De Gennes. "Polymers at an interface; a simplified view". In: *Adv. Colloid Interface Sci.* 27 (1987), pp. 189–209.

[DG91] P.-G. De Gennes. "A second type of phase separation in polymer solutions". In: *C.R. Acad. Sci. Paris II* 313 (1991), pp. 1117–1122.

[DH23] P. Debye and E. Hückel. "The theory of electrolytes. I. Freezing point depres-sion and related phenomena [Zur Theorie der Elektrolyte. I. Gefrierpunktserniedrigung und verwandte Erscheinungen]". In: *Phys. Z.* 24 (1923), pp. 185–206.

[Ebe+14] B. Ebeling, S. Eggers, M. Hendrich, A. Nitschke, and P. Vana. "Flipping the pressure-and temperature-dependent cloud-point behavior in the cononsolvency system of poly(*N*-isopropylacrylamide) in water and ethanol". In: *Macromolecules* 47 (2014), pp. 1462–1469.

[Fer+10] P. A. Fernandes, S. Schmidt, M. Zeiser, A. Fery, and T. Hellweg. "Swelling and mechanical properties of polymer gels with crosslinking gradient". In: *Soft Matter* 6 (2010), pp. 3455–3458.

[Fra+11] T. Franosch, M. Grimm, M. Belushkin, F. M. Mor, G. Foffi, L. Forró, and S. Jeney. "Resonances arising from hydrodynamic memory in Brownian motion". In: *Nature* 478 (2011), pp. 85–88.

[GKB04] D. Goodman, J. N. Kizhakkedathu, and D. E. Brooks. "Attractive Bridging Interactions in Dense Polymer Brushes in Good

Solvent Measured by Atomic Force Microscopy". In: *Langmuir* 20 (2004), pp. 2333–2340.

[Gil+00] T. Gilányi, I. Varga, R. Mészáros, G. Filipcsei, and M. Zrínyi. "Characterisation of monodisperse poly(*N*-isopropylacrylamide) microgel particles". In: *Phys. Chem. Chem. Phys.* 2 (2000), pp. 1973–1977.

[HD09] S. M. Hashmi and E. R. Dufresne. "Mechanical properties of individual microgel particles through the deswelling transition". In: *Soft Matter* 5 (2009), pp. 3682–3688.

[HG68] M. Heskins and J. E. Guillet. "Solution Properties of Poly(*N*-isopropyl-acrylamide)". In: *J. Macromol. Sci., Chem.* 2 (1968), pp. 1441–1455.

[HHT87] S. Hirotsu, Y. Hirokawa, and T. Tanaka. "Volume-phase transitions of ionized *N*-isopropylacrylamide gels". In: *J. Chem. Phys.* 87 (1987), pp. 1392–1395.

[HKW15] A. Halperin, M. Kröger, and F. M. Winnik. "Poly(*N*-isopropylacrylamide) Phase Diagrams: Fifty Years of Research". In: *Angew. Chem. Int. Ed.* 54 (2015), pp. 15342–15367.

[HWW18] B. A. Humphreys, E. J. Wanless, and G. B. Webber. "Effect of ionic strength and salt identity on poly(*N*-isopropylacrylamide) brush modified colloidal silica particles". In: *J. Colloid Interface Sci.* 516 (2018), pp. 153–161.

[Har+03] M. Hartmann, F. Pfeifer, G. Dornheim, and K. Sommer. "HPDS-Hochdruckzelle zur Beobachtung mikroskopischer Phänomene unter Hochdruck". In: *Chem. Ing. Tech.* 75 (2003), pp. 1763–1767.

[Hel+16] J. Hellwig, S. Micciulla, J. Strebe, and R. von Klitzing. "Separation of Storage and Loss Modulus of Polyelectrolyte Multilayers on a Nanoscale: a Dynamic AFM Study". In: *Langmuir* 32 (2016), pp. 10505–10512.

[Hir91] S. Hirotsu. "Softening of bulk modulus and negative Poisson's ratio near the volume phase transition of polymer gels". In: *J. Chem. Phys.* 94 (1991), pp. 3949–3957.

[Hum+16] B. A. Humphreys, J. D. Willott, T. J. Murdoch, G. B. Webber, and E. J. Wanless. "Specific ion modulated thermoresponse of poly(*N*-isopropylacrylamide) brushes". In: *Phys. Chem. Chem. Phys.* 18 (2016), pp. 6037–6046.

[Hum+19a] B. A. Humphreys, S. W. Prescott, T. J. Murdoch, A. Nelson, E. P. Gilbert, G. B. Webber, and E. J. Wanless. "Influence of molecular

weight on PNIPAM brush modified colloidal silica particles". In: *Soft Matter* 15 (2019), pp. 55–64.

[Hum+19b] B. A. Humphreys, E. C. Johnson, E. J. Wanless, and G. B. Webber. "Poly(*N*-isopropylacrylamide) Response to Salt Concentration and Anion Identity: A Brush-on-Brush Study". In: *Langmuir* 35 (2019), pp. 10818–10830.

[IB07] N. Ishida and S. Biggs. "Direct Observation of the Phase Transition for a Poly(*N*-isopropylacrylamide) Layer Grafted onto a Solid Surface by AFM and QCM-D". In: *Langmuir* 23 (2007), pp. 11083–11088.

[IB10] N. Ishida and S. Biggs. "Effect of Grafting Density on Phase Transition Behavior for Poly(*N*-isopropylacrylamide) Brushes in Aqueous Solutions Studied by AFM and QCM-D". In: *Macromolecules* 43 (2010), pp. 7269–7276.

[Isr11a] J. N. Israelachvili. "Electrostatic Forces between Surfaces in Liquids". In: *Intermolecular and Surface Forces*. Third Edition. Academic Press, 2011. Chap. 14, pp. 291–340.

[Isr11b] J. N. Israelachvili. "Steric (Polymer-Mediated) and Thermal Fluctuation Forces". In: *Intermolecular and Surface Forces*. Third Edition. Academic Press, 2011. Chap. 16, pp. 381–413.

[Ito+05] Y. Ito, T. Ito, H. Takaba, and S.-i. Nakao. "Development of gating membranes that are sensitive to the concentration of ethanol". In: *J. Membr. Sci.* 261 (2005), pp. 145–151.

[JBJ10] M. J. N. Junk, R. Berger, and U. Jonas. "Atomic Force Spectroscopy of Thermoresponsive Photo-Cross-Linked Hydrogel Films". In: *Langmuir* 26 (2010), pp. 7262–7269.

[KFA90] K. Kubota, S. Fujishige, and I. Ando. "Solution properties of poly(*N*-isopropylacrylamide) in water". In: *Polym. J.* 22 (1990), pp. 15–20.

[KM15] M. Kuroda and Y. Murayama. "Simple method to measure and analyze the fluctuations of a small particle in biopolymer solutions". In: *Rev. Sci. Instrum.* 86 (2015), p. 125105.

[Kam+17] S. Kametani, S. Sekine, T. Ohkubo, T. Hirano, K. Ute, H. N. Cheng, and T. Asakura. "NMR studies of water dynamics during sol-to-gel transition of poly(*N*-isopropylacrylamide) in concentrated aqueous solution". In: *Polymer* 109 (2017), pp. 287–296.

[Kha+12] I. S. Khattab, F. Bandarkar, M. A. A. Fakhree, and A. Jouyban. "Density, viscosity, and surface tension of water+ ethanol mixtures from 293 to 323K". In: *Korean J. Chem. Eng.* 29 (2012), pp. 812–817.

[Klo15] L. Klouda. "Thermoresponsive hydrogels in biomedical applications: A seven-year update". In: *Eur. J. Pharm. Biopharm.* 97 (2015), pp. 338–349.

[Koo+12] E. S. Kooij, X. Sui, M. A. Hempenius, H. J. Zandvliet, and G. J. Vancso. "Probing the Thermal Collapse of PNIPAM Grafts by Quantitative in Situ Ellipsometry". In: *J. Phys. Chem. B* 116 (2012), pp. 9261–9268.

[Kyr+16] K. Kyriakos, M. Philipp, L. Silvi, W. Lohstroh, W. Petry, P. Müller-Buschbaum, and C. M. Papadakis. "Solvent Dynamics in Solutions of PNIPAM in Water/Methanol Mixtures — A Quasi-Elastic Neutron Scattering Study". In: *J. of Phys. Chem. B* 120 (2016), pp. 4679–4688.

[LG97] D. S. Lemons and A. Gythiel. "Paul Langevin's 1908 paper "on the theory of Brownian motion"["Sur la théorie du mouvement brownien," CR Acad. Sci.(Paris) 146, 530–533 (1908)]". In: *Am. J. Phys.* 65 (1997), pp. 1079–1081.

[LMF16] E. W. Lemmon, M. O. McLinden, and D. G. Friend. *Thermophysical Properties of Fluid Systems in NIST Chemistry WebBook, NIST Standard Reference Database Number 69, edited by P.J. Linstrom and W.G. Mallard (National Institute of Standards and Technology, Gaithersburg MD, 20899)*. 2016.

[LR13] T. C. Li and M. G. Raizen. "Brownian motion at short time scales". In: *Ann. Phys. (Berlin, Ger.)* 525 (2013), pp. 281–295.

[LS09] L. Limozin and K. Sengupta. "Quantitative reflection interference contrast microscopy (RICM) in soft matter and cell adhesion". In: *ChemPhysChem* 10 (2009), pp. 2752–2768.

[LZ15] D. Lohse and X. Zhang. "Surface nanobubbles and nanodroplets". In: *Rev. Mod. Phys.* 87 (2015), p. 981.

[Lan08] P. Langevin. "Sur la théorie du mouvement brownien". In: *C. R. Acad. Sci. (Paris)* 146 (1908), pp. 530–533.

[Liu+12] L. Liu, X.-L. Song, X.-J. Ju, R. Xie, Z. Liu, and L.-Y. Chu. "Conversion of alcoholic concentration variations into mechanical force via core–shell capsules". In: *J. Phys. Chem. B* 116 (2012), pp. 974–979.

[Lor07] H. A. Lorentz. *Abhandlungen über theoretische Physik*. BG Teubner, 1907.

[Luk+07] B. Lukić, S. Jeney, Z. Sviben, A. J. Kulik, E. L. Florin, and L. Forró. "Motion of a colloidal particle in an optical trap". In: *Phys. Rev. E* 76 (2007), p. 011112.

[MCC93] A. Mencke, A.-c. Cheng, and M. Caffrey. "A simple apparatus for time-resolved x-ray diffraction biostructure studies using static and oscillating pressures and pressure jumps". In: *Rev. Sci. Instrum.* 64 (1993), pp. 383–389.

[MDT06] S. A. Mukai, S. Deguchi, and K. Tsujii. "A high-temperature and -pressure microscope cell to observe colloidal behaviors in subcritical and supercritical water: Brownian motion of colloids near a wall". In: *Colloids Surf., A* 282 (2006), pp. 483–488.

[MK17] D. Mukherji and K. Kremer. "How does poly (*N*-isopropylacrylamide) trigger phase separation in aqueous alcohol?" In: *Polymer Science, Series C* 59 (2017), pp. 119–124.

[MMK14] D. Mukherji, C. M. Marques, and K. Kremer. "Polymer collapse in miscible good solvents is a generic phenomenon driven by preferential adsorption". In: *Nat. Commun.* 5 (2014).

[MMK20] D. Mukherji, C. M. Marques, and K. Kremer. "Smart Responsive Polymers: Fundamentals and Design Principles". In: *Annu. Rev. Condens. Matter Phys.* 11 (2020), pp. 271–299.

[MRI06] E. E. Meyer, K. J. Rosenberg, and J. Israelachvili. "Recent progress in understanding hydrophobic interactions". In: *Proc. Natl. Acad. Sci. U.S.A.* 103 (2006), pp. 15739–15746.

[MSR03] A. Milewska, J. Szydlowski, and L. P. N. Rebelo. "Viscosity and Ultrasonic Studies of Poly(*N*-isopropylacrylamide)-Water Solutions". In: *J. Polym. Sci., Part B: Polym. Phys.* 41 (2003), pp. 1219–1233.

[Mic+16] S. Micciulla, O. Soltwedel, O. Löhmann, and R. von Klitzing. "Temperature responsive behavior of polymer brush/polyelectrolyte multilayer composites". In: *Soft Matter* 12 (2016), pp. 1176–1183.

[Mur+16] T. J. Murdoch, B. A. Humphreys, J. D. Willott, K. P. Gregory, S. W. Prescott, A. Nelson, E. J. Wanless, and G. B. Webber. "Specific Anion Effects on the Internal Structure of a Poly(*N*-isopropylacrylamide) Brush". In: *Macromolecules* 49 (2016), pp. 6050–6060.

[Nie+17] B.-J. Niebuur, K.-L. Claude, S. Pinzek, C. Cariker, K. N. Raftopoulos, V. Pipich, M.-S. Appavou, A. Schulte, and C. M. Papadakis. "Pressure-Dependence of Poly (*N*-isopropylacrylamide) Mesoglobule Formation in Aqueous Solution". In: *ACS Macro Lett.* 6 (2017), pp. 1180–1185.

[ODG94] A. Okhulkov, Y. N. Demianets, and Y. E. Gorbaty. "X-ray scattering in liquid water at pressures of up to 7.7 kbar: Test of a fluctuation model". In: *J. Chem. Phys.* 100 (1994).

[Oh+08] J. K. Oh, R. Drumright, D. J. Siegwart, and K. Matyjaszewski. "The development of microgels/nanogels for drug delivery applications". In: *Prog. Polym. Sci.* 33 (2008), pp. 448–477.

[Ota+93] K. Otake, R. Karaki, T. Ebina, C. Yokoyama, and S. Takahashi. "Pressure effects on the aggregation of poly (*N*-isopropylacrylamide) and poly (*N*-isopropylacrylamide-co-acrylic acid) in aqueous solutions". In: *Macromolecules* 26 (1993), pp. 2194–2197.

[PC86] R. Pelton and P Chibante. "Preparation of aqueous latices with *N*-isopropylacrylamide". In: *Colloids Surf.* 20 (1986), pp. 247–256.

[Pel10] R. Pelton. "Poly(*N*-isopropylacrylamide)(PNIPAM) is never hydrophobic". In: *J. Colloid Interface Sci.* 348 (2010), pp. 673–674.

[Pil+16] D. W. Pilat, B. Pouligny, A. Best, T. A. Nick, R. Berger, and H.-J. Butt. "Surface forces between colloidal particles at high hydrostatic pressure". In: *Phys. Rev. E* 93 (2016), p. 022608.

[Pil16] D. W. Pilat. "Surface force measurement at high hydrostatic pressure". PhD thesis. Johannes Gutenberg-Universität Mainz, 2016.

[Plu+06] K. N. Plunkett, X. Zhu, J. S. Moore, and D. E. Leckband. "PNIPAM Chain Collapse Depends on the Molecular Weight and Grafting Density". In: *Langmuir* 22 (2006), pp. 4259–4266.

[Pol] M. N. Polyanskiy. *Refractive index database*. URL: `https://refractiveindex.info` (visited on 11/27/2019).

[Pue+09] R. A. Álvarez Puebla, R. Contreras-Cáceres, I. Pastoriza-Santos, J. Pérez-Juste, and L. M. Liz-Marzán. "Au@pNIPAM Colloids as Molecular Traps for Surface-Enhanced, Spectroscopic, Ultra-Sensitive Analysis". In: *Angew. Chem., Int. Ed.* 48 (2009), pp. 138–143.

[RC+03] M. Rubinstein, R. H. Colby, et al. *Polymer physics*. Vol. 23. Oxford university press New York, 2003.

[Rov+19] L. Rovigatti, N. Gnan, A. Ninarello, and E. Zaccarelli. "Connecting elasticity and effective interactions of neutral microgels: The validity of the Hertzian model". In: *Macromolecules* 52 (2019), pp. 4895–4906.

[SM+11] B Sierra-Martin, Y Laporte, A. South, L. A. Lyon, and A Fernández-Nieves. "Bulk modulus of poly(*N*-isopropylacrylamide) microgels through the swelling transition". In: *Phys. Rev. E* 84 (2011), p. 011406.

[SR00] A. K. Soper and M. A. Ricci. "Structures of high-density and low-density water". In: *Phys. Rev. Lett.* 84 (2000), p. 2881.

[SR99] H. Senff and W. Richtering. "Temperature sensitive microgel suspensions: Colloidal phase behavior and rheology of soft spheres". In: *J. Chem. Phys.* 111 (1999), pp. 1705–1711.

[Sch+10] S. Schmidt, M. Zeiser, T. Hellweg, C. Duschl, A. Fery, and H. Möhwald. "Adhesion and Mechanical Properties of PNIPAM Microgel Films and Their Potential Use as Switchable Cell Culture Substrates". In: *Adv. Funct. Mater.* 20 (2010), pp. 3235–3243.

[Sch+14] C. Scherzinger, A. Schwarz, A. Bardow, K. Leonhard, and W. Richtering. "Cononsolvency of poly-*N*-isopropyl acrylamide (PNIPAM): Microgels versus linear chains and macrogels". In: *Curr. Opin. Colloid Interface Sci.* 19 (2014), pp. 84–94.

[Sch92] H. G. Schild. "Poly(*N*-Isopropylacrylamide): Experiment, Theory and Application". In: *Prog. Polym. Sci.* 17 (1992), pp. 163–249.

[Sch+98] F. J. Schmitt, C. Park, J. Simon, H. Ringsdorf, and J. Israelachvili. "Direct Surface Force and Contact Angle Measurements of an Adsorbed Polymer with a Lower Critical Solution Temperature". In: *Langmuir* 14 (1998), pp. 2838–2845.

[Sha+04] J. Shan, J. Chen, M. Nuopponen, and H. Tenhu. "Two Phase Transitions of Poly(*N*-isopropylacrylamide) Brushes Bound to Gold Nanoparticles". In: *Langmuir* 20 (2004), pp. 4671–4676.

[Sha+07] N. Shamim, L. Hong, K. Hidajat, and M. S. Uddin. "Thermosensitive polymer (*N*-isopropylacrylamide) coated nanomagnetic particles: preparation and characterization". In: *Colloids Surf., B* 55 (2007), pp. 51–58.

[Ste+19] A. Z. Stetten, D. S. Golovko, S. A. Weber, and H.-J. Butt. "Slide electrification: charging of surfaces by moving water drops". In: *Soft Matter* 15 (2019), pp. 8667–8679.

[Stu+10] M. A. Stuart, W. T. Huck, J. Genzer, M. Müller, C. Ober, M. Stamm, G. B. Sukhorukov, I. Szleifer, V. V. Tsukruk, M. Urban, F. Winnik, S. Zauscher, I. Luzinov, and S. Minko. "Emerging applications of stimuli-responsive polymer materials". In: *Nat. Mater.* 9 (2010), pp. 101–113.

[Sui+11] X. Sui, Q. Chen, M. A. Hempenius, and G. J. Vancso. "Probing the Collapse Dynamics of Poly(*N*-isopropylacrylamide) Brushes by AFM: Effects of Co-nonsolvency and Grafting Densities". In: *Small* 7 (2011), pp. 1440–1447.

[TZC18] L Tavagnacco, E Zaccarelli, and E Chiessi. "On the molecular origin of the cooperative coil-to-globule transition of poly(*N*-isopropylacrylamide) in water". In: *Phys. Chem. Chem. Phys.* 20 (2018), pp. 9997–10010.

[TZW14] H. Tang, B. Zhang, and P. Wu. "On the two-step phase transition behavior of the Poly(*N*-isopropylacrylamide) (PNIPAM) brush: different zones with different orders". In: *Soft Matter* 10 (2014), pp. 7278–7284.

[Vou+13] P. Voudouris, D. Florea, P. van der Schoot, and H. M. Wyss. "Micromechanics of temperature sensitive microgels: dip in the Poisson ratio near the LCST". In: *Soft Matter* 9 (2013), pp. 7158–7166.

[WB05] H.-J. Wu and M. A. Bevan. "Direct Measurement of Single and Ensemble Average Particle-Surface Potential Energy Profiles". In: *Langmuir* 21 (2005), pp. 1244–1254.

[WC76] S. Weinbaum and C. G. Caro. "A macromolecule transport model for the arterial wall and endothelium based on the ultrastructural specialization observed in electron microscopic studies". In: *J. Fluid Mech.* 74 (1976), pp. 611–640.

[Wal+12] J. Walter, J. Sehrt, J. Vrabec, and H. Hasse. "Molecular dynamics and experimental study of conformation change of poly(*N*-isopropylacrylamide) hydrogels in mixtures of water and methanol". In: *J. Phys. Chem. B* 116 (2012), pp. 5251–5259.

[Wir+17] F. J. Wirkert, C. Hölzl, M. Paulus, P. Salmen, M. Tolan, D. Horinek, and J. Nase. "The Hydrophobic Gap at High Hydrostatic Pressures". In: *Angew. Chem.* (2017).

[Wu+07] T. Wu, Y. Zhang, X. Wang, and S. Liu. "Fabrication of Hybrid Silica Nanoparticles Densely Grafted with Thermoresponsive Poly(*N*-isopropylacrylamide) Brushes of Controlled Thickness

via Surface-Initiated Atom Transfer Radical Polymerization". In: *Chem. Mater.* 20 (2007), pp. 101–109.

[XBS06] Y. Xia, N. A. Burke, and H. D. Stöver. "End Group Effect on the Thermal Response of Narrow-Disperse Poly(*N*-isopropylacrylamide) Prepared by Atom Transfer Radical Polymerization". In: *Macromolecules* 39 (2006), pp. 2275–2283.

[Yim+05] H. Yim, M. S. Kent, S. Satija, S. Mendez, S. S. Balamurugan, S. Balamurugan, and G. P. Lopez. "Evidence for vertical phase separation in densely grafted, high-molecular-weight poly(*N*-isopropylacrylamide) brushes in water". In: *Phys. Rev. E* 72 (2005), p. 051801.

[Yon+18] H. Yong, S. Rauch, K.-J. Eichhorn, P. Uhlmann, A. Fery, and J.-U. Sommer. "Cononsolvency Transition of Polymer Brushes: A Combined Experimental and Theoretical Study". In: *Materials* 11 (2018), p. 991.

[Yon+19] H. Yong, E. Bittrich, P. Uhlmann, A. Fery, and J.-U. Sommer. "Cononsolvency transition of poly(*N*-isopropylacrylamide) brushes in a series of binary mixtures". In: *Macromolecules* 52 (2019), pp. 6285–6293.

[Yon+20] H. Yong, H. Merlitz, A. Fery, and J.-U. Sommer. "Polymer Brushes and Gels in Competing Solvents: The Role of Different Interactions and Quantitative Predictions for Poly(*N*-isopropylacrylamide) in Alcohol–Water Mixtures". In: *Macromolecules* 53 (2020), pp. 2323–2335.

[Yu+15] Y. L. Yu, B. D. Kieviet, F. Liu, I. Siretanu, E. Kutnyánszky, G. J. Vancso, and S. de Beer. "Stretching of collapsed polymers causes an enhanced dissipative response of PNIPAM brushes near their LCST". In: *Soft Matter* 11 (2015), pp. 8508–8516.

[Yu+16] Y. Yu, M. Cirelli, B. D. Kieviet, E. S. Kooij, G. J. Vancso, and S. de Beer. "Tunable friction by employment of co-non-solvency of PNIPAM brushes". In: *Polymer* 102 (2016), pp. 372–378.

[Yu+17] Y. Yu, R. A. L. de la Cruz, B. D. Kieviet, H. Gojzewski, A. Pons, G. J. Vancso, and S. de Beer. "Pick up, move and release of nanoparticles utilizing co-non-solvency of PNIPAM brushes". In: *Nanoscale* 9 (2017), pp. 1670–1675.

[ZN94] P. W. Zhu and D. H. Napper. "Experimental Observation of Coil-to-Globule Type Transitions at Interfaces". In: *J. Colloid Interface Sci.* 164 (1994), pp. 489–494.

[ZN96] P. W. Zhu and D. H. Napper. “Interfacial coil-to-globule transitions: the effects of molecular weight”. In: *Colloids Surf.* 113 (1996), pp. 145–153.

[ZPD95] J. Zhang, R. Pelton, and Y. Deng. “Temperature-Dependent Contact Angles of Water on Poly(*N*-isopropylacrylamide) Gels”. In: *Langmuir* 11 (1995), pp. 2301–2302.

[Zha+11] X. B. Zhang, C. L. Pint, M. H. Lee, B. E. Schubert, A. Jamshidi, K. Takei, H. Ko, A. Gillies, R. Bardhan, J. J. Urban, M. Wu, R. Fearing, and A. Javey. “Optically- and Thermally-Responsive Programmable Materials Based on Carbon Nanotube-Hydrogel Polymer Composites”. In: *Nano Lett.* 11 (2011), pp. 3239–3244.

[Zhu+91] E. B. Zhulina, O. V. Borisov, V. A. Pryamitsyn, and T. M. Birshtein. “Coil-Globule Type Transitions in Polymers. 1. Collapse of Layers of Grafted Polymer Chains”. In: *Macromolecules* 24 (1991), pp. 140–149.

[vBB19] D. van Duinen, H.-J. Butt, and R. Berger. “Two-Stage Collapse of PNIPAM Brushes: Viscoelastic Changes Revealed by an Interferometric Laser Technique”. In: *Langmuir* (2019).